

Simulation and diagnosis of stratosphere-troposphere exchange

Citation for published version (APA):

Meloan, J. (2002). *Simulation and diagnosis of stratosphere-troposphere exchange*. [Phd Thesis 1 (Research TU/e / Graduation TU/e), Applied Physics and Science Education]. Technische Universiteit Eindhoven. <https://doi.org/10.6100/IR556135>

DOI:

[10.6100/IR556135](https://doi.org/10.6100/IR556135)

Document status and date:

Published: 01/01/2002

Document Version:

Publisher's PDF, also known as Version of Record (includes final page, issue and volume numbers)

Please check the document version of this publication:

- A submitted manuscript is the version of the article upon submission and before peer-review. There can be important differences between the submitted version and the official published version of record. People interested in the research are advised to contact the author for the final version of the publication, or visit the DOI to the publisher's website.
- The final author version and the galley proof are versions of the publication after peer review.
- The final published version features the final layout of the paper including the volume, issue and page numbers.

[Link to publication](#)

General rights

Copyright and moral rights for the publications made accessible in the public portal are retained by the authors and/or other copyright owners and it is a condition of accessing publications that users recognise and abide by the legal requirements associated with these rights.

- Users may download and print one copy of any publication from the public portal for the purpose of private study or research.
- You may not further distribute the material or use it for any profit-making activity or commercial gain
- You may freely distribute the URL identifying the publication in the public portal.

If the publication is distributed under the terms of Article 25fa of the Dutch Copyright Act, indicated by the "Taverne" license above, please follow below link for the End User Agreement:

www.tue.nl/taverne

Take down policy

If you believe that this document breaches copyright please contact us at:

openaccess@tue.nl

providing details and we will investigate your claim.

**Simulation and Diagnosis
of
Stratosphere-Troposphere Exchange**

PROEFSCHRIFT

ter verkrijging van de graad van doctor aan de
Technische Universiteit Eindhoven, op gezag van de
Rector Magnificus, prof.dr. R.A. van Santen, voor een
commissie aangewezen door het College voor
Promoties in het openbaar te verdedigen
op donderdag 20 juni 2002 om 16.00 uur

door

Jojanneke Meloen

geboren te Nieuwkoop

Dit proefschrift is goedgekeurd door de promotoren:

prof.dr. H. Kelder
en
prof.dr. A. Ebel

Copromotor:
dr. P.C. Siegmund

Druk: Universiteitsdrukkerij Technische Universiteit Eindhoven

CIP-DATA LIBRARY TECHNISCHE UNIVERSITEIT EINDHOVEN

Meloen, Jojanneke

Simulation and diagnosis of stratosphere-troposphere exchange / by
Jojanneke Meloen. - Eindhoven : Technische Universiteit Eindhoven, 2002.
Proefschrift. - ISBN 90-386-1999-5

NUR 912

Trefwoorden: atmosferische dynamica / potentiële vorticheit / stratosfeer-troposfeer
uitwisseling / trajectorieën / modelvergelijking

Subject headings: potential vorticity / upper troposphere / lower stratosphere /
stratosphere-troposphere exchange / trajectories / model intercomparison

Voor mijn ouders

Front cover

–Folding events can be found everywhere–

Dent Blanche (4357 m)

Valais, Switzerland

Photograph: Wouter Knap

Editing: Pieter Valks

Contents

Voorwoord	9
Inleiding en samenvatting	11
1 Introduction	19
1.1 Conserved quantities	20
1.2 Overworld, middleworld and underworld	22
1.3 Overview of the dynamical aspects of STE	23
1.3.1 Global-scale dynamical aspects: the Brewer-Dobson circulation	23
1.3.2 Processes near the tropopause	25
1.4 Models and methods used to estimate and diagnose STE	29
1.5 Overview of this thesis	30
2 On the conservation of moist potential vorticity versus potential vorticity	33
2.1 Introduction	34
2.2 Potential and moist potential vorticity equations	35
2.2.1 The potential vorticity	35
2.2.2 The moist potential vorticity	36
2.2.3 Simplification of the Q_d and Q_m equation	37
2.3 Comparing Q_m with Q_d	37
2.3.1 Meteorological situation	37
2.3.2 Data description	38
2.3.3 Results	39
2.4 Discussion and conclusion	48
3 Stratosphere-troposphere exchange in an extratropical cyclone calculated with a Lagrangian method	53
3.1 Introduction	54

3.2	Method and data	56
3.2.1	Calculation of the air-mass flux across a Q -surface	56
3.2.2	Trajectory model	58
3.2.3	ECMWF data	58
3.3	Results	59
3.3.1	Synoptic situation	59
3.3.2	Geographical distribution of the flux across Q -surfaces	59
3.3.3	Decomposition of the flux	62
3.3.4	Vertical cross-sections: air-mass flux across Q -surfaces	62
3.3.5	Area-averaged upward and downward fluxes	64
3.4	Discussion	65
3.4.1	Parameterisation of Q -mixing in the ECMWF model	66
3.4.2	Method for calculating the flux across a Q -surface	67
3.4.3	Comparison of F_{up}/F_{down} with previous studies	69
3.5	Conclusions	70
4	A Lagrangian computation of stratosphere-troposphere exchange in a tropopause folding event in the subtropical Southern Hemisphere	71
4.1	Introduction	72
4.2	Method and Data	73
4.2.1	Flux calculation	73
4.2.2	ECMWF data	75
4.2.3	Trajectory model	75
4.2.4	The TRACAS experiment	76
4.3	Results	76
4.3.1	Evaluation of F	76
4.3.2	Exchange in the fold: time and area integration	82
4.4	Discussion and conclusions	85
5	Stratosphere-troposphere exchange: model and method intercomparison	87
5.1	Introduction	88
5.2	Intercomparison: set-up, models and methods	90
5.2.1	Intercomparison set-up	90
5.2.2	Models and methods	91
5.3	Meteorological situation	95
5.4	The model and method intercomparison	95
5.4.1	Cross-tropopause mass fluxes	97
5.4.2	Stratospheric tracer concentration and flux at the 700 hPa surface	99

5.4.3	Time versus height plots of the stratospheric tracer concentration	106
5.5	Discussion and conclusions	108
6	Summary and outlook	111
6.1	Summary	111
6.2	Outlook	113
	References	117
	Curriculum vitae	123

Voorwoord

Zo, het zit er bijna op. De KNMI-tijd van in het zonnetje zitten en nadenken over hoe het komt dat de ene grafiek op een kameel lijkt en de ander op een dromedaris is (voorlopig?) voorbij. Een half jaar geleden, toen de datum voor mijn promotie vastgelegd werd, had ik nooit verwacht dat ik die 20 juni ook inderdaad zou halen. Tussendoor heb ik zelfs overwogen om mijn promotie uit te stellen, zodat ik niet de hele commissie zou belasten met het vrijhouden van een datum die later toch weer verzet zou worden. Van hoger af heb ik toen de opdracht gekregen om struisvogelpolitiek te gaan bedrijven: kop in het zand, je nergens druk over maken (zeker niet over de agenda's van de commissie), en zelf het hardst van allemaal geloven dat je die datum gewoon gaat halen! Dat ik de datum inderdaad gehaald heb, is een teken dat ik de struisvogelpolitiek erg goed onder de knie heb weten te krijgen. Voor deze wijze les en voor heel veel andere grote of kleine bijdragen aan de totstandkoming van dit proefschrift, wil ik hier de nodige mensen bedanken.

Allereerst Peter Siegmund, mijn begeleider. Dat we in de loop van de vier jaar wetenschappelijk gezien dichter tot elkaar zijn gekomen werd mij duidelijk toen je dit voorjaar ineens een aantal weken ziek was. Wat was ik blij dat je terug was en er eindelijk weer iemand dezelfde ideeën over mijn onderzoek had als ik. Ook de snelheid waarmee je dingen doet ben ik steeds meer gaan waarderen. Vooral in de laatste vier maanden toen de tijdsdruk hoog was, kwam ik er achter dat het heel erg handig is als je 's ochtends leeswerk in kan leveren en het dan 's middags gecorrigeerd terugkrijgt. Ook je eerlijke mening over hoe het ging of wat je van mijn artikelen vond heb ik altijd zeer gewaardeerd. Peter, ontzettend bedankt!

Peter van Velthoven had eigenlijk niet zo heel veel met mij te maken, maar ik heb je min of meer gestrikt als tweede begeleider. Als 'mijn' Peter er niet was, of als ik een 'second opinion' wilde, dan ging ik naar jou toe. Ook als (nu en dan) hart-onderde-riem-steker heb ik zeker een goeie aan je gehad. En mede door jouw inzet voor de financiële middelen heb ik hier ruim vier jaar kunnen zitten. Volgens mij was je af en toe zenuwachtiger dan ik dat er geen nieuw geldpotje gevonden zou worden!

Hennie wil ik ook bedanken. Als promotor en als hoofd van de groep heb je me

alle vrijheid gegeven. Op het eind heb je de touwtjes stevig in handen genomen en me door de laatste zes maanden van de promotiebureaucratie heen geloodst. Je rust en je alles-komt-goed-mentaliteit zal ik zeker niet vergeten!

Dan natuurlijk al mijn collega's. Ik kan me amper voorstellen dat het wat collega's betreft beter kan. Niet alleen bij Atmosferische Samenstelling, maar ook bij andere groepen waren jullie altijd even aardig en behulpzaam, in voor een babbeltje of de lunch, voor het beantwoorden van vragen of het oplossen van technische ellende. In die tijden dat ik mijn werk even niet meer zag zitten, hebben jullie als KNMI-lijm gefungeerd!

Twee wil ik uiteraard nog even apart noemen: Mijke en Renske. Jullie hebben mijn tijd op het KNMI echt tot een feestje gemaakt, en ik ga ervan uit dat jullie buiten het KNMI daar gewoon mee doorgaan. Vooral Mijke is onmisbaar geweest in de afgelopen tijd. Je bent rond dezelfde tijd begonnen aan je promotie en we zijn tegelijkertijd door alle bergen en dalen, onzekerheden en zevendaagse werkweken van het promovendus zijn heen gegaan. Hierdoor had ik altijd maar een half woord nodig, want je snapte als geen ander hoe ik me voelde. Meiden, ontzettend bedankt!

Bart van den Hurk is ook zeker onmisbaar geweest om mijn KNMI-tijd te maken tot wat het was. Als muzikaal talent heb je regelmatig één van mijn grootste hobbies KNMI-leven ingeblazen: zingen. Ik heb het altijd met veel plezier gedaan en vond het erg jammer dat destijds het KNMI-koor opgeheven werd. Desondanks bleek er altijd nog wel wat gelegenheid om te zingen binnen het KNMI en verder kon ik gelukkig mijn zingei kwijt bij Bon Ton, het leukste koor van Utrecht!

Ik mag natuurlijk mijn vrienden niet vergeten. Allemaal zijn jullie trouwe toehoorders van het wel en wee van alles wat met mij te maken heeft, en altijd staan jullie klaar voor de leuke dingen buiten het werk. Ik ben me ervan bewust dat ik jullie de laatste zes maanden erg verwaarloosd heb, maar reken maar dat ik het weer goed ga maken!

Als laatste wil ik mijn ouders, zus en zwager bedanken voor al hun steun en vertrouwen die ze tijdens de afgelopen vier jaar, maar ook daarvoor, in me hebben gesteld. Zonder jullie was ik nooit zover gekomen. Door alle drukte is het alweer een hele poos geleden dat ik in Tholen langs ben geweest, maar ook dat gaat helemaal goed komen. Dit jaar kom ik zeker een dagje wieden! Ook ga ik er vanuit dat Matthijs over een jaar een beter beeld heeft van zijn tante dan dat hij nu heeft, want in zijn leventje tot nu toe heeft hij me nog veel te weinig gezien.

Er zijn vast mensen die ik niet genoemd heb. Het is bijna onmogelijk om in twee bladzijden iedereen te noemen en het ook nog een beetje onderhoudend te houden. Daarom hierbij mijn dank voor iedereen die op welke manier ook aanwezig was in mijn leven de afgelopen vier jaar, jij in het bijzonder!

Inleiding en samenvatting

In dit hoofdstuk geef ik een inleiding op, en een korte samenvatting van de inhoud van dit proefschrift. Het is geschreven voor de leek, in de hoop dat jullie een paar bladzijden verder zullen komen dan alleen de stellingen, het voorwoord en mijn curriculum vitae, en daarbij ook nog snappen wat ik in die vier jaar zoal gedaan heb. Allereerst worden de voor het onderzoek in dit proefschrift belangrijke delen van de atmosfeer beschreven. Vervolgens wordt een overzicht gegeven van de uitwisseling tussen de verschillende delen van de atmosfeer. Tenslotte worden de belangrijkste resultaten van dit proefschrift samengevat.

De atmosfeer

Voor het onderzoek gedaan voor dit proefschrift zijn drie delen van de atmosfeer van belang: de troposfeer, de stratosfeer en het grensvlak hiertussen, de tropopauze. Deze opbouw van de atmosfeer is weergegeven in de figuur op bladzijde 14. De troposfeer is de laag die aan het aardoppervlak grenst, en waar het merendeel van het menselijk leven en het dagelijkse weer zich afspelen. De hoogte van deze laag varieert van ongeveer acht kilometer boven het poolgebied tot zestien kilometer boven de tropen. De stratosfeer is de laag die zich boven de troposfeer bevindt en zich uitstrekt tot een hoogte van ongeveer vijftig kilometer. Het vlak dat de troposfeer en de stratosfeer scheidt, heet de tropopauze.

De samenstelling van de troposfeer en de stratosfeer is niet hetzelfde. Water bevindt zich bijvoorbeeld vooral onder in de troposfeer. Naar boven toe neemt de hoeveelheid waterdamp snel af en in de stratosfeer is het vrijwel afwezig. Een belangrijk gas dat vooral in de stratosfeer te vinden is, is ozon. In de ozonlaag, op een hoogte tussen 25 en 35 kilometer, is de concentratie aan ozon het grootst. Toch is zelfs op die hoogte de hoeveelheid ozon ten opzichte van andere gassen heel klein, namelijk minder dan twee deeltjes per miljoen andere deeltjes. Deze ozonlaag absorbeert het grootste deel van de ultraviolette straling van de zon en is dus van groot belang voor het leven op aarde.

Ook de dynamische eigenschappen van de troposfeer en de stratosfeer zijn niet hetzelfde. In de troposfeer bijvoorbeeld is de menging van de lucht erg groot. Als een stof aan het aardoppervlak losgelaten zou worden, zou je datzelfde stofje een aantal uur later al terug kunnen vinden boven in de troposfeer. Als hetzelfde experiment in de stratosfeer gedaan zou worden, zou het maanden duren voor je hetzelfde stofje op een hele andere hoogte tegen zou komen. Dit verschil in transportsnelheid is een gevolg van de verschillen in temperatuursopbouw tussen de troposfeer en de stratosfeer. In de troposfeer is de temperatuursopbouw vaak niet stabiel, met warme lucht onderin en koude lucht boven in de troposfeer. Omdat de warme lucht onderin lichter is dan de koude lucht bovenin, zal de warme lucht de neiging hebben om op te stijgen (hierbij kunnen wolken ontstaan als de lucht genoeg waterdamp bevat). In de stratosfeer daarentegen bevindt de zware koude lucht zich onderin, en de lichte warme lucht zich bovenin, wat een stabiele opbouw geeft van de lucht in de stratosfeer.

De tropopause vormt een barrière tussen de troposfeer en stratosfeer. Lucht die zich in de stratosfeer bevindt, kan niet zomaar de troposfeer in waaien. Ozon uit de stratosfeer kan dus niet zomaar in de troposfeer terechtkomen. Andersom kan het waterdamp uit de troposfeer ook niet zomaar in de stratosfeer terechtkomen. Toch vindt er transport plaats van lucht van de troposfeer naar de stratosfeer en vice versa, de zogenaamde stratosfeer-troposfeer uitwisseling.

Hoeveel lucht er uitgewisseld wordt tussen de stratosfeer en troposfeer, en hoe en waar die uitwisseling plaatsvindt, is belangrijk om te weten. Dit is dan ook het centrale thema van dit proefschrift. Als er meer bekend is over de uitwisseling tussen de stratosfeer en troposfeer, dan kunnen we de opbouw en samenstelling van de atmosfeer beter gaan begrijpen, bijvoorbeeld hoe het komt dat de stratosfeer zo ontzettend droog is. Het geeft ook inzicht in de manier waarop menselijke activiteiten aan het aardoppervlak de ozonafbraak in de stratosfeer beïnvloeden, of hoe en waar de uitlaatgassen van vliegtuigen de samenstelling van de atmosfeer beïnvloeden. Ook kan met een beter begrip van de uitwisseling tussen de stratosfeer en troposfeer onderzocht worden hoe deze uitwisseling zal veranderen als bijvoorbeeld de troposfeer opwarmt ten gevolge van de toename van broeikasgassen.

Uitwisseling tussen troposfeer en stratosfeer

De uitwisseling tussen de stratosfeer en de troposfeer en vice versa kan het best begrepen worden als er onderscheid gemaakt wordt tussen uitwisseling die te maken heeft met luchtbewegingen die de hele wereld beslaan, het grootschalige proces, en uitwisseling die te maken heeft met plaatselijke, kleinschalige processen.

Grootschalige proces van stratosfeer-troposfeer uitwisseling

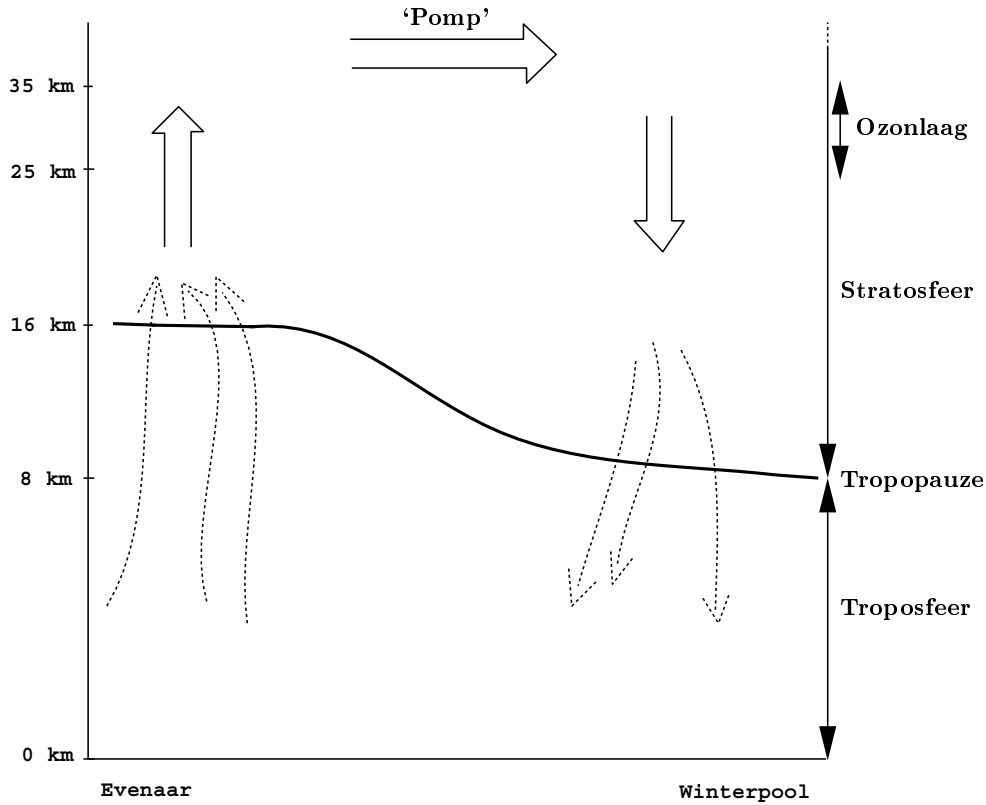
De lucht in de atmosfeer beweegt voortdurend. Behalve de luchtverplaatsingen in de troposfeer, die merkbaar zijn als wind, bestaat er een grootschalige langzame luchtcirculatie die plaatsvindt in de troposfeer en stratosfeer. Deze luchtcirculatie wordt de Brewer-Dobson circulatie genoemd. Deze luchtcirculatie bestaat uit opgaande bewegingen in de troposfeer in de tropen. De lucht gaat hier door de tropopauze en komt terecht in de stratosfeer. In de stratosfeer verplaatst de meeste lucht zich in de richting van het poolgebied waar het winter is, een kleiner gedeelte van de lucht gaat in de richting van het poolgebied waar het zomer is. In de buurt van de polen zakt de lucht weer naar beneden, waarbij de tropopauze wederom gepasseerd wordt. Deze Brewer-Dobson circulatie is in de figuur op bladzijde 14 aangegeven door de dubbele pijlen.

De Brewer-Dobson circulatie is een gevolg van een ‘pomp’ in de stratosfeer die de lucht hier in poolwaartse richting stuwt. Hierdoor wordt de lucht uit de tropen de stratosfeer ingezogen, en in de poolgebieden de troposfeer ingepompt. Zoals gezegd zijn de luchtbewegingen in de stratosfeer erg langzaam. Het duurt dan ook maanden voor de lucht die in de tropen de stratosfeer ingaat, er bij de polen weer uitkomt. Toch is dit de weg die elk luchtdeeltje in de atmosfeer ongeveer elke twee jaar een keer aflegt. Ook de vervuilende stoffen uit de troposfeer die boven de polen voor ozongaten in de stratosfeer zorgen, komen in de polaire stratosfeer terecht door in de tropen de tropopauze te passeren.

Kleinschalige processen van stratosfeer-troposfeer uitwisseling

De Brewer-Dobson circulatie bepaalt hoeveel lucht er in totaal uitgewisseld wordt tussen de stratosfeer en de troposfeer. De kleinschalige processen daarentegen bepalen waar en wanneer in de atmosfeer deze lucht uitgewisseld wordt. Er zijn verschillende kleinschalige processen die de uitwisseling tussen de troposfeer en stratosfeer bepalen. Ze vinden plaats rond de tropopauze, en zijn in de figuur op bladzijde 14 aangegeven door de gestippelde pijlen. Door de zuigende werking van de Brewer-Dobson circulatie in de tropen, vinden hier voornamelijk kleinschalige processen plaats waarbij de lucht van de troposfeer naar de stratosfeer getransporteerd wordt, en buiten de tropen voornamelijk kleinschalige processen waarbij de lucht van de stratosfeer naar de troposfeer getransporteerd wordt. Voor dit proefschrift zijn vooral de laatste kleinschalige transportprocessen onderzocht.

Een voorbeeld van zo’n kleinschalig proces is een front. De tropopauze ter plaatse van een front (waar de regen in Nederland vaak uit valt) ziet eruit zoals op de voorkant van dit proefschrift: het lijkt alsof de stratosfeer schuin naar beneden de troposfeer



Opbouw van de atmosfeer. Op de verticale as staat de hoogte aangegeven in kilometers. De tropopauze is aangegeven door de dikke lijn die loopt van 8 km op de winterpool tot 16 km bij de evenaar. De laag eronder is de troposfeer, die erboven de stratosfeer. De ozonlaag bevindt zich tussen 25 en 35 km in de stratosfeer. De grootschalige circulatie (Brewer-Dobson circulatie) is aangegeven door de dubbele pijlen, de gestippelde pijlen geven de kleinschalige processen rond de tropopauze aan.

instroomt. Omdat de tropopauze in principe een barrière vormt voor lucht, zou de stratosfeer enige tijd later weer terug kunnen stromen zonder dat er uitwisseling tussen de stratosfeer en troposfeer plaats heeft gevonden. Het lijkt dan op een tijdelijke 'deuk' in de tropopauze. Om transport van lucht door de tropopauze te krijgen zijn er nog kleinschaligere effecten nodig, die hier 'bijkomende effecten' worden genoemd. Door de bijkomende effecten van zo'n front vindt er uitwisseling plaats tussen de stratosfeer en troposfeer. Ze bestaan bijvoorbeeld uit het mengen van luchtmassa's als gevolg van grote verschillen in lichtsnelheid (denk aan een trein die voorbij raast als je op het perron staat, door de snelheid van de trein gaat de lucht waar de trein

doorheen rijdt bewegen en mengen, wat je voelt als wind). Een ander bijkomend effect is opwarming of afkoeling van de lucht. Door opwarming of afkoeling kan de lucht stijgen of dalen waardoor er uitwisseling plaats kan vinden. Een voorbeeld van zo'n effect dat bij fronten een rol speelt is opwarming van lucht door de omzetting van waterdamp naar vloeibaar water (dit proces heet condensatie). Bij condensatie van waterdamp komt de warmte vrij die nodig was om vloeibaar water om te zetten naar waterdamp (wat bijvoorbeeld ook gebeurt bij het koken van water). Deze warmte komt vrij bij de afkoeling van vochtige lucht door bijvoorbeeld opwaartse luchtbewegingen. De afgekoelde lucht kan minder waterdamp bevatten en de waterdamp zal daarom omgezet worden in vloeibaar water. De warmte die hierbij vrijkomt, warmt de door opwaartse luchtbeweging afgekoelde lucht weer op. Als de lucht hierbij warmer wordt dan zijn omgeving zal hij nog verder op kunnen stijgen, koelt hij weer af, en komt er weer warmte vrij door condensatie van waterdamp. Op deze manier kan de lucht uiteindelijk de tropopauze bereiken, en hier zorgen voor de menging van lucht tussen de troposfeer en stratosfeer.

Deze twee bijkomende effecten, menging ten gevolge van verschillen in windsnelheid en opwarming door het omzetten van waterdamp naar vloeibaar water, zijn de twee belangrijkste processen die uitwisseling veroorzaken rond een front. Ook voor de meeste andere kleinschalige processen zijn één of beide bijkomende effecten de oorzaak van de uiteindelijke uitwisseling.

Een voorbeeld van een ander kleinschalig proces is een lagedrukgebied. In deze lagedrukgebieden is de tropopauze relatief laag. Ook hier zijn menging van lucht-massa's ten gevolge van verschillen in windsnelheid en opwarming door het omzetten van waterdamp naar water de oorzaak van de uiteindelijke uitwisseling van lucht tussen stratosfeer en troposfeer.

Een ander proces waarbij uitwisseling plaats vindt tussen de stratosfeer en troposfeer is de straalstroom. De straalstroom is een smalle strook van zeer hoge windsnelheden ter hoogte van de tropopauze. De wind in deze straalstroom waait vanuit het westen richting het oosten. Deze strook is doorgaans duizenden kilometers lang in oost/west richting, enkele honderden kilometers breed in noord/zuid richting en enkele kilometers dik. Er bevindt zich een straalstroom boven de oceanen ter hoogte van Europa en ter hoogte van de subtropen (de straalstroom ter hoogte van Europa zorgt voor de constante aanvoer van lagedrukgebieden in ons land, en voor het feit dat de vliegtijd naar Amerika gemiddeld een uur langer duurt (wind tegen) dan de terugreis (wind mee)). Omdat de straalstroom zo'n smalle strook is van zeer hoge windsnelheden en zich rond de tropopauze bevindt, vindt hier, net als bij de voorbijrazende trein, menging van lucht uit de stratosfeer en de troposfeer plaats vindt. Het andere bijkomende effect, het vrijkomen van warmte door het omzetten van water-

damp naar water, speelt bij de straalstroom geen rol.

Er zijn nog andere kleinschalige processen die stratosfeer-troposfeer uitwisseling veroorzaken, maar dit zijn de drie belangrijkste. Samenvattend kun je dus zeggen dat de Brewer-Dobson circulatie bepaalt hoeveel uitwisseling er in totaal plaatsvindt tussen de stratosfeer en de troposfeer, en dat de kleinschalige processen bepalen waar op de wereld en wanneer deze uitwisseling tussen de stratosfeer en troposfeer plaatsvindt. Voor het begrijpen van stratosfeer-troposfeer uitwisseling is kennis van beide processen dus belangrijk. Voor dit proefschrift is vooral onderzoek gedaan naar de kleinschalige processen in de atmosfeer.

Overzicht van dit proefschrift

De term potentiële vortciteit wordt veel gebruikt in dit proefschrift. Voor een meteoroloog is de potentiële vortciteit net zoiets als de temperatuur. Zoals met de temperatuur wordt aangegeven hoe warm de lucht is, zo wordt met de potentiële vortciteit aangegeven hoe snel de lucht ronddraait. Dit kan vergeleken worden met bijvoorbeeld een kopje koffie. Als je niet in de koffie roert is de potentiële vortciteit van de koffie nul, zodra je in de koffie gaat roeren, neemt de draaiing van de koffie en dus ook de potentiële vortciteit van de koffie toe. Zo is het ook in de atmosfeer. Rond een lagedrukgebied bijvoorbeeld draait de lucht tegen de wijzers van de klok in. Deze draaiende lucht zorgt ervoor dat in een lagedrukgebied de potentiële vortciteit hoog is ¹.

Potentiële vortciteit wordt veel gebruikt in de meteorologie omdat (in afwezigheid van bijvoorbeeld warmte die vrijkomt bij condensatie) de potentiële vortciteit van een luchtdeeltje behouden is. Dit wil zeggen dat in de loop van de tijd de potentiële vortciteit van een luchtdeeltje niet verandert. In **hoofdstuk 2** zijn twee verschillende soorten potentiële vortciteit gedefiniëerd, de gebruikelijke potentiële vortciteit waarvan de waarde kan veranderen door het vrijkomen van condensatiewarmte, en een ‘natte’ potentiële vortciteit waar het vrijkomen van condensatiewarmte geen invloed op heeft. Omdat de troposfeer over het algemeen behoorlijk nat is, zou je verwachten dat de natte potentiële vortciteit een beter behouden grootte is dan de in de meteorologie meest gebruikte potentiële vortciteit. In hoofdstuk 2 is onderzocht of dit ook daadwerkelijk zo is. Het resultaat van dit onderzoek was dat de natte potentiële vortciteit dicht bij het aardoppervlak slechter behouden is dan de gebruikelijke po-

¹Eigenlijk klopt dit beeld niet helemaal. De term vortciteit geeft de hoeveelheid draaiing van de lucht aan zoals hierboven beschreven. De term potentiële vortciteit geeft aan hoe hard de lucht zou draaien als je deze naar een bepaalde plek op aarde zou brengen met een bepaalde temperatuursopbouw. Maar lucht die sowieso al draait en dus een relatief grote draaiing heeft ten opzichte van zijn omgeving, zal op deze referentieplek op aarde ook een relatief grote draaiing hebben. Daarom heb ik hier voor de eenvoud de begrippen vortciteit en potentiële vortciteit door elkaar gebruikt.

tentiële vortciteit. Dit is dus niet zoals verwacht omdat bij het aardoppervlak de lucht het vochtigst is en hier dus de meeste warmte vrij kan komen door condensatie van waterdamp. Wat hoger in de troposfeer is de natte potentiële vortciteit wel beter behouden. Mogelijke verklaringen voor dit verrassende resultaat zijn beschreven in het tweede hoofdstuk.

Een nog niet genoemd voordeel van de potentiële vortciteit is dat de lucht in de troposfeer een hele lage waarde van potentiële vortciteit heeft, in de stratosfeer een hele hoge waarde, en dat de tropopauze gedefiniëerd kan worden door een bepaalde vaste waarde van potentiële vortciteit. Dit laatste houdt in dat alle deeltjes die zich op een bepaald moment op de tropopauze bevinden dezelfde waarde van potentiële vortciteit hebben. De potentiële vortciteit van een luchtdeeltje wordt daarom in dit proefschrift gebruikt om luchtdeeltjes te karakteriseren, omdat het aangeeft waar in de atmosfeer een luchtdeeltje zich bevindt. De hoge waarde van potentiële vortciteit in de stratosfeer en de lage waarde in de troposfeer heeft ook als voordeel dat een deeltje die van de stratosfeer, door de tropopauze, naar de troposfeer gaat (wat dus kan als er condensatiewarmte vrijkomt, zoals beschreven in het stuk over de kleinschalige effecten) in de stratosfeer een hoge potentiële vortciteit zal hebben en op zijn weg naar de troposfeer een steeds lagere waarde voor de potentiële vortciteit zal krijgen. Met behulp van de potentiële vortciteit is dus de uitwisseling van lucht tussen de stratosfeer en de troposfeer (en andersom) te achterhalen.

In **hoofdstuk 3** is van deze voordelen van de potentiële vortciteit is gebruik gemaakt. In dit hoofdstuk is een methode ontwikkeld om de hoeveelheid en plaats van stratosfeer-troposfeer uitwisseling te bepalen. Deze methode is gebaseerd op het trajectoriemodel van het KNMI. Het trajectoriemodel is een computermodel dat in staat is om met behulp van windvelden de beweging van luchtdeeltjes door de atmosfeer te berekenen. Deze windvelden komen van het Europees Centrum voor Middellange Weersvoorspellingen (ECMWF) in Reading, Engeland. Hier staat een supercomputer, die continu de atmosferische bewegingen, temperatuur, druk enzovoorts berekent. Continu worden aan deze modelberekeningen waarnemingen toegevoegd, zodat het model in overeenstemming blijft met de werkelijke weerssituatie. Elke dag wordt een voorspelling gemaakt van het weer voor de komende tien dagen. Het zijn deze voorspellingen die in onze weerberichten gebruikt worden. In de methode ontwikkeld in hoofdstuk 3 worden luchtdeeltjes die zich op de tropopauze bevinden gevolgd met behulp van het trajectoriemodel. In eerste instantie hebben al deze luchtdeeltjes dus dezelfde potentiële vortciteitswaarde. Na verloop van tijd, als de luchtdeeltjes die zich op de tropopauze bevonden de gelegenheid hebben gehad alle kanten op te waaien, kan met behulp van de nieuwe potentiële vortciteitswaarde van deze luchtdeeltjes gekeken worden of en hoeveel luchtdeeltjes zich verplaatst hebben naar de

stratosfeer of naar de troposfeer. Uit de resultaten bleek dat deze nieuw ontwikkelde methode een goede manier is om de stratosfeer-troposfeer uitwisseling te bepalen.

In **hoofdstuk 4** is de methode van hoofdstuk 3 toegepast op een front in de subtropen op het Zuidelijk Halfrond (deze had ook de vorm zoals getoond op de voorkant van dit proefschrift). Voor beide gebieden, de subtropen in het algemeen en het Zuidelijk Halfrond, is nog weinig bekend over de hoeveelheid lucht die uitgewisseld wordt tussen de stratosfeer en de troposfeer. De kleinschalige processen zijn wel ongeveer hetzelfde als bij ons in de buurt, maar kunnen toch op wezenlijke punten verschillen. Met de methode van hoofdstuk 3 is berekend hoeveel kilogram lucht uitgewisseld is in dit front. In het gebied wat bekeken is (ongeveer 2.5 keer zo groot als Europa, het front nam hiervan 10% in beslag) ging over een periode van 4.5 dag 20×10^{13} kg lucht naar de troposfeer. In het front werd 200 keer zoveel lucht uitgewisseld als buiten het front. De methode ontwikkeld in hoofdstuk 3 is in hoofdstuk 4 gecontroleerd met behulp van metingen. De resultaten van deze controle geven vertrouwen in de toepasbaarheid van de methode gebruikt in hoofdstuk 3 en 4.

Als laatste worden in **hoofdstuk 5** verschillende modellen en methoden vergeleken die in Europa gebruikt worden om stratosfeer-troposfeer uitwisseling te bepalen. Om te zorgen dat de uitvoer van de modellen en methoden vergeleken kon worden is er een simpel stratosferisch gas bedacht waarmee de modellen en methoden de uitwisseling tussen stratosfeer en troposfeer hebben berekend. Met de vergelijking is geprobeerd om inzicht te krijgen in de sterke en zwakke kanten van elk model en elke methode, en is de betrouwbaarheid van de resultaten bepaald. Een conclusie van dit onderzoek was dat de modellen en methoden vergelijkbare resultaten geven. Een oorzaak van verschillen tussen de resultaten van de modellen en methoden zijn de verschillen in grootte van de luchtpakketjes waarmee het model of de methode rekent. Het bleek ook dat voor een exactere bepaling van de sterke en zwakke kanten van de modellen en methoden, de modellen en methoden zoveel mogelijk op dezelfde manier de uitwisseling moeten berekenen. In deze vergelijking waren er zoveel verschillen in die berekening, dat de precieze oorzaken van de verschillen in de resultaten niet altijd te achterhalen waren.

1

Introduction

The transport of air from the stratosphere to the troposphere and vice versa plays an important role in the dynamics and composition of the atmosphere. The extreme dryness of the stratosphere, for example, is a result of the transport from the troposphere to the stratosphere in the tropics, where the air is strongly dried when it passes the very cold tropopause. Stratosphere-troposphere exchange (STE) is also important for the human impact on the atmosphere. CFCs, for example, which cause enhanced chemical ozone destruction in the stratosphere, are released at the earth's surface due to human activities and are transported into the stratosphere in the tropics. From here the CFCs are transported toward the poles where the ozone depletion takes place.

Despite extensive research on STE, there are still large uncertainties in several important qualitative and quantitative aspects of STE. For example, there are still uncertainties in the knowledge of the temporal and spatial distribution of STE. This knowledge is essential for modelling the human impact on atmospheric chemistry and climate, since anthropogenic pollutants are emitted non-uniformly in time and space.

For assessing the detailed influence of STE on the dynamics and composition of the atmosphere, not only more research on the dynamical and chemical aspects of the exchange processes is required, but also the accuracy of and confidence in the used diagnostic methods need to be increased. Also for assessing the impact of future climate change on the composition of the atmosphere through circulation changes, the knowledge of STE needs to be increased. Recently, *Butchart and Scaife* [2001] predicted an increase of the air-mass exchange between the troposphere and the stratosphere with 3% per decade due to enhanced greenhouse gas concentrations. In order to investigate the impact of enhanced greenhouse gas concentrations on STE, it is important to simulate the involved transport processes correctly.

In this thesis several aspects of STE are discussed. In this introduction first a description is given of conserved quantities used in this thesis (section 1.1). A further

classification of the stratosphere and troposphere which is relevant to STE is given in section 1.2. Section 1.3 describes the known mechanisms of STE, divided in global-scale processes and processes near the tropopause. Section 1.4 gives an overview of the models and methods that have been used for the simulation and diagnosis of STE. Finally, in section 1.5 an overview of this thesis is given.

1.1 Conserved quantities

Conserved quantities are quantities that have a constant value in materially conserved flows. Several conserved quantities are used to describe the atmosphere. One of the strengths of these quantities is that on material conserved surfaces their flow is two-dimensional. On such surfaces conserved quantities can be followed in time and space.

One commonly used conserved quantity is the potential temperature. This is the temperature that a dry air parcel attains if it is adiabatically displaced to a reference pressure. 'Adiabatically' means that there is no exchange of heat between the air parcel and its environment. The potential temperature implicitly takes into account the effects of compressibility of the air. It is used to remove cooling (warming) effects associated with the adiabatic expansion (compression), allowing the comparison of the temperature of air parcels at different levels in the atmosphere. A surface of constant potential temperature is called an isentropic surface. Transport of air parcels across such a surface only occurs in the presence of diabatic heating.

There are three main sources of diabatic heating in the atmosphere: latent heating, radiative heating and sensible heating. Latent heat is the energy released when water vapour condensates, radiative heating is the net result of absorption and emission of solar and infrared radiation by the atmosphere. Sensible heating is the heat which is transferred from the earth's surface to the atmosphere.

A second used conserved quantity is the equivalent potential temperature. This is the potential temperature an air parcel would have if all moisture is condensed and the resulting latent heat is used to warm the air parcel. It is conserved in dry and wet processes when radiative heating and sensible heating are absent. The equivalent potential temperature lacks therefore a diabatic source that does exist for the potential temperature.

The potential vorticity is another conserved quantity. The potential vorticity is the vorticity of an air parcel when it is brought to a standard latitude and static stability. It is useful to understand Rossby wave propagation, the structure, origin and persistence of cut-off cyclones and blocking anti-cyclones, and it can be used for the initialisation of numerical weather-prediction models [*Hoskins et al.*, 1985; *Hoskins*, 1991]. The potential vorticity is often used to define the tropopause, often

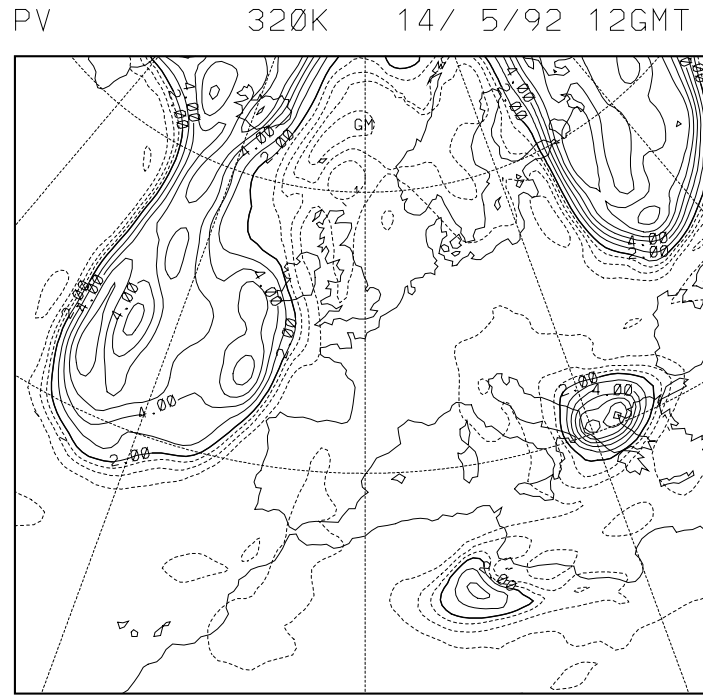


Figure 1.1: Isentropic contours of potential vorticity on the 320 K surface for 14 May 1992 at 12 UTC, calculated from the European Centre for Medium-Range Weather Forecasts operational analysis. The tropopause appears as the first solid contour (2 pvu). Higher potential vorticity values indicate stratospheric air, lower values tropospheric air [from Appenzeller *et al.*, 1995].

by a potential vorticity value of 2 pvu (pvu is the potential vorticity unit, 1 pvu is equal to $10^{-6} \text{ m}^2 \text{ K kg}^{-1} \text{ s}^{-1}$). The magnitude of the tropospheric potential vorticity is about a factor of ten smaller than the magnitude of the stratospheric potential vorticity. Due to this large difference, potential vorticity generation and destruction can be used as a tracer for the transport of air from the troposphere to the stratosphere and vice versa.

Because the potential temperature and the potential vorticity are conserved quantities, the flow of potential vorticity on an isentropic surface is two-dimensional for adiabatic and frictionless flow. This means that potential vorticity structures on an isentropic surface can be followed in time and space [Hoskins *et al.*, 1985]. An example of the potential vorticity on an isentropic surface is shown in Figure 1.1.

As for the potential temperature, a potential vorticity quantity can be defined

that is constant when latent heat is released. In this thesis this quantity is called the moist potential vorticity. The moist potential vorticity is conserved in adiabatic, barotropic and frictionless flow. The flow of the moist potential vorticity on an equivalent potential temperature surface is therefore two-dimensional for such a flow, and moist potential vorticity can be followed in time and space on these surfaces.

1.2 Overworld, middleworld and underworld

For this thesis, two parts of the atmosphere are particularly important: the troposphere and the stratosphere. The troposphere is characterised by low potential vorticity and low static stability, the stratosphere by high potential vorticity and high static stability. The tropopause acts as a dynamical and chemical barrier between the troposphere and the stratosphere [Ambaum, 1997]. The high stability of the stratosphere represses vertical mixing. Here mixing takes place on timescales of the order of months. The mixing in the troposphere is more rapid, with a timescale for mixing in the order of hours to days. There are no differences between the stratosphere and troposphere for quasi-horizontal mixing along isentropic surfaces.

To clarify the roles of the different mechanisms involved in STE, another classification is useful. Hereto, the stratosphere and the troposphere are subdivided into the overworld, the middleworld and the underworld (Figure 1.2). The overworld is the part of the stratosphere where isentropic surfaces lie entirely in the stratosphere, and the underworld is the part of the troposphere where isentropic surfaces lie entirely in the troposphere. In the middle world the isentropic surfaces lie partly in the troposphere and partly in the stratosphere. The stratospheric part of the middle world is called the lowermost stratosphere. The lower boundary of the overworld more or less coincides with the 380 K isentropic surface. Air in the overworld cannot reach the troposphere without first slowly descending across isentropic surfaces, a process that must be accompanied by diabatic cooling, which takes place on a timescale of the order of months. Conversely, air in the underworld cannot reach the stratosphere without first rising across isentropic surfaces, a process that takes place on a timescale ranging from hours to days. In the middle world, air can be transported from the lowermost stratosphere to the troposphere and vice versa by transport along isentropic surfaces. The overworld can be viewed as the classical stratosphere: low water vapour mixing ratios and high ozone mixing ratios. The lowermost stratosphere is made up of a mix of stratospheric air that descended adiabatically from the overworld and air from the troposphere that crossed the extratropical tropopause.

From the above it is clear that it is advantageous to distinguish between transport from the overworld into the lowermost stratosphere and from transport from the

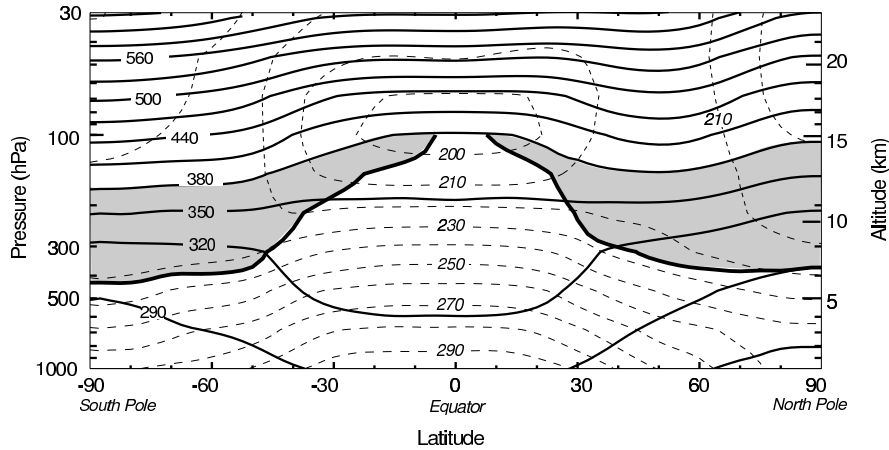


Figure 1.2: Latitude-altitude cross-section for January 1993 showing longitudinally averaged potential temperature (solid contours) and temperature (dashed contours). The heavy solid contour (cut off at the 380 K isentrope) denotes the 2 pvu potential vorticity contour, which approximates the tropopause outside the tropics. Shaded areas denote the 'lowermost stratosphere', whose isentropic surfaces cross the tropopause. The region above the 380 K surface is the 'overworld', in which isentropes lie entirely in the stratosphere. The region below 300 hPa is the 'underworld', in which isentropes lie entirely in the troposphere [from Holton et al., 1995].

lowermost stratosphere into the troposphere. The first type of transport depends on the global-scale dynamical aspects and defines the total amount of air and tracers that will be exchanged. The second type of transport requires consideration of the details of processes at the tropopause and defines the temporal and spatial distribution of the exchange.

1.3 Overview of the dynamical aspects of STE

1.3.1 Global-scale dynamical aspects: the Brewer-Dobson circulation

The Brewer-Dobson circulation consists of upward motion into the tropical stratosphere, poleward motion in the stratosphere towards the winter pole, and downward motion in the extratropical stratosphere (Figure 1.3). As described by Holton et al. [1995], the force behind this circulation is a wave-induced 'pumping' which takes place in the stratosphere. Westward moving Rossby and gravity waves propagate into the stratosphere and mesosphere. If these waves break they induce a persistent westward force, which can be seen as the force that makes the air parcels move slower towards

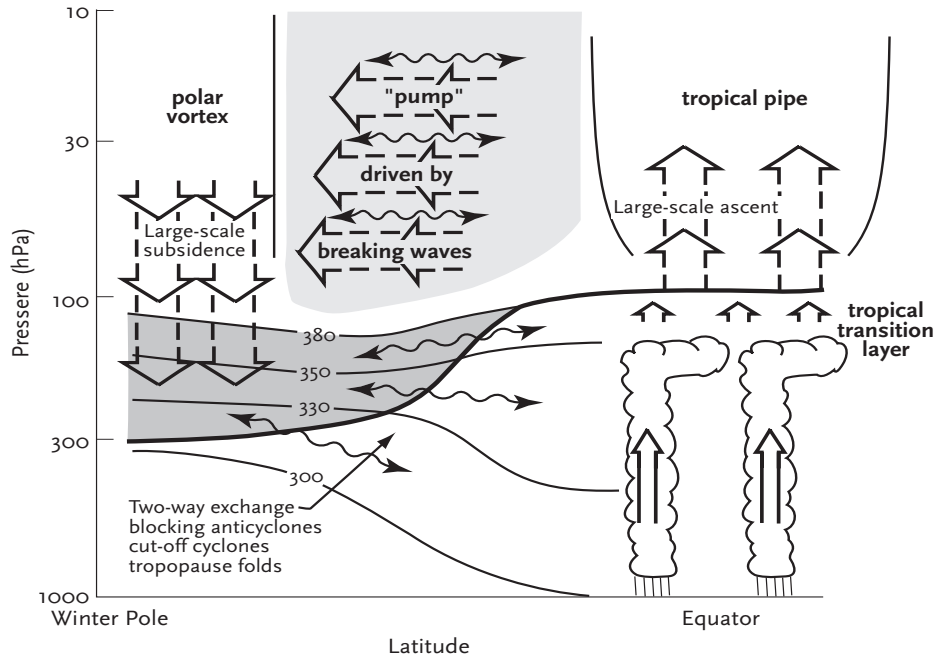


Figure 1.3: *Dynamical aspects of stratosphere-troposphere exchange. The tropopause is shown by the thick line. Thin lines are isentropic surfaces. The heavily shaded region is the lowermost stratosphere. Light shading in the overworld denotes wave-induced forcing (the extratropical ‘pump’). Isentropic transport processes are indicated by the wavy double-headed arrows. The broad arrows show transport by the global-scale circulation, which is driven by the extratropical pump.*

the east. In the extratropics this force destroys the balance between the poleward pressure gradient force and the equatorward Coriolis force, because the Coriolis force decreases accordingly to the slower moving air parcels. The air parcels will therefore be forced poleward in the direction of the dominating pressure gradient force, and a new balance between the westward induced force and the (now eastward) Coriolis force will be established. Because of mass conservation this poleward movement acts as a suction pump on the air in the tropics, causing upward motion from approximately 15°N to 15°S . In the extratropics and polar regions there will be downward movement of air because of mass conservation.

The strength of this circulation depends on the strength of the jet streams, which

in turn depends on the temperature gradient between the equator and the poles. With a stronger jet stream Rossby waves can break more easily, through which the poleward force that drives the Brewer-Dobson circulation will be stronger. The average pole-to-equator temperature gradient in the troposphere is larger in winter than in summer, and is larger in the Northern Hemisphere winter than in the Southern Hemisphere winter. The Brewer-Dobson circulation is therefore more intense on the winter hemisphere, and is strongest in the Northern Hemisphere winter. The smaller temperature gradient between the equator and the poles on the Southern Hemisphere is mainly due to the large thermal inertia of the oceans together with the greater fraction of the surface that is covered by oceans.

Despite this global-scale dynamical pump, there is still a sharp distinction in the overworld between the tropics and the extratropics. This is evident from the observation that in the overworld many chemical species have different tropical and extratropical mixing ratios [*Randel et al.*, 1993]. This suggests that isentropic mixing in the extratropical overworld is isolated from the tropical overworld [*Plumb*, 1996]. This exchange barrier is indicated as ‘tropical pipe’ (Figure 1.3).

This global scale circulation is the process that determines the total amount of air that is exchanged between the stratosphere and the troposphere. On the other hand, the local exchange across the tropopause is determined by the temporal and spatial distribution of processes near the tropopause like tropopause folds. This does not imply that at every instant the downward flux into the lowermost stratosphere needs to equal the flux across the extratropical tropopause. It is only on long enough timescales that fluxes across the 380 K surface and the tropopause must be the same, assuming that there is no source or sink in the lowermost stratosphere.

1.3.2 Processes near the tropopause

There are several processes by which air is exchanged through the tropopause. These processes are responsible for the temporal and spatial distribution of the exchange. The most important processes responsible for STE are:

- transport from the troposphere to the stratosphere in the tropics
- seasonal mass variation of the lowermost stratosphere
- isentropic mass exchange
- tropopause folding
- cut-off lows
- other synoptic- and smaller-scale processes

Transport from the troposphere to the stratosphere in the tropics

The pumping action of the Brewer-Dobson circulation causes large-scale upward transport of mass from the tropical troposphere into the tropical stratosphere, at a rate that is largely independent of local conditions near the tropical tropopause. This pumping encourages the formation of deep cumulonimbus clouds and produces higher and colder tropopauses. The cumulonimbus clouds inject air from the lower troposphere into the upper troposphere (the 'tropical transition layer' in Figure 1.3), and from there the air slowly ascends into the tropical stratosphere [Folkins *et al.*, 1999]. Because the tropopause in the tropics is very cold, the saturation vapour pressure is very low, so that the air that passes the tropopause is extremely dry. Therefore the stratosphere contains almost no water vapour.

Seasonal mass variation of the lowermost stratosphere

The mass of the lowermost stratosphere has a distinct annual cycle, particularly for the Northern Hemisphere. Appenzeller *et al.* [1996] found that the net mass variation of the lowermost stratosphere substantially contributes to the net mass flux across the tropopause. This mass flux has a minimum in early autumn and a maximum in late spring. However, the maximum downward mass flux across the upper boundary of the lowermost stratosphere, which is due to the Brewer-Dobson circulation, occurs during the winter season, the minimum flux in early summer. It was found that it is the combined effect of the seasonal variation of the global-scale circulation and the seasonal variation of the mass of the lowermost stratosphere that determines the net mass transport across the tropopause into the troposphere. Measurements of radioactive tracers in the troposphere confirm this result (Figure 1.4).

Isentropic mass exchange

The transport of air along isentropic surfaces can lead to a displacement of stratospheric air towards the Equator. An example of this isentropic transport is shown in Figure 1.1. This transport is an adiabatic process and does not lead directly to STE. For STE secondary processes are needed, such as diabatic processes or turbulent mixing. Isentropic transport across the tropopause often occurs near the subtropical and polar tropopause breaks (Figure 1.5). These tropopause breaks are accompanied by the subtropical and polar jet streams. A cause for STE at the subtropical tropopause break is small-scale filamentation, which is caused by Rossby wave breaking. Because of the large wind shear near the jet, these stratospheric filaments are rapidly mixed into the troposphere. This transport of air across the subtropical tropopause break has been clearly established in a case study using ECMWF data [Baray *et al.*, 1998].

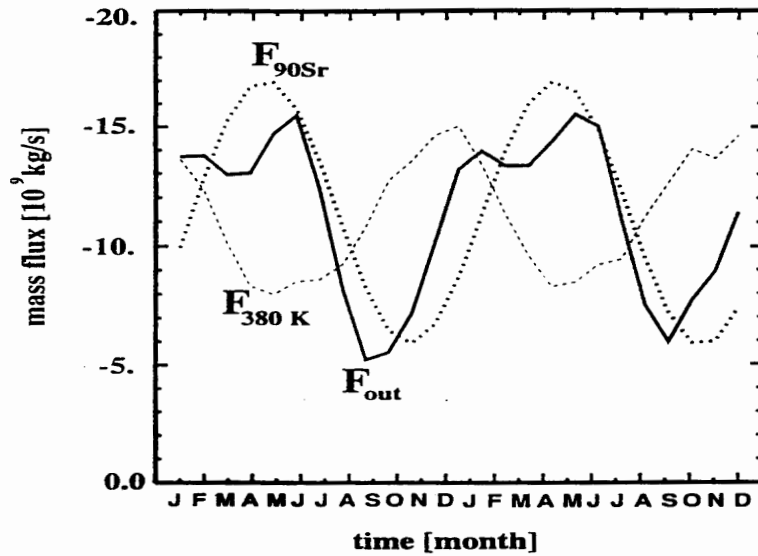


Figure 1.4: Annual variation of the net downward mass transport across the extratropical tropopause (F_{out} , solid line) and the 380 K isentropic surface (F_{380} , dashed line), and mass flux according to measurements of a radioactive tracer (F_{90Sr} , dotted line) for the Northern Hemisphere. Shown are the two years 1992 and 1993. Negative values denote a downward mass flux [from Appenzeller et al., 1996].

Tropopause folding

Tropopause folding occurs in the presence of low pressure systems. In the vicinity of a low pressure area the air is drawn down- and southward, which is an adiabatic process and therefore takes place along surfaces of equal potential temperature. The stratospheric air in the tropopause fold therefore originates from the lowermost stratosphere. The actual STE occurs only when diabatic processes or turbulent mixing occur, which mix the stratospheric air gradually into the troposphere.

The air in a tropopause fold is transported into two different directions [Vaughan, 1988]. The air in the lowest part of the fold is transported towards the equator and usually stays in the troposphere. The air in the upper part of the fold, on the other hand, is transported back to the lowermost stratosphere. This gives rise to two difficulties for the calculation of STE. First, it is not clear how much of the air transported into the tropopause fold will stay in the troposphere, and second, the air that returns to the lowermost stratosphere will be mixed with an unknown amount of tropospheric air.

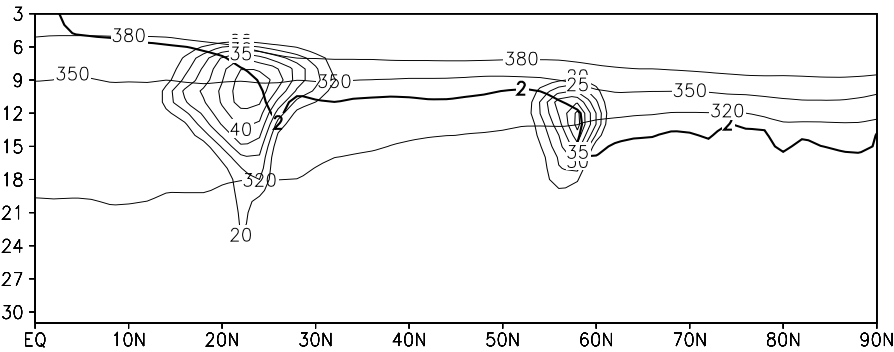


Figure 1.5: Latitude-height cross-section of the 380 K, 350 K and 320 K isentropes, the 2 pvu contour, and the maximum values of u (in units of m/s), defining the location of the jet streams. The 350 K and 320 K isentropes cross the tropopause at the subtropical and polar tropopause break, respectively.

Cut-off lows

A cut-off low is created when there is a large equatorward extrusion of stratospheric air on a isentropic surface, which is cut off from the stratospheric reservoir. It is characterised by a low tropopause and a reduction of the tropospheric static stability. An example of the start of such a process is shown in Figure 1.1 at the left, an actually ‘cut-off’ low can be seen on the right. The formation of a cut-off low is an adiabatic process. STE in cut-off lows occurs by deep convective mixing, radiative erosion of the anomalously low tropopause, or by turbulent mixing near the jet stream associated with the cut-off system. *Price and Vaughan* [1993] suggested that only a relatively small percentage of STE is associated with cut-off lows.

Other synoptic- and smaller-scale processes

Also other synoptic- and small-scale processes occur that cause STE. Clear air turbulence, e.g., is encountered in the wind shear regions of jet streams and cause mixing of stratospheric with tropospheric air. In warm conveyor belts moist lower tropospheric air is transported to the upper troposphere and possibly across the tropopause [*Saraber and Heijboer*, 1994]. Convective motions due to latent heat release enforce the upward motion in such warm conveyor belts. Also regional variations in radiative heating and cooling can cause STE [*Zierl and Wirth*, 1997]. Finally, non-linear or breaking gravity waves near the tropopause can cause mixing of tropospheric and stratospheric air [*Moustaoui et al.*, 1999].

1.4 Models and methods used to estimate and diagnose STE

For the estimation and diagnosis of STE a range of models and methods exists. One method used to study STE is tropospheric measurements of stratospheric constituents. Several quantitative estimates of STE have been obtained from observations of ozone, nitrogen oxides, radioactive tracers, and various other stratospheric constituents that are conserved on a relatively long timescale.

Also three-dimensional model fields of wind and temperature can be used to estimate STE. Several methods use analyses from numerical weather prediction models. *Appenzeller et al.* [1996] e.g., estimated the global-scale stratospheric meridional circulation and the seasonal mass variation of the stratosphere. Several other studies calculated instantaneous spatial distributions of air-mass exchange using the method described by *Wei* [1987]. A disadvantage of this method is that it can be less reliable, because it suffers from an almost cancellation of large terms [*Wirth and Egger*, 1999].

Numerical weather prediction model data are also often used as input for other models. For example, various methods exist to investigate STE with the help of trajectories. These trajectory methods are often applied to specific events, but can also be applied for the estimation of global cross-tropopause mass fluxes.

Another technique that requires input from numerical weather prediction models is contour advection. With this technique isentropic transport of potential vorticity contours can be simulated. The contour advection technique was used by e.g. *Dethof et al.* [2000] to quantify the global quasi-horizontal, isentropic mass transport across the tropopause.

Also three-dimensional transport models are used to simulate STE. These models use model output of numerical weather prediction models to calculate the transport of air and chemical species. *Chen* [1995], e.g., calculated isentropic cross-tropopause mass exchange using a semi-Lagrangian transport model.

General circulation models are also used to calculate STE. An advantage of general circulation models is that they can be coupled to chemistry models with which they have the ability to simulate stratospheric and tropospheric chemistry. With a relaxation technique these models can be used to simulate actual meteorological situations. For this technique the general circulation models is relaxed towards analysed fields of a numerical weather prediction model [*Jeuken et al.*, 1996]. The advantage of this technique is that general circulation models are able to reproduce strong and fast actual meteorological developments. *Kentarchos et al.* [1999] coupled a global chemistry model with a general circulation model to estimate STE events and the associated amount of stratospheric ozone transferred into the troposphere.

Combinations of the above described approaches are also often used. *Ancellet et al.* [1991] combined lidar measurements with trajectories to calculate air-mass exchange for several specific cases. *Gouget et al.* [2000] investigated mechanisms for STE and the associated mass flux in a cut-off low with the help of trajectories and MOZAIC (Measurement of OZone and water vapour by Airbus In-service airCraft) data.

1.5 Overview of this thesis

This thesis has been focussed on four subjects:

1. The difference between the moist potential vorticity and the commonly used potential vorticity.
2. A new Lagrangian method to diagnose STE.
3. Application of this method to a subtropical Southern Hemisphere tropopause fold.
4. Intercomparison of nine different models and methods that are used for the simulation and diagnosis of STE.

In **Chapter 2** the conservation of the potential vorticity is compared with the conservation of the moist potential vorticity. This is done by investigating the differences between the spatial distributions of the potential vorticity and the moist potential vorticity, and by investigating the differences in conservation by means of trajectories. This chapter is a draft manuscript that will be submitted to *Journal of Atmospheric Sciences*.

A new method to diagnose air-mass exchange is described in **Chapter 3**. It is applied to a Northern Hemisphere extratropical cyclone. In this study special emphasis is put on the statistical significance of the results and on the reliability of the method. The author of this thesis was involved in the development of the method, including the statistical approach, the evaluation of the method, and the validation of the results. Chapter 3 appeared as *Sigmond et al.* [2000].

In **Chapter 4** this method has been applied to a case study in the Southern Hemisphere subtropics. Previous studies of STE were mostly restricted to the Northern Hemisphere. The knowledge of Southern Hemisphere exchange processes is much smaller. With previous methods the tropopause in tropopause folds is generally truncated to a single level, mostly because of technical reasons. The consequence of this truncation is that any amount of stratospheric air that enters the fold is assumed to be irreversibly transferred to the troposphere. In this chapter, the spatial and temporal

distribution of the exchange through all tropopause levels are calculated. Chapter 4 appeared as *Meloen et al.* [2001].

Although a large range of models and methods is used for the simulation of STE, there are still large uncertainties in the qualitative and quantitative characteristics of STE. **Chapter 5** presents therefore an intercomparison of nine models and methods used for simulating and diagnosing STE. The present STE intercomparison study adds to the small amount of existing studies on three aspects. First, the number of applied models and methods is larger, second, the range of the applied models and methods is larger, finally, the model results are evaluated with measurements in a companion study by *Cristofanelli et al.* [2002]. Chapter 5 has been submitted to *Journal of Geophysical Research*.

The following general reference books and review papers were used in preparing this text. A complete reference list is given at the end of this thesis.

Holton, J. R., Introduction to Dynamic Meteorology. Academic Press, 507 pp., 1992.

Holton, J. R., P. H. Haynes, M. E. McIntyre, A. R. Douglass, R. B. Rood, and L. Pfister, Stratosphere-troposphere exchange. *Rev. Geophys.*, **33**, 403-439, 1995.

Peixoto, J. P. and A. H. Oort, Physics of climate, American Institute of Physics, 520 pp., 1992.

2

On the conservation of moist potential vorticity versus potential vorticity

The potential vorticity (Q_d) is a materially conserved quantity in the absence of diabatic effects and friction. In the boundary layer of the earth's atmosphere friction plays a role, but in the free atmosphere it is so small that it is often neglected. The three diabatic effects that are able to change Q_d are radiative heating, latent heating and sensible heating. These effects are also often neglected. To account for latent heat release, one can define the moist potential vorticity (Q_m). Q_m has no source term for latent heat release, but it has an additional source term due to baroclinicity. Differences between Q_m and Q_d are mainly determined by the vertical gradient of the specific humidity. In the higher atmosphere, Q_m differs little from Q_d because the humidity and its vertical gradient are very small on those heights. Lower in the atmosphere, approximately below 6 km, the differences in Q_d and Q_m are larger. Differences in material conservation between Q_d and Q_m have been investigated with the help of trajectories. It was found that for altitudes higher than 600 hPa, Q_m is indeed better conserved than Q_d . For altitudes lower than 600 hPa Q_m is less conserved than Q_d , for which four possible reasons are discussed.

2.1 Introduction

Potential vorticity (Q_d) is an important and often used quantity. It is used as an approach to e.g. understand Rossby wave propagation, the structure, origin and persistence of cut-off cyclones and blocking anti-cyclones, and can be used for the initialisation of numerical weather-prediction models [Hoskins *et al.*, 1985; Hoskins, 1991]. It is based on vorticity and on potential temperature. The latter is a conserved quantity in dry adiabatic flow. Q_d has two major properties which make it so useful for meteorological dynamics. The first is the material conservation of Q_d in adiabatic and frictionless flow [e.g. Pedlosky, 1987]. Together with the material conservation of potential temperature this implies that on a potential temperature surface, structures in Q_d can be followed in time and space [Hoskins *et al.*, 1985]. Another advantage of Q_d is the existence of the invertibility principle [Hoskins *et al.*, 1985], which states that under certain conditions the distribution of Q_d determines all the other dynamical meteorological fields in the atmosphere.

On longer timescales the conservation of Q_d is actually not valid anymore, and requires that diabatic effects should be taken into account. The three diabatic effects that can change Q_d are radiative heating, latent heating and sensible heating. In the presence of e.g. cut-off lows, latent heat release may become quite significant [Wirth, 1995].

A way to take account of the release of latent heat, i.e. the presence of condensation, is to define the moist potential vorticity (Q_m). Q_m is based on the equivalent potential temperature (θ_e), in contrast to Q_d which is based on θ . Because the θ_e is a conserved quantity in a flow in which latent heat is released, Q_m implicitly includes the effects of this diabatic process. Latent heat release is therefore an adiabatic process for Q_m , in contrast to Q_d [Bénard *et al.*, 1992].

Hoskins *et al.* [1985] made an estimate of the source terms in the Q_d equation. They distinguished between cut-off lows and blocking anticyclones. In the case of a cut-off low Hoskins *et al.* stated that the most pronounced effect of latent heat release is in the region of the tropopause (between 1.5 and 2 pvu, 1 pvu is equal to $10^{-6} \text{ m}^2 \text{ K kg}^{-1} \text{ s}^{-1}$). At 300 K, typical tendencies of -1 pvu per day through radiative heating and latent heat release are estimated. Over continental areas during wintertime the moisture and heat supply are usually insufficient for much convection, and latent heat release is less important. In the case of a blocking anticyclone the convection is generally suppressed. No latent heat is released, and the most important diabatic effect that changes the Q_d is radiative cooling. In this case a tendency of $+1$ pvu per 5 days is typical. The diabatic modification of Q_d is therefore much faster for cut-off lows than for blocking anticyclones.

Wirth [1995] used a model to investigate the role of diabatic heating in the dynamic evolution of an axisymmetric cut-off cyclone. He found that the release of latent heat in the troposphere can lead to the decay of the upper level Q_d anomaly within a few days. The magnitude of the diabatic source in the Q_d equation through the release of latent heat in his model was about -1 pvu per day. The largest changes occurred at an altitude of approximately 9 km, again near the tropopause. In the presence of latent heat release and radiative cooling at cloud tops, the decrease in Q_d was estimated to be more than 4 pvu per day.

Knowing that Q_m might be a better conserved quantity because it takes account of latent heat release, it is useful to investigate whether it is indeed better conserved than Q_d and to know whether Q_m has other advantages, or disadvantages, compared to Q_d . It can be expected that the differences between Q_d and Q_m are largest in the lower troposphere, because here the humidity is largest. Q_m has already been used in investigations of moist circumstances by e.g. *Zhang and Cho* [1992], who investigated squall lines and by *Cao and Cho* [1995], who used the Q_m flux as an indicator of cyclone development and cyclone motion.

To our knowledge, studies of the differences and similarities between Q_d and Q_m have not been published yet. Therefore, in this study the spatial pattern and the conservation of Q_m compared to those of Q_d is investigated. The spatial pattern is investigated in a single case study in which a considerable amount of humidity was present. The conservation of Q_m compared to that of Q_d is studied for the same case with the use of trajectories.

In section 2.2, the derivation of the Q_d and Q_m equations are given. Section 2.3.3 investigates Q_d and Q_m in the atmosphere on the basis of a case study. The conservation of Q_d and Q_m is also investigated in this section by means of trajectories. In section 2.4 the results are discussed and the conclusions that can be drawn from this study are given.

2.2 Potential and moist potential vorticity equations

2.2.1 The potential vorticity

When formulating the potential vorticity Q_d , the temperature used is the potential temperature (θ). θ is a conserved quantity for adiabatic motion. Q_d can be written as [*Holton*, 1992]:

$$Q_d = \frac{\vec{\omega}_a}{\rho} \cdot \vec{\nabla} \theta. \quad (2.1)$$

Here $\vec{\omega}_a$ is the absolute vorticity and ρ the air density. Q_d is often expressed in potential vorticity units (pvu). One pvu is equal to $10^{-6} \text{ m}^2 \text{ K kg}^{-1} \text{ s}^{-1}$.

When discussing the time evolution of Q_d , it is usually assumed that the atmospheric flow is frictionless and adiabatic, so that Q_d is materially conserved. As discussed above, this is not always true, at least not on a timescale beyond a few hours or in an area where diabatic effects are large. There are three diabatic effects that can change Q_d : radiative heating (R), latent heating (L) and sensible heating (S). Friction plays a role only in the boundary layer of the atmosphere and is neglected in this study.

The potential vorticity equation [Pedlosky, 1987] can be written as

$$\frac{DQ_d}{Dt} = \frac{\vec{\omega}_a}{\rho} \cdot \vec{\nabla} \Psi_d, \quad (2.2)$$

with

$$\Psi_d = \frac{D\theta}{Dt} = R + L + S. \quad (2.3)$$

2.2.2 The moist potential vorticity

If condensation of water vapour is taken into account, another potential vorticity quantity can be defined. This potential vorticity is called the moist potential vorticity (Q_m), and is conserved when latent heat is released. Q_m is based on the equivalent potential temperature (θ_e). θ_e is the potential temperature of an air parcel when all moisture is condensed and the resulting latent heat is used to warm the air parcel.

The moist potential vorticity is defined as:

$$Q_m = \frac{\vec{\omega}_a}{\rho} \cdot \vec{\nabla} \theta_e, \quad (2.4)$$

the moist potential vorticity equation [Pedlosky, 1987] can be written as:

$$\frac{DQ_m}{Dt} = \frac{\vec{\omega}_a}{\rho} \cdot \vec{\nabla} \Psi_m + \vec{\nabla} \theta_e \cdot \left(\frac{\vec{\nabla} \rho \times \vec{\nabla} p}{\rho^3} \right), \quad (2.5)$$

with

$$\Psi_m = \frac{D\theta_e}{Dt} = R + S. \quad (2.6)$$

Because Q_m is based on θ_e , which is conserved if latent heat is released, Q_m is also conserved when latent heat is released [Bénard *et al.*, 1992]. This means that the structures of Q_m are conserved and can be followed in time and space on a θ_e surface, similar to the behaviour of Q_d on a θ surface.

Comparing the equation for Q_m with the equation for Q_d , the Q_d equation has an extra diabatic term. On the other hand, the Q_m equation has an extra baroclinic

term. This is because for unsaturated circumstances θ_e is, unlike θ , not only a function of p and ρ , but also of the specific humidity [Pedlosky, 1987]. Equations (2.1), (2.2), (2.4) and (2.5) will now be rewritten in a form that is more suitable for computations.

2.2.3 Simplification of the Q_d and Q_m equation

Equations (2.2) and (2.5) will be expressed in spherical coordinates, and then simplified by assumptions similar to those made to derive the primitive equations. One assumption is hydrostatic balance. A second assumption is neglecting the latitudinal component of the earth's rotation vector [Holton, 1992]. With a scale analysis [Holton, 1992] the equations can be further simplified to:

$$Q \approx -g (\zeta_z + f) \frac{\partial \theta}{\partial p}, \quad (2.7)$$

$$Q_m \approx -g (\zeta_z + f) \frac{\partial \theta_e}{\partial p}, \quad (2.8)$$

$$\frac{DQ_d}{Dt} \approx -g (\zeta_z + f) \frac{\partial \Psi_d}{\partial p} \quad (2.9)$$

and

$$\begin{aligned} \frac{DQ_m}{Dt} \approx & -g (\zeta_z + f) \frac{\partial \Psi_m}{\partial p} + \\ & \frac{-g}{\rho^2 a^2 \cos \phi} \left[\left[\frac{\partial \theta_e}{\partial \lambda} \right]_z \left(\left[\frac{\partial \rho}{\partial \phi} \right]_z - \frac{\partial \rho}{\partial p} \left[\frac{\partial p}{\partial \phi} \right]_z \right) + \left[\frac{\partial \theta_e}{\partial \phi} \right]_z \left(\frac{\partial \rho}{\partial p} \left[\frac{\partial p}{\partial \lambda} \right]_z - \left[\frac{\partial \rho}{\partial \lambda} \right]_z \right) \right], \end{aligned} \quad (2.10)$$

with Ψ_d and Ψ_m as in Equations (2.3) and (2.6), respectively. ζ_z is the z-component of the relative vorticity, f is planetary vorticity and a the radius of the earth. These equations are invariant under a change of the vertical coordinate z , i.e. they do not change when using another vertical coordinate like the model coordinate η as will be used from now on.

2.3 Comparing Q_m with Q_d

2.3.1 Meteorological situation

When selecting a situation in which differences between Q_d and Q_m can be expected, one should look for a situation in which a substantial amount of humidity is present. This occurred over the Atlantic Ocean on 12 May 1997. Figure 2.1 shows a satellite image of this situation. Between the cold and warm front, which are part of a low pressure system, the warm sector is situated which contains a considerable amount of humidity. This is also visible in Figure 2.2, which shows a horizontal section of the

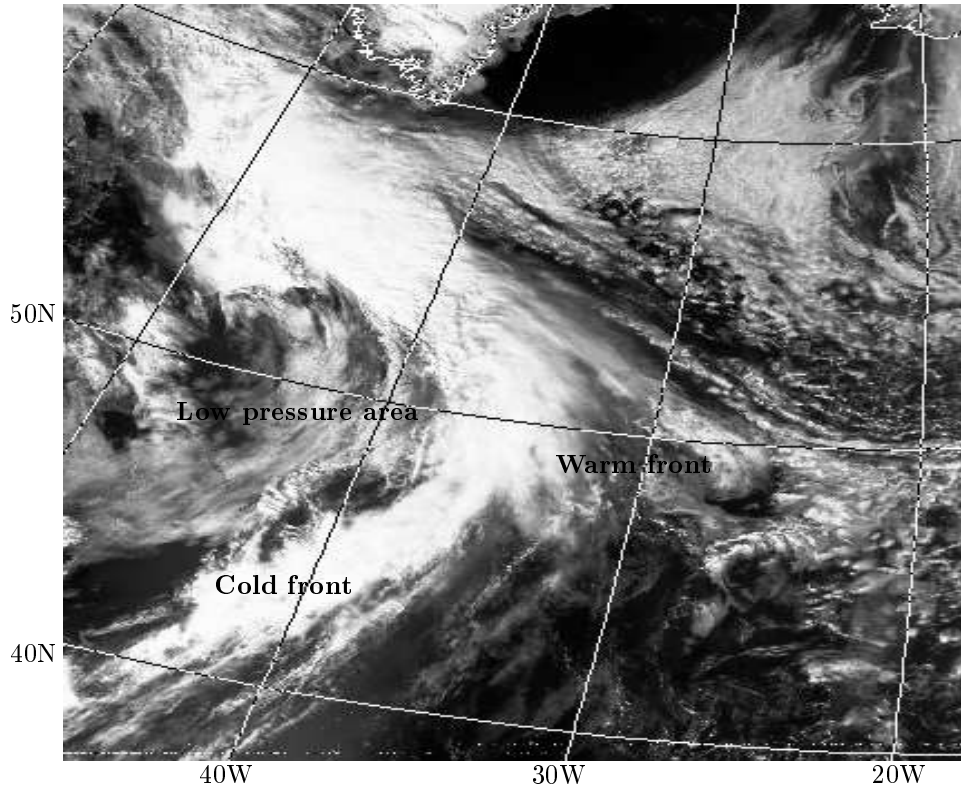


Figure 2.1: Satellite image from the visible channel for 12 May 1997 16 UTC. The low pressure area, together with the accompanying cold and warm front are indicated. Between the two fronts the warm sector is situated, which contains a considerable amount of humidity.

specific humidity (q). The centre of the high humidity area is situated at about 46°N and 40°W . From the vertical section of the specific humidity (Figure 2.3c), it can be seen that the humidity around this centre reaches relatively high levels.

2.3.2 Data description

The meteorological data for this study are taken from the ECMWF. These data are first guess fields with $2^\circ \times 2^\circ$ horizontal resolution, on 31 model levels. For the trajectories forecast data are used with a $1^\circ \times 1^\circ$ horizontal resolution. An advantage of forecast data is that the data remain physically consistent during the entire trajectory computation because the evolution of the meteorological fields is not perturbed by assimilation of observations. The analysis date of the forecast is 9 May 1997 12 UTC, and the applied forecast length is 6 days. For the calculation of θ_e the used formulas are described by Bolton [1980].

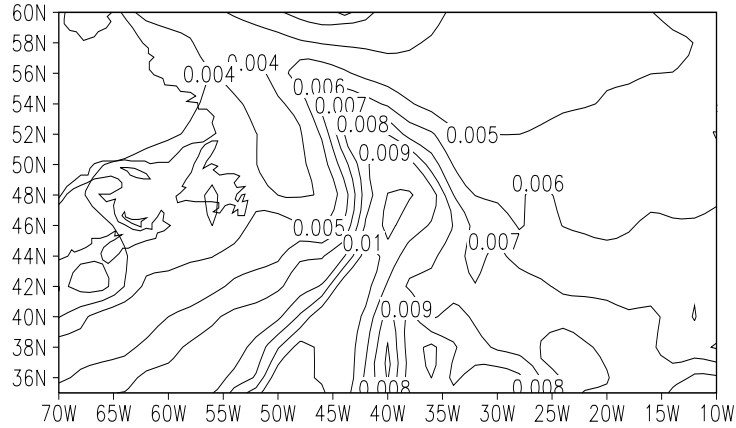


Figure 2.2: Specific humidity in units of kg/kg for 12 May 1997 12 UTC. This horizontal section is made on model level 29.

2.3.3 Results

Q_m versus Q_d : spatial structure

In Figure 2.3 vertical cross-sections of θ , θ_e and q are shown. The pattern of the difference between θ_e and θ (not shown) is similar to the pattern of q . From the definition of θ_e it follows that θ_e only differs from θ where a substantial amount of water vapour is in the air. As can be seen in Figure 2.3c, this only is the case in the lowest 6 or 7 km (about model level 18) of the atmosphere, and the difference decreases higher up. Also it can be seen that θ_e is always equal or larger than θ , as is evident from the definition of θ_e .

Another difference between θ_e and θ is that near fronts, where gradients in both the temperature and humidity are large, a very pronounced front in θ_e can be seen. This can be verified in Figure 2.3b, where at 30°W the cold front and at 25°W the warm front can be seen. θ_e is therefore a useful quantity to analyse fronts. As can be seen in Figure 2.3b, the interpolation of Q_m to a θ_e surface could give serious problems when the same θ_e surface occurs at more than one altitude. This favours the use of Q_d on θ surfaces rather than the use of Q_m on θ_e surfaces.

In Figure 2.4 vertical sections of Q_d , Q_m and $Q_d - Q_m$ at 45°N are shown. Figure 2.4a shows that Q_d has values between 0 and 1 pvu in the troposphere. Except in the frontal zone between 60°W and 45°W close to the earth's surface, the value of Q_d is relatively large, which is probably due to surface friction. Above the tropopause its value rapidly increases. The boundary between low uniform and high rapidly

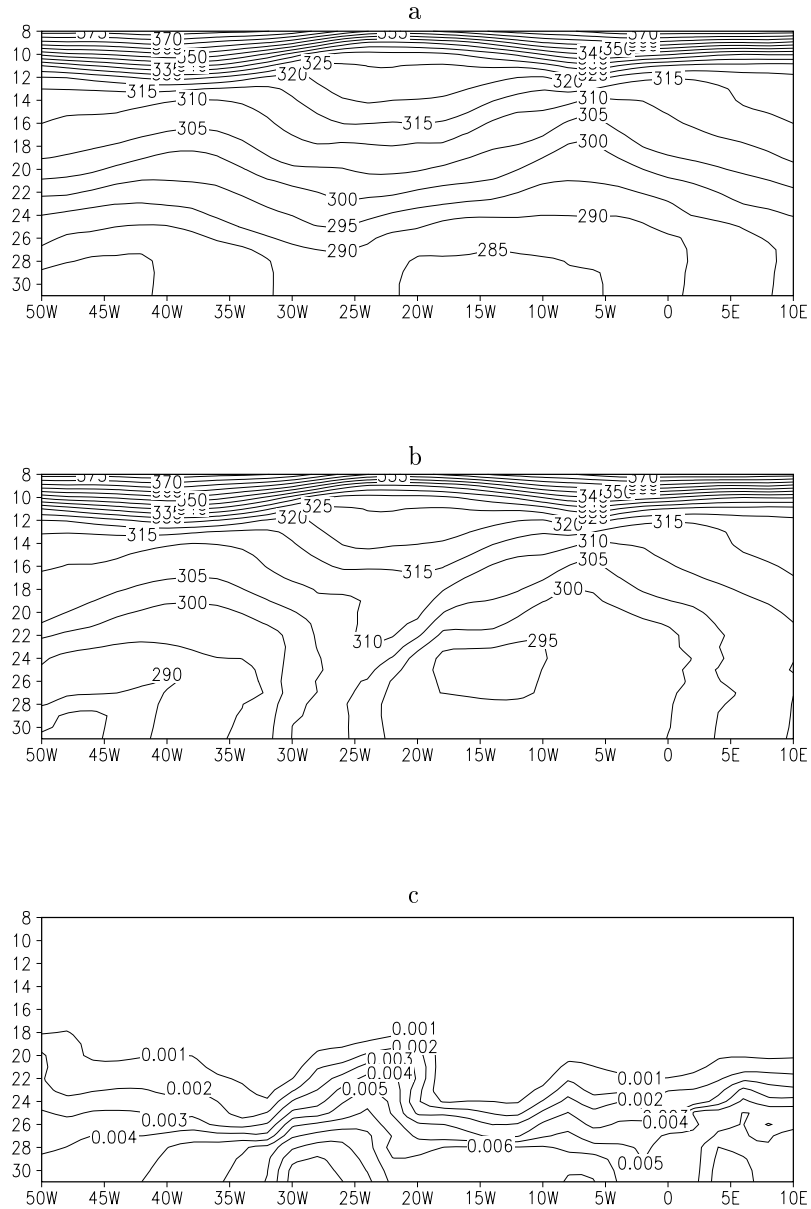


Figure 2.3: θ (a), θ_e (b) both in units of K, and q (c) in units of kg/kg for 13 May 1997 12 UTC. This section is made at latitude 48°N. The horizontal axis displays the longitude, the vertical axis the model level. The tropopause lies near model level 12. A front can be seen between 35°W and 22°W.

increasing Q_d is wavy.

Figure 2.4b shows Q_m , which gives the same overall picture. Only in the troposphere were Q_d and Q_m are relatively small, small differences can be seen. Here Q_m can even become negative, in contrast to Q_d which is rarely negative on the Northern Hemisphere. This can be understood from the sign of the vertical gradient in θ and θ_e , on which the sign of Q_d and Q_m depend, respectively. Comparing Figures 2.3a and 2.3b, it can be seen that θ increases monotonically with height, whereas θ_e does not. The vertical gradient in θ_e can therefore become negative as can be seen in Figure 2.3b between longitude 20°W and 10°W and model level 31 and 24.

This difference between θ and θ_e can also be seen in Figure 2.5 which shows the zonal- and annual-mean cross-sections of the vertical gradient of θ and θ_e . For pressures lower than 800 hPa the vertical gradient of θ_e is indeed generally smaller than the vertical gradient of θ . For pressures above 800 hPa the zonal- and annual-mean vertical gradient of θ_e is negative and large. The implication of this is that Q_m is generally negative below the 800 hPa surface, and can become very large near the earth's surface. It also implies that Q_m is more variable than Q_d in the troposphere.

Figure 2.4c shows that the largest differences between Q_d and Q_m are about 1 pvu and occur in the troposphere, and that the differences become negligibly small near and above the tropopause (about model level 13). Generally, Q_d is larger than Q_m . This is as expected because the vertical gradient in θ is generally larger than the vertical gradient in θ_e . Features that may be useful for detecting interesting weather situations could not be found in Q_m or in the difference between Q_d and Q_m for this specific case.

Figure 2.6 shows scatterplots of the difference between Q_d and Q_m versus several variables on which this difference might depend. It shows that only the vertical gradient in q depends approximately linearly on the difference between Q_d and Q_m . This means e.g. that in the case of a high pressure area with descending air, where the gradient of q increases in the lower troposphere (not shown), the difference in Q_d and Q_m is relatively large. This shows that care must be taken when relating large differences between Q_d and Q_m to large values of q , as is also evident from Figure 2.6a.

Q_m versus Q_d : material conservation

The material conservation of Q_d and Q_m is compared with the help of trajectories. Along a trajectory, which tracks an air parcel in the atmosphere, quantities like Q_d and Q_m are constant in the absence of diabatic or frictional forces. For the reasons explained in Section 2.2, Q_m is expected to be more constant along a trajectory than Q_d . However, the baroclinic term in Equation (2.10) is also capable of changing Q_m ,

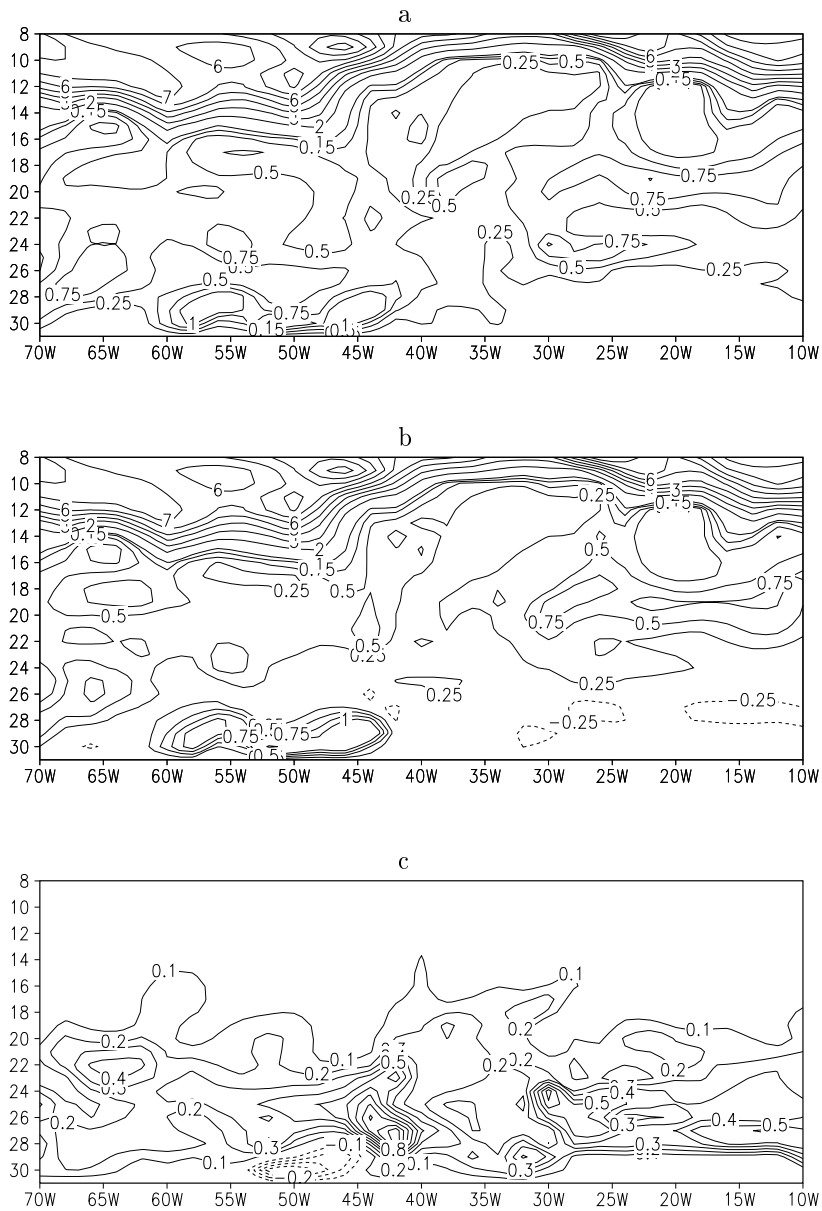


Figure 2.4: Q_d (a), Q_m (b) and $Q_d - Q_m$ (c) all in units of pvu for 12 May 1997 12 UTC. The sections are made at 45°N. The vertical axis displays the model level.

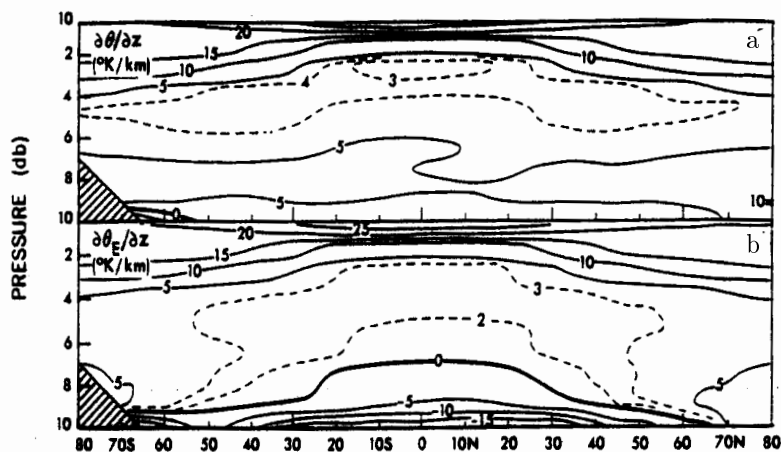


Figure 2.5: Zonal- and annual-mean cross-sections of the vertical gradient of θ (a) and θ_e (b), both in K/km [from Peixoto and Oort, 1992].

a term of which Q_d does not suffer.

The trajectories are started in a column near the centre of the moist structure shown in Figure 2.2, on 12 May 1997 12 UTC on 17 vertical levels from 900 hPa to 200 hPa. At each vertical level 25 points were chosen on a regular horizontal grid, from 30°W to 50°W and from 40°N to 56°N. At each gridpoint a 2.5 day back trajectory and a 2.5 day forward trajectory is started, together forming a trajectory of 5 days. Hence in total 425 5-day trajectories were computed. Along the trajectories θ , θ_e , Q_d , Q_m , $\partial\theta/\partial p$ and $\partial\theta_e/\partial p$ were calculated.

An example of a trajectory is shown in Figure 2.7. This trajectory shows a strong ascent, from 850 hPa to 300 hPa (Figure 2.7a). It is expected that during this ascent a large amount of humidity will condense, releasing a large amount of latent heat which will change Q_d but not Q_m . Q_d and Q_m are shown in Figure 2.7b. One striking feature is that Q_m is negative at pressures higher than 700 hPa, whereas Q_d is positive along the whole trajectory. The reason for Q_m being negative is the negative vertical gradient of θ_e , as shown in Figure 2.7d. When the air parcel has been lifted above 700 hPa, Q_m becomes positive. From here on the difference between the values of Q_d and Q_m remains small. It is also clear from Figure 2.7b that during the ascent from -17 to 10 hours the change in Q_m is indeed smaller than the change in Q_d . When the air parcel reaches it's highest point, 300 hPa, the difference between Q_d and Q_m has become very small, and remains small during the final descent to

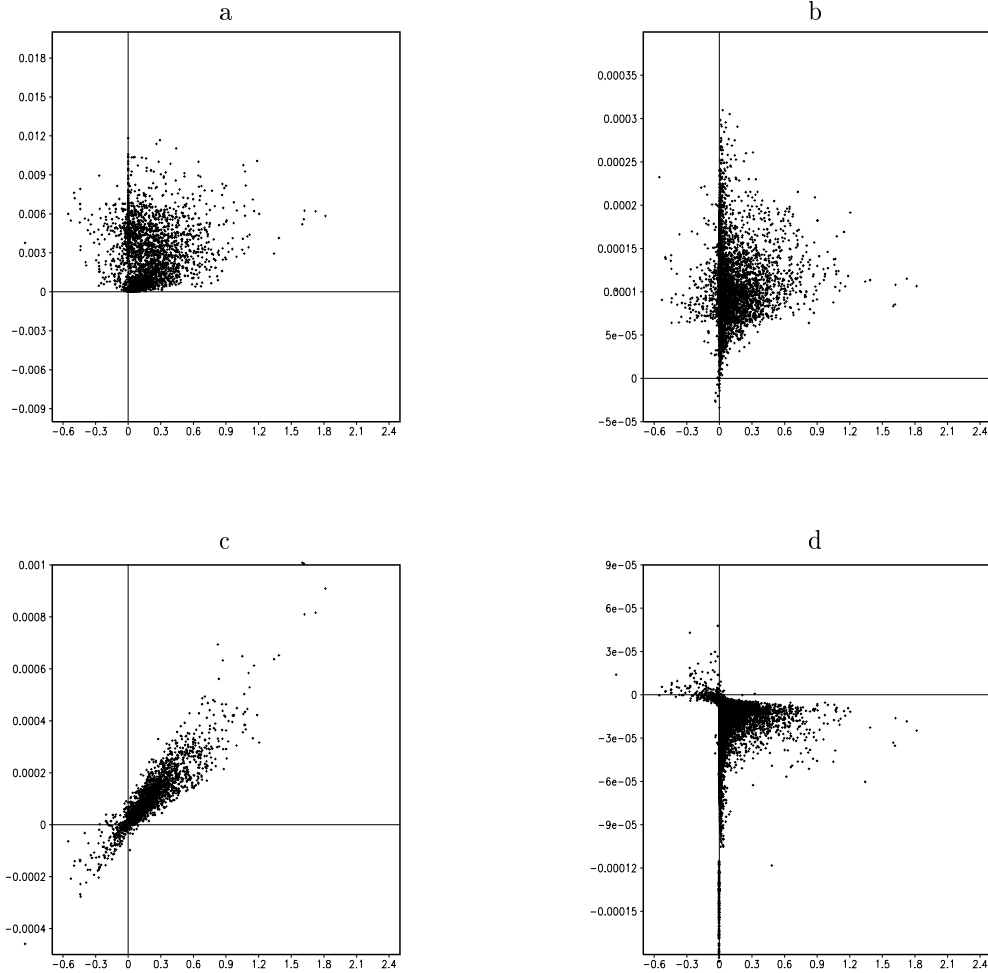


Figure 2.6: Scatterplots of $Q_d - Q_m$, which is displayed on the horizontal axis (in units of pvu), versus q (a, in units of kg/kg), $\zeta_\eta + f$ (b, in units of s^{-1}), $\partial q / \partial p$ (c, in units of $kg\ kg^{-1}\ Pa^{-1}$) and $\partial(1/T_{ice}) / \partial p$ (d, in units of $K^{-1}\ Pa^{-1}$) which are displayed on the vertical axis. The grid points that are plotted in the scatterplots are from the whole $45^\circ N$ parallel of latitude and model level 31 to 1, for 12 May 1997 12 UTC.

about 500 hPa at the end of the trajectory. Figure 2.7c shows that θ_e is less variable than θ along the trajectory, especially during the ascent. This is as expected, and it indicates that the change in Q_d and θ during the ascent of the trajectory is mainly caused by latent heat release. Because latent heat release has no impact on Q_m , it is more constant during the ascent.

The difference between conservation of Q_d and Q_m has also been investigated

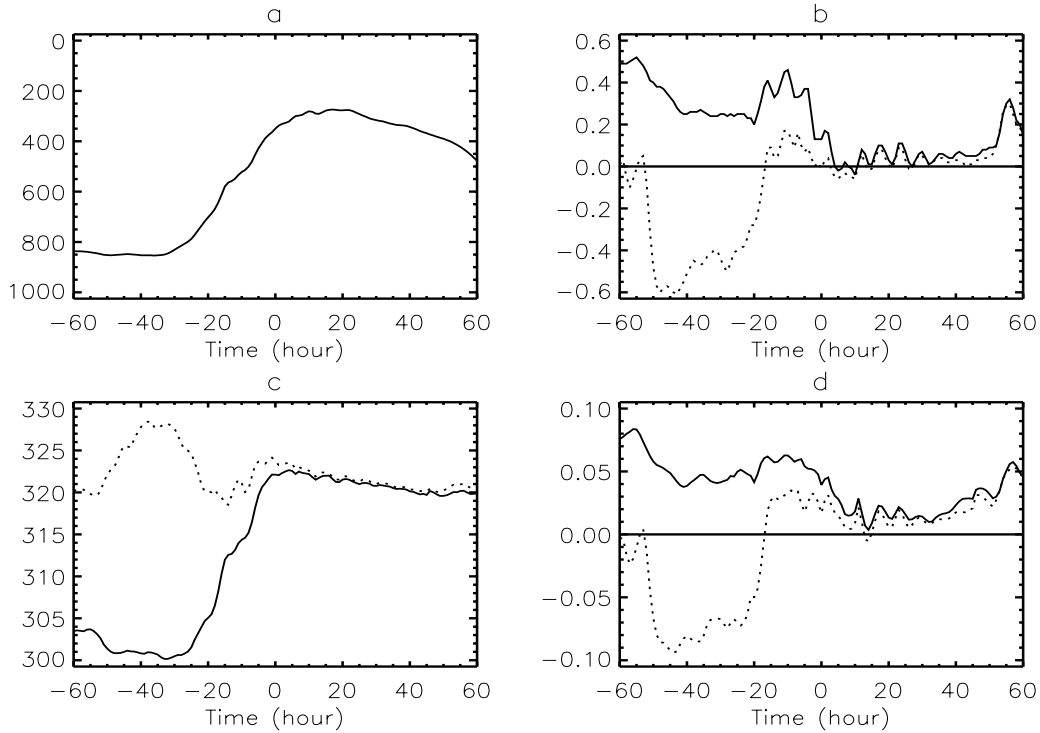


Figure 2.7: Pressure in hPa (a), Q_d (solid line) and Q_m (dotted line) in pvu (b), θ (solid line) and θ_e (dotted line) in K (c), and vertical gradient of θ (solid line) and θ_e (dotted line) in K/m (d) along a trajectory. The 2.5 day forward trajectory and 2.5 day backward trajectory were started at $t=0$, which corresponds with 12 May 1997 12 UTC.

statistically for all 425 trajectories. It turned out Q_m was less conserved than Q_d . This can be understood from Figure 2.7b, where the variation of Q_m is more variable than the variation of Q_d , which is due to the first part of the trajectory where Q_m is negative. However, if the trajectories are analysed separately for the parts in the upper and lower troposphere, significant differences exist. This has been done by selecting the trajectories which had a minimum ascent of 200 hPa, and by separating each of these trajectories in two parts, below and above 600 hPa (Figure 2.8). For these two parts the mean values and the deviations of Q_d and Q_m from these values are calculated. The distribution of these deviations are shown in Figure 2.9, separately for the parts of the trajectory below and above 600 hPa. A broad distribution, which is measured here with the standard deviation, implies that changes along the trajectory are large.

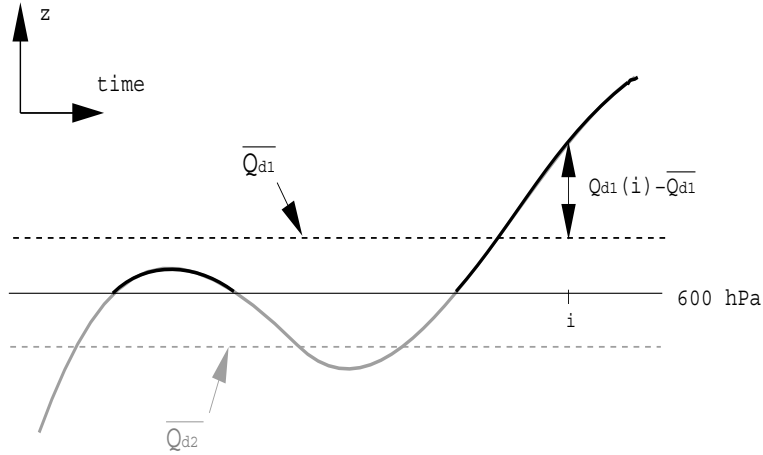


Figure 2.8: Schematic diagram of the altitude of a trajectory versus time. The trajectory is separated in a part above 600 hPa and a part below 600 hPa. In these parts Q_d is denoted by, respectively, Q_{d1} and Q_{d2} . For each part the mean value of Q_d , $\overline{Q_{d1}}$ and $\overline{Q_{d2}}$, are calculated. For every time step along the trajectory the deviation of Q_d from its mean value (i.e., $Q_{d1} - \overline{Q_{d1}}$ or $Q_{d2} - \overline{Q_{d2}}$) is calculated. This procedure is repeated for Q_m .

The standard deviations are shown below the distributions for all four panels. An F-test showed that both below and above 600 hPa there is a more than 95% probability that the distributions of Q_d and Q_m have significantly different standard deviations. The results show that Q_d has a broader distribution than Q_m above 600 hPa, implying that Q_m is indeed a better conserved quantity than Q_d in the upper troposphere. Below 600 hPa, the distribution for Q_m is broader than that of Q_d and Q_m is therefore less conserved than Q_d at these levels. When considering all trajectories in the upper troposphere ($p < 600$ hPa), and not only those with a minimum ascent of 200 hPa, the same conclusions apply although the differences between Q_d and Q_m are smaller then (not shown).

There are four possible reasons which can make Q_m less conserved than Q_d in the lower troposphere. These differences are due to differences between the magnitudes of the right-hand side of Equations (2.9) and (2.10). The first possible reason is that the sum of the vertical gradient of the diabatic sources, $\partial(L + R + S)/\partial p$, in the Q_d equation is not necessarily larger than for the Q_m equation, $\partial(R + S)/\partial p$. This is shown in Figure 2.10. $\partial R/\partial p$ is relatively small in the troposphere, whereas $\partial L/\partial p$ and $\partial S/\partial p$ are considerable. $\partial L/\partial p$ even becomes negative in the first 3 km above the earth's surface, i.e. acts as a sinkterm for Q_d . Therefore, it is very well possible that $\partial(L + R + S)/\partial p$ is smaller than $\partial(R + S)/\partial p$ in the first 3 km above the earth's

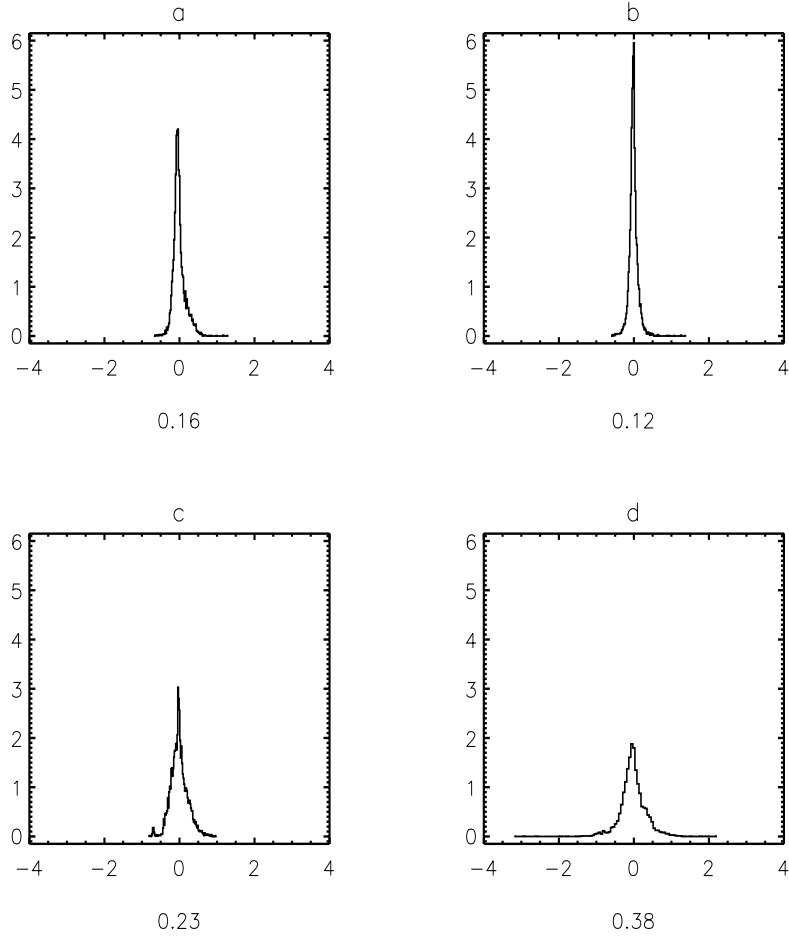


Figure 2.9: Distribution of $Q_{d1} - \overline{Q_{d1}}$ (a), $Q_{m1} - \overline{Q_{m1}}$ (b), $Q_{d2} - \overline{Q_{d2}}$ (c) and $Q_{m2} - \overline{Q_{m2}}$ (d), for trajectories ascending more than 200 hPa. The standard deviations of the distributions are shown below each panel.

surface.

The second reason for Q_m to be less conserved is the extra term due to baroclinicity in the Q_m equation. A mean value of the baroclinicity term has been calculated directly from ECMWF data (not shown). It was found that the mean baroclinicity is negligibly small above 6 km, and below 6 km it is an order of magnitude smaller than the total change in Q_m . But it is possible that in specific circumstances this term has a non-negligible contribution to the change in Q_m .

The third reason because of which Q_m can be less conserved than Q_d is mixing. Mixing is not included in the equations of Q_d and Q_m because the potential vorticity of an infinite small air parcel should not be influenced by mixing. But for a trajectory this is not true. Here the potential vorticity calculated along the trajectory represents the mean potential vorticity of the total air parcel. If the air which is represented by the trajectory mixes with air in the vicinity of the trajectory with a different potential vorticity, the potential vorticity will change accordingly. This mixing, and therefore the change in potential vorticity, will be larger when the gradients in the potential vorticity are large. If mixing is a reason for Q_m being less conserved than Q_d in the vicinity of the earth's surface, then the gradients in Q_m should be larger than the gradients in Q_d . Even though the differences in gradient have not been clearly found in Section 2.3.3, the contribution of mixing can be expected to be considerable in specific cases, especially in the lower troposphere where turbulence is frequent.

The fourth reason because of which Q_m can be less conserved is friction. Although the friction was neglected in this study, its impact on Q_m might be larger than on Q_d .

2.4 Discussion and conclusion

In this study the differences between the potential vorticity (Q_d) and the moist potential vorticity (Q_m) have been investigated. This was done by calculating the spatial distributions of Q_d and Q_m and by calculating Q_d and Q_m along trajectories in a case study involving a large amount of humidity. The conservation of Q_d is only valid in an atmosphere which is not diabatically or mechanically forced. When condensation of water vapour takes place, this conservation is not valid anymore. When defining Q_m , latent heat release is taken into account, so that Q_m is conserved when condensation of water vapour takes place. However, compared to Q_d , Q_m has a baroclinic term which can make Q_m less conservative.

In diagnosing the atmosphere, the use of Q_m instead of Q_d makes no large difference. In the upper troposphere, approximately above 6 km, Q_m and Q_d are almost equal. In the lower troposphere the differences become more significant, up to 1 pvu. A disadvantage of Q_m is that in the lower troposphere θ_e surfaces occur at more than one altitude and do not increase monotonically with height. This is a disadvantage when interpolating Q_m to a θ_e surface on which it is conserved in adiabatic and barotropic flow. An important difference between Q_d and Q_m is furthermore that close to the earth's surface the vertical gradient in θ_e can become negative, so that Q_m will be negative too. This is in contrast to Q_d , which is mainly positive on the Northern Hemisphere.

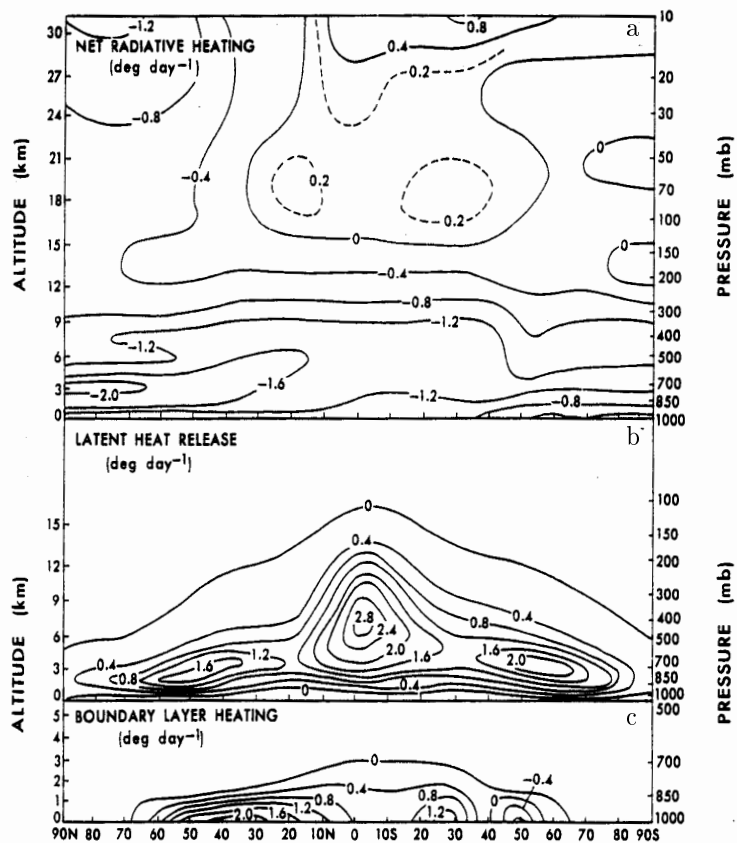


Figure 2.10: The components of the diabatic heating rate for the atmosphere for December-February, i.e. the net radiative heating (a), the latent heat release (b) and the sensible heating in the boundary layer (c) in units of $^{\circ}\text{C day}^{-1}$ (From Peixoto and Oort [1992]).

One of the reasons that Q_m has not proven to be more useful than Q_d , is that moisture is not transported to sufficiently high altitudes to give substantial differences between Q_d and Q_m in the upper atmosphere, where the potential vorticity concept is most frequently applied. However, Wirth [1995] and Hoskins *et al.* [1985] indicate that in cut-off lows moisture is transported up to the tropopause. Therefore, a thunder storm that occurred on 7 June 1997 above the Netherlands was also investigated on a four times finer grid (not shown). However, also in this event the difference between the computed Q_d and Q_m at high altitudes is small.

Schubert *et al.* [2001] extended the potential vorticity conservation principle to a nonhydrostatic, moist, precipitating atmosphere. Hereto they used a generalisation

of the Ertel potential vorticity, using the virtual potential temperature. When using the virtual potential temperature, the baroclinic term in Equation (2.2) vanishes, but the diabatic sources are virtually the same as for Q_d . Also, the virtual potential temperature and the potential temperature are almost equal, because of which this potential vorticity is not supposed to differ much from Q_d . An advantage of this approach is that the invertibility principle exists for their potential vorticity, which does not exist for Q_m .

The difference in conservation between Q_d and Q_m was investigated with the help of trajectories. As has been shown in Section 2.2, the Q_d equation has an extra diabatic source term, latent heating, and the Q_m equation has an extra term due to baroclinicity. Because of the considerable amount of latent heat released in the case studied in this chapter, Q_d is expected to be worse conserved than Q_m . In Section 2.3.3 it was shown that above 600 hPa Q_m is indeed better conserved than Q_d . In the vicinity of the tropopause the humidity is small and so is the difference between Q_d and Q_m . Below 600 hPa, Q_m is less conserved than Q_d . Here Q_m can become negative due to negative values of $\partial\theta_e/\partial z$, which enhance the variability of Q_m . This larger variability of Q_m compared to Q_d in the lower troposphere has to be accompanied by a larger magnitude of the sum of sinks and sources in the Q_m equation, i.e. the right-hand side in Equation (2.10).

There are four possible reasons which can make Q_m less conserved than Q_d in the lower troposphere. The first reason is that the vertical gradient of the diabatic sources for Q_m is not necessarily smaller than for Q_d . The second reason is that the baroclinic term in the Q_m equation could have a non-negligible contribution. A third reason is that mixing along a trajectory has a larger impact on Q_m than on Q_d because the gradients in Q_m are larger than the gradients in Q_d near the earth's surface. A fourth reason why Q_m is less conserved than Q_d could be that the friction, which was neglected in this study, has a larger impact on Q_m than Q_d .

Which of these reasons are the explanation for the worse conservation of Q_m compared to Q_d in the vicinity of the earth's surface, cannot be told from this study. Hereto the vertical gradient should be calculated separately for each diabatic source, and the contribution of the mixing to the change of Q_m and Q_d should be quantified. Also should the impact of friction on Q_m and Q_d be further investigated.

When thinking of using Q_m instead of Q_d , care must be taken with the following issues. First, the interpolation of Q_m on θ_e surfaces can cause problems, because θ_e can be very irregular in the lower troposphere. Second, in the lower troposphere up to about 600 hPa Q_m is less conserved than Q_d . Third, near the tropopause the differences between Q_d and Q_m become vanishingly small, as becomes the difference in conservation. Finally, the invertibility principle does not exist for Q_m as defined

in this study [*Schubert et al.*, 2001]. However, it was found in this study that Q_m is a better conserved quantity for pressure values lower than 600 hPa. This result was also found for a cut-off low which was investigated (not shown), implying that this better conservation of Q_m is a general feature, which does make Q_m an attractive quantity to use.

3

Stratosphere-troposphere exchange in an extratropical cyclone calculated with a Lagrangian method

In this chapter a Lagrangian technique is developed and applied to calculate stratosphere-troposphere exchange (STE) in an extratropical cyclone. This exchange is computed from the potential vorticity or Q along trajectories, calculated from ECMWF circulation data. Special emphasis is put on the statistical significance of the results. The computed field of the cross-tropopause flux is dominated by elongated patterns of statistically significant large downward and small upward fluxes. The downward fluxes mainly occur in the lower part of the considered tropopause folds. The upward fluxes are found near the entrance of the folds, in the tropopause ridges. The ratio between the area-averaged downward and upward cross-tropopause fluxes increases with increasing strength of the cyclone. Since the largest fluxes are shown to occur in the regions with the largest wind shear, where Q -mixing is thought to cause large cross-tropopause fluxes, the results are expected to be reliable, at least in a qualitative sense. The position of a tropopause fold along the northwest coast of Africa is confirmed by total ozone observations. The results indicate that the applied Lagrangian technique is an appropriate tool for diagnosing STE.

3.1 Introduction

Understanding and quantifying human impact on the climate system is one of the most challenging questions in atmospheric sciences. The importance of STE for understanding this impact is widely acknowledged [e.g. *Holton et al.*, 1995]. The transport of specific anthropogenic emissions from the ground to the stratosphere is believed to be the main cause of stratospheric ozone depletion [*WMO*, 1995], whereas the increasing amount of aircraft emissions in the tropopause region could have a substantial impact on climate and the atmospheric composition [*IPCC*, 1999]. The global scale STE is realised by a mean meridional cell, which is called the Brewer-Dobson circulation. The cell consists of upward cross-tropopause transport in the tropics, poleward drift in the stratosphere towards the winter pole, and downward transport into the extratropical winter troposphere [*Brewer*, 1949; *Dobson*, 1956].

At smaller scales, however, STE is not dominated by mean circulations, but by synoptic scale eddy processes, such as tropopause folds associated with cut-off lows, that can lead to rapid exchange of air across the tropopause [*Holton et al.*, 1995]. Therefore, apart from downward cross-tropopause transport, upward cross-tropopause transport occurs in the extratropics, which can bring anthropogenic species directly into the extratropical lower stratosphere [e.g. *Hoerling et al.*, 1993]. Knowledge of the instantaneous bidirectional cross-tropopause fluxes rather than the time-mean net flux is, in the presence of a cross-tropopause gradient of a chemical species, necessary to determine the fluxes of this species across the tropopause [*Gettelman and Sobel*, 1998]. Moreover, since the anthropogenic species are emitted non-uniformly in time and space, the knowledge of the distribution of the instantaneous cross-tropopause flux is essential for modelling the human impact on the climate.

Many efforts have been made to determine the cross-tropopause flux. In these studies, Eulerian diagnostic methods have been dominant. The cross-tropopause flux is generally computed with one of the versions of the diagnostic formula derived by *Wei* [1987] (hereafter called the Wei- x formula, where x is the vertical coordinate, see later).

Hoerling et al. [1993] diagnosed the net global-scale cross-tropopause flux by applying Wei's equation to twice-daily global circulation data with a horizontal resolution of $3.75^\circ \times 3.75^\circ$. *Siegmund et al.* [1996] investigated the STE with a more accurate numerical method and with circulation data at higher temporal and spatial resolution. They calculated the magnitudes of the upward and downward cross-tropopause fluxes separately. They found that for an accurate estimation of the local and instantaneous cross-tropopause flux, the spatial and temporal resolution should be at least $1^\circ \times 1^\circ$ and 6 hours, respectively. To cope with practical problems of time and space

differencing, a complicated numerical scheme is applied. *Siegmund et al.* [1996] as well as *Gettelman and Sobel* [1998] both used the Wei- p formula (where p denotes pressure) and found strong dipole structures in the computed cross-tropopause flux field.

Wirth and Egger [1999] examined five different methods to diagnose the cross-tropopause flux in a cut-off low. They found that both the Wei- p and the Wei- θ formula (where θ denotes potential temperature) are unreliable. In these formulas, the cross-tropopause flux is a small residual of three relatively large terms, so that small errors in the individual terms can result in a large relative error in the computed cross-tropopause flux. A third method examined by *Wirth and Egger* [1999] is the Wei- Q formula, where potential vorticity is taken as the vertical coordinate. The advantage of this method is that if the tropopause is defined as a Q -surface, the formula consists of only one term. The method therefore does not suffer from the problem of strong cancellation, provided that the Q -sources can be calculated with reasonable accuracy.

Apart from these Eulerian diagnostic methods, *Wirth and Egger* [1999] also examined a Lagrangian method, by starting multiple trajectories on the tropopause. The pressure difference between the endpoint of a trajectory and the tropopause at that point is then considered as a measure for the STE in the considered time interval.

Wernli and Davies [1996] describe how their Lagrangian method can be applied for diagnosing the cross-tropopause flux in an extratropical cyclone. Coherent ensembles of trajectories with a period of 10 days, which cross the tropopause (defined as the 2 pvu surface, $1 \text{ pvu} = 10^{-6} \text{ K m}^2 \text{ kg}^{-1} \text{ s}^{-1}$), are identified. Only a small part (5–25%) of these trajectories indicate significant STE (i.e. reside within the stratosphere (troposphere) during (at least) the first four days and within the troposphere (stratosphere) for (at least) the last four days). Although this method is an appropriate tool for studying the spatial structure of STE in an extratropical cyclone, it does not give a numerical estimate of the cross-tropopause flux.

In the present study a Lagrangian technique is used to calculate STE in an extratropical cyclone. Although this technique is to some extent similar to that applied by *Wirth and Egger* [1999], there are several new aspects in it. The main concept of the method of the present study is the evaluation along trajectories of the air-mass flux across several Q -surfaces. Unlike in previous studies, the errors in the calculated data will be discussed.

In section 3.2 the method, input data and the trajectory model will be described. The results will be presented in section 3.3, discussed in section 3.4 and summarised in section 3.5.

3.2 Method and data

3.2.1 Calculation of the air-mass flux across a Q -surface

In the present study Wei's [1987] general formula is used with Q as the vertical coordinate. The air-mass flux across a Q -surface per unit surface area (F) is then defined by:

$$F = -\frac{1}{g} \frac{\partial p}{\partial Q} \frac{dQ}{dt}, \quad (3.1)$$

where g is the acceleration due to gravity. The unit of F is $\text{kg m}^{-2} \text{s}^{-1}$.

For consistency, it is desired that positive values of F near the tropopause would denote transport from the troposphere to the stratosphere in all cases. In order to accomplish this, Equation (3.1) should be altered in the case of tropopause folds. A tropopause is folded where the Q -surface is multivalued with respect to pressure, i.e. at a particular longitude and latitude where three heights are found where Q is constant. Consider the tropopause fold as in Figure 3.1, where the air is transported from the troposphere to the stratosphere in all parts of the fold. Since the surface is turned upside down in the middle part of the fold, $\partial p/\partial Q$ is positive in that part. Calculating F with Equation (3.1) would then give a negative F through this middle surface, whereas a positive value is desired. This problem can be solved by calculating F as:

$$F = \frac{1}{g} \left| \frac{\partial p}{\partial Q} \right| \frac{dQ}{dt}, \quad (3.2)$$

so that the sign of F is determined by the sign of dQ/dt . Positive values of F are then always associated with transport from the troposphere to the stratosphere.

To compute the right-hand side of Equation (3.2), Q and $|\partial p/\partial Q|$ along trajectories are calculated. An example of Q along a trajectory is shown in Figure 3.2. As can be inferred from Figure 3.2, Q is partially fluctuating due to noise. The instantaneous dQ/dt is therefore not reliable. In order to reduce this noise, Q should be averaged over a certain period. F is therefore approximated as:

$$\tilde{F} = \frac{1}{g} \left| \overline{\frac{\partial p}{\partial Q}} \right|^{12h} \overline{\frac{dQ}{dt}}^{12h}, \quad (3.3)$$

where $\overline{\frac{dQ}{dt}}^{12h}$ is the mean dQ/dt in the 12-hour time interval obtained by a linear least square regression of Q along the trajectory versus time, and $\left| \overline{\frac{\partial p}{\partial Q}} \right|^{12h}$ is the mean of $|\partial p/\partial Q|$ along the 12-hour trajectory.

The value of \tilde{F} is calculated for each gridpoint of the three-dimensional domain (described in section 3.3), by calculating Q and $|\partial p/\partial Q|$ along the 6-hour forward and backward trajectory that start at the gridpoint. The value of \tilde{F} is then attributed to

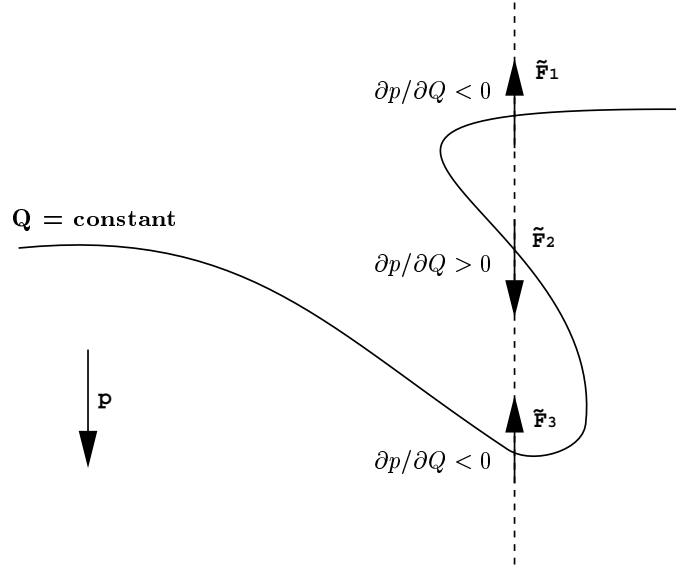


Figure 3.1: Illustration of a tropopause fold. The tropopause is denoted by the solid line. \tilde{F}_1 , \tilde{F}_2 and \tilde{F}_3 are the air-mass fluxes through the tropopause at different altitudes for the same gridpoint.

the gridpoint and the starting time of the trajectories. To compute the flux \tilde{F} in a tropopause fold at a particular latitude and longitude, the fluxes through the three surfaces where Q is constant are summed so that Equation (3.3) becomes:

$$\tilde{F} = \tilde{F}_1 + \tilde{F}_2 + \tilde{F}_3, \quad (3.4)$$

where subscript 1 denotes calculation at the top of the fold, 2 at the middle tropopause and 3 at the bottom of the fold (see Figure 3.1).

According to Equation (3.2), an air-mass flux across a Q -surface implies a material change of Q . The Q of a single air parcel can be changed by diabatic heating gradients and friction [Hoskins *et al.*, 1985]. In addition, the gridbox-mean Q can be changed by mixing [Shapiro, 1980]. The computed fluxes also suffer from noise due to errors in the atmospheric data-set, the computed trajectories and the numerical method to calculate Q .

\tilde{F} is called statistically significant if the probability that \tilde{F} differs from zero is more than 99%. Hereto a Student's t-test is applied to the value of \tilde{F} and its standard deviation, where the standard deviation of \tilde{F} is computed from the standard deviations of $\overline{dQ/dt}^{12h}$ and $|\partial p / \partial Q|^{12h}$.

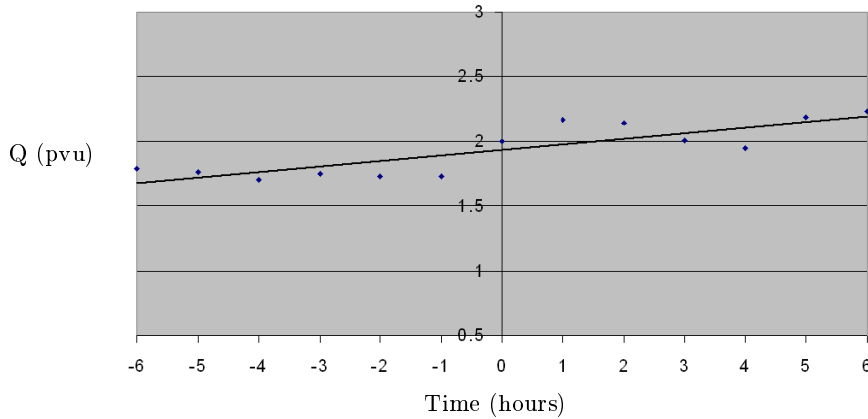


Figure 3.2: Determination of the 12-hour mean dQ/dt with a linear regression of Q versus time. The trajectory model gives output data every hour. $1 \text{ pvu} = 10^{-6} \text{ K m}^2 \text{ kg}^{-1} \text{ s}^{-1}$.

3.2.2 Trajectory model

To calculate the trajectories, the KNMI trajectory model is used as described by *Scheele et al.*, [1996]. This model calculates the three-dimensional displacement of air parcels for each time step δt using the iterative scheme after *Petterssen* [1940]. In the present study $\delta t = 10$ minutes. The input circulation data are obtained from the ECMWF (see section 2.3). Spatial interpolation (linear in the horizontal and linear in the vertical with $\log(p)$) and temporal interpolation (quadratic) are applied to the input data. In the present study three-dimensional rather than isentropic trajectories are calculated in order to include diabatic effects in the calculations of \tilde{F} . Moreover, the three-dimensional trajectories are believed to be more accurate as is concluded, e.g., by *Stohl et al.* [1995]. To calculate Q at place X and at time t , Q is first calculated at the three data input times closest to time t at place X and is then quadratically interpolated to time t .

3.2.3 ECMWF data

For this study ECMWF circulation and temperature data of the first five days of a forecast run are used, which is initialised on 13 April 1998 12 UTC. The data are at a $1^\circ \times 1^\circ$ horizontal grid, at 31 vertical levels. Around the tropopause the vertical resolution is about 25 hPa. The model data are stored every 6 hours. Forecast data are used rather than analysed data in order to have a physically consistent data-set, in which the modelled quantities (in particular Q) are not disturbed by the addition

of new observations. Since the difference between the +96 hour model forecast of the 500 hPa geopotential height field for 17 April 1998 12 UTC and the verifying analysis is very small, the forecast data give a realistic representation of the synoptic-scale processes in the considered period.

3.3 Results

The air-mass flux across a Q -surface (\tilde{F}) is calculated for an extratropical cyclone over the North Sea between 14 and 17 April 1998. \tilde{F} is calculated on two different three-dimensional grids with a horizontal resolution of $1^\circ \times 1^\circ$: one with Q as the vertical coordinate (fluxes are calculated across the 1, 1.5, 2, 3, 4, 6, 8 and 10 pvu surfaces) and one with pressure as the vertical coordinate (from 600 hPa to 100 hPa, with a vertical resolution of 25 hPa). The horizontal domain is the area between 35°W and 25°E and between 20°N and 75°N .

3.3.1 Synoptic situation

The solid lines in Figure 3.3 show the 500 hPa geopotential height field for the period between 14 and 17 April 1998. On 14 April the cyclone has already reached maturity, on 16 April the strength of the cyclone is maximal and on 17 April the cyclone has weakened considerably. The centre of the cyclone as seen on the 500 hPa geopotential height map hardly moves; it lies at the northern part of the North Sea during the entire considered period.

3.3.2 Geographical distribution of the flux across Q -surfaces

The tropopause is generally defined as a surface of constant Q . The values mostly used vary between 1.5 and 3.5 pvu. When the tropopause is defined as the 2 pvu surface, which is an often used value, the flux across that surface can be considered as the cross-tropopause flux.

Figure 3.3 also shows the field of \tilde{F} across the 2 pvu surface for the four different days. The field is dominated by elongated patterns of large downward and small upward fluxes. During the entire period a region with large downward fluxes far south of the cyclone centre (along the northwest coast of Africa) is visible. On 14 and 16 April (Figure 3.3a and Figure 3.3c, respectively), a region with large upward fluxes can be found just south of this region.

Two other regions with large downward fluxes are present on 14 April: one north of the cyclone centre and one southwest of the cyclone centre, west of the 500 hPa trough. On 15 April the latter region has separated into two regions, one west and

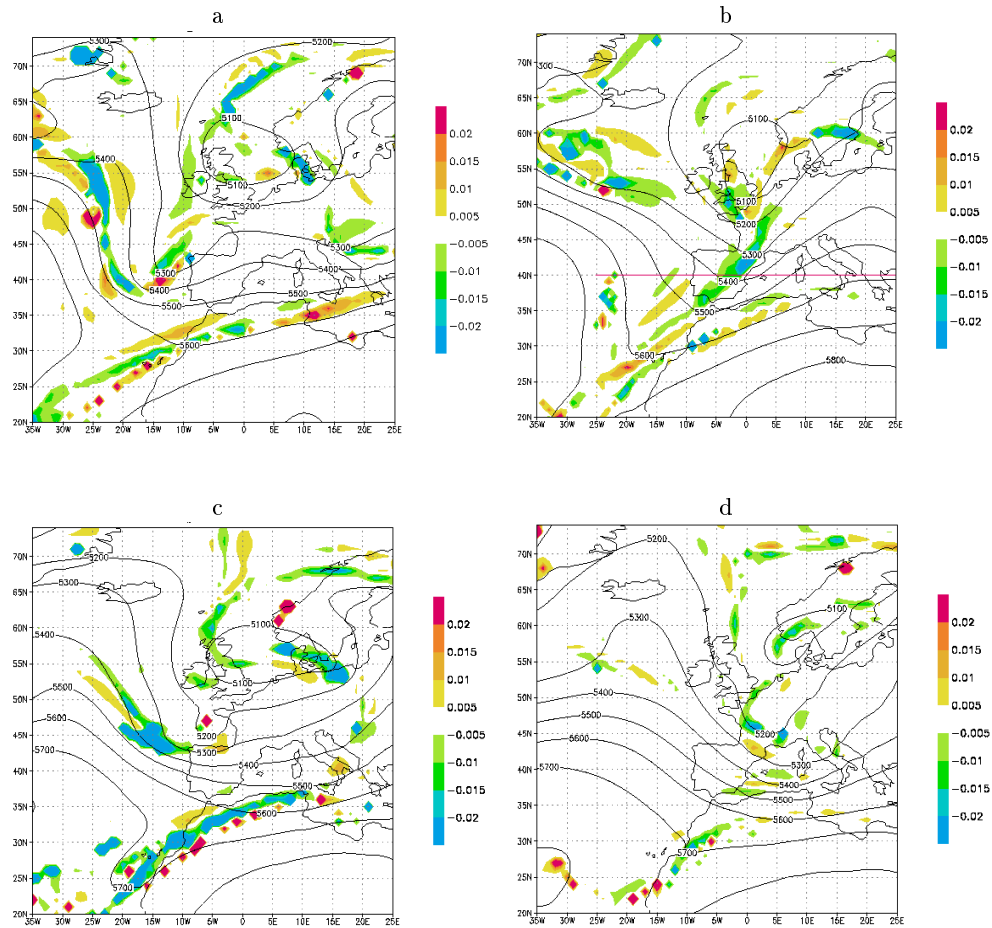


Figure 3.3: \tilde{F} across the 2 pvu surface (shaded, in $\text{kg m}^{-2} \text{s}^{-1}$) together with the 500 hPa geopotential height (contours, in m). Positive values denote transport from the troposphere to the stratosphere. \tilde{F} is shown for 14 April (a), 15 April (b), 16 April (c) and 17 (d) April 1998, all at 12 UTC.

one south of the cyclone centre, in the middle of the 500 hPa trough. The region with large downward fluxes north of the centre on the 14th has moved eastward towards southeast Scandinavia. On 16 April a region with large downward fluxes is again identified southwest of the cyclone centre. Two other bands with large downward fluxes are present: the first just east of the cyclone centre, the other starting in the cyclone centre and then curling to the north. On 17 April the large downward fluxes southwest of the cyclone have vanished. The regions with large downward fluxes occur near the cyclone centre and just south of it.

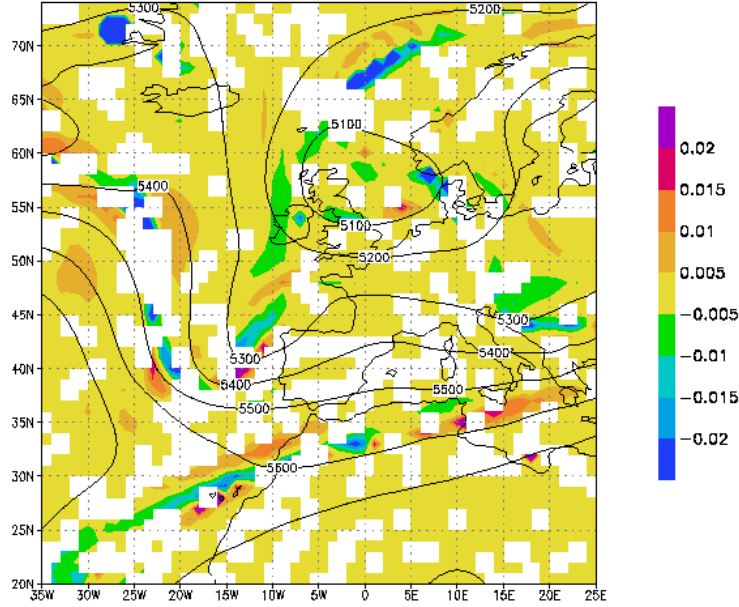


Figure 3.4: \tilde{F} across the 2 pvu surface (shaded, in $\text{kg m}^{-2} \text{s}^{-1}$) together with the 500 hPa geopotential height (contours, in m) on 14 April 1998 12 UTC, with significance criterion. Where \tilde{F} is statistically insignificant, the corresponding gridbox has been left blank.

For the air-mass fluxes across the other Q -surfaces differences are found compared with the air-mass flux across the 2 pvu surface. The flux across the Q -surfaces e.g. decreases with increasing Q . Another difference found is that the $|\partial p/\partial Q|$ -field and thus the \tilde{F} -field across Q -surfaces lower than 2 pvu is very noisy (not shown).

Figure 3.4 shows \tilde{F} across the 2 pvu surface on 14 April at 12 UTC with significance criterion, as described in section 3.2.1. Although the three areas with large downward fluxes can still be identified, it is clear that in large parts of these areas the computed fluxes are not significant. This can be understood as follows. Along trajectories passing a tropopause fold, Q is changing relatively rapid. dQ/dt along those trajectories is relatively large but noisy. As a result, the signal to noise ratio along a trajectory passing a fold is generally low and consequently the computed \tilde{F} is often not statistically significant, i.e. the probability that the real flux differs from zero is less than 99%. In other areas where the flux is statistically insignificant, the flux itself is very small. In the entire domain 87% of the gridpoints in Figure 4 have significant fluxes, 88% have significant dQ/dt and 99% have significant $|\partial p/\partial Q|$. Similar values are found for the other days.

3.3.3 Decomposition of the flux

In order to gain understanding of the structures in the \tilde{F} -field, \tilde{F} across the 2 pvu surface on 14 April is decomposed in dQ/dt (Figure 3.5a) and $|\partial p/\partial Q|$ (Figure 3.5b). After comparing Figure 3.5a and Figure 3.5b with Figure 3.3a, one can conclude that a condition for large (downward) fluxes is a large $|\partial p/\partial Q|$. A large dQ/dt does not imply a large flux when $|\partial p/\partial Q|$ is small. In the southwestern part of Iceland, for example, a large dQ/dt but a small $|\partial p/\partial Q|$ is present, which results in a small flux. When $|\partial p/\partial Q|$ is small, the vertical distance between the different Q -surfaces is small so that a large Q -change does not imply that much air has crossed a Q -surface.

The $|\partial p/\partial Q|$ -field at the 2 pvu surface appears to be directly coupled to the pressure field at this surface (Figure 3.5c), i.e. the tropopause height. The $|\partial p/\partial Q|$ and thus the flux is large in the areas where the tropopause pressure gradient is large (i.e. where the tropopause slopes) and in small-scale areas where the tropopause pressure itself is high (i.e. where the tropopause height is small), which can be understood from Figure 3.6. These conditions are valid in the tropopause folds, where the slope of the tropopause is very large (see Figure 3.1), and at the edge of a more extended lowering of the tropopause in the centre of a cyclone.

3.3.4 Vertical cross-sections: air-mass flux across Q -surfaces

In order to obtain a clearer understanding of the structure of the field of \tilde{F} in tropopause folds, vertical cross-sections of \tilde{F} across these folds have been calculated. Figure 3.7 shows a vertical cross-section of \tilde{F} on 15 April 12 UTC along 40°N, with pressure as the vertical coordinate. A region with large downward fluxes on the eastside of the tropopause trough and a region with smaller upward fluxes in the tropopause ridges west and east of this trough are clearly distinguished. Many insignificant fluxes are found below the 1 pvu surface, where $|\partial p/\partial Q|$ is very large and noisy, resulting in a low signal to noise ratio. In other tropopause folds (not shown), the region with the largest downward fluxes is also found on the eastside; in some folds this maximum is found in the middle of the fold, but not in the western part. The presence of regions with upward fluxes in tropopause ridges is also found to be a returning feature.

The maximum found in downward fluxes in tropopause folds is expected to be a reliable result for the following reason. A tropopause fold can be looked at as a small-scale lowering of the tropopause. Above a lowered tropopause, Q is anomalously high. According to the definition of Q , this would mean an anomalously high positive relative vorticity and an anomalously high $\partial\theta/\partial p$ in this Q -anomaly. The wind speed is therefore highest on both sides of the Q -anomaly, as can be verified from ECMWF

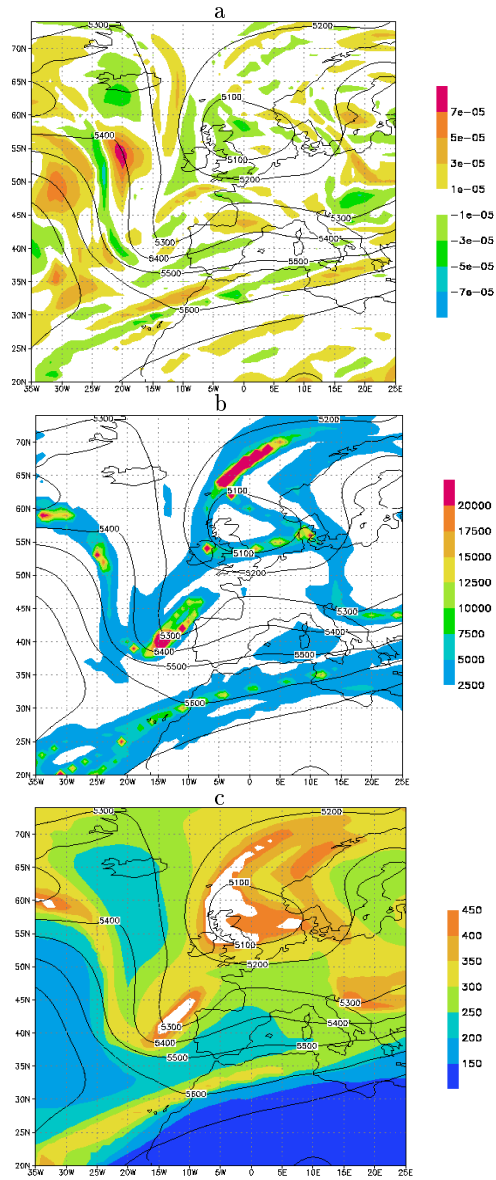


Figure 3.5: Decomposition of \tilde{F} across the 2 pvu surface on 14 April 1998 12 UTC (as shown in Figure 3.3a) in dQ/dt (a, shaded, in pvu s^{-1}) and $|\partial p / \partial Q|$ (b, shaded, in Pa pvu^{-1}) together with the 500 hPa geopotential height (contours, in m). The colours in panel c show the pressure (in hPa) of the 2 pvu surface.

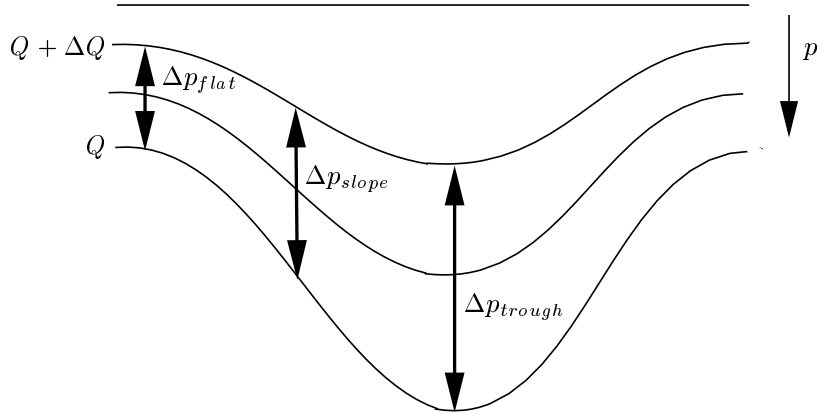


Figure 3.6: Illustration of $|\partial p/\partial Q|$ around a tropopause trough. $|\partial p/\partial Q|$ at a sloping tropopause and at a tropopause trough is generally larger than $|\partial p/\partial Q|$ at a flat tropopause.

data for 15 April as seen in Figure 3.8. The wind maxima cause a large shear in the surrounding areas. This wind shear causes strong mixing of air-masses in the tropopause fold. Since the Q -gradient is relatively high in this region, this mixing of air-masses implies a strong Q -mixing. Comparing Figure 3.8 with Figure 3.7, one can clearly see that the fluxes are largest in the regions where the wind shear is maximal. In these regions, Q -mixing is thought to cause the large fluxes. The large downward fluxes found in tropopause folds are therefore thought to be a reliable result, at least in a qualitative sense.

The tropopause fold found along the northwest coast of Africa is thought to lie on a peculiar position. To validate the position of this tropopause fold, GOME (Global Ozone Monitoring Experiment) total ozone columns have been considered. These data (not shown) show a maximum in the total ozone column, which implies a lowering of the tropopause, virtually along the tropopause fold. The tropopause fold found with its large downward fluxes along the northwest coast of Africa is, therefore, expected to be a reliable result.

3.3.5 Area-averaged upward and downward fluxes

As described in the introduction, the ratio between the upward and downward fluxes should be known in order to calculate the cross-tropopause fluxes of chemical species. To get an impression of this ratio, all upward and downward fluxes (without signif-

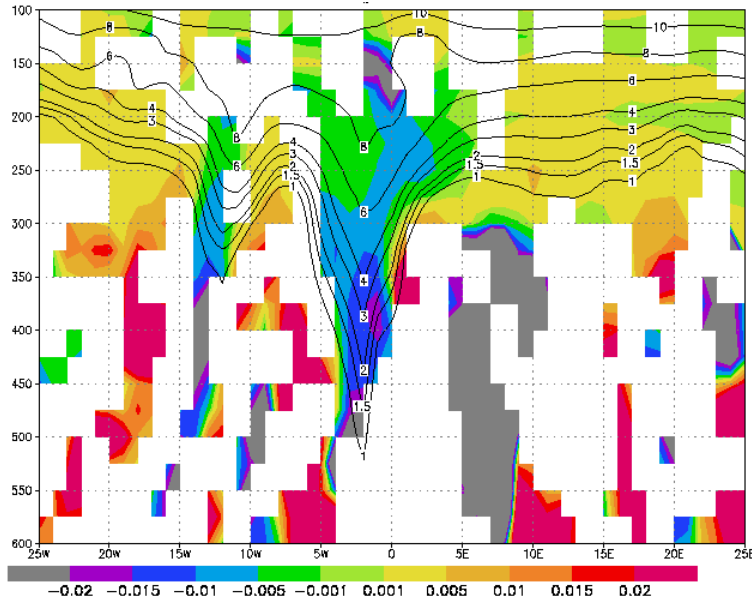


Figure 3.7: Vertical cross-section of \tilde{F} (shaded, in $\text{kg m}^{-2} \text{s}^{-1}$) on 15 April 1998 12 UTC along 40°N (which is the red line in Figure 3b), with significance criterion (i.e. spaces are left blank where \tilde{F} is statistically insignificant), with pressure as the vertical coordinate, together with isolines of Q (in pVU).

ificance criterion) are added separately and are then averaged over the entire domain (see Table 3.1). In this calculation, fluxes larger than $0.1 \text{ kg m}^{-2} \text{ s}^{-1}$ and smaller than $-0.1 \text{ kg m}^{-2} \text{ s}^{-1}$ are assumed to be non-physical and are set to $0.1 \text{ kg m}^{-2} \text{ s}^{-1}$ and $-0.1 \text{ kg m}^{-2} \text{ s}^{-1}$, respectively. It is striking to see that the ratio R is smallest on 16 April, when the strength of the cyclone is maximal, and largest on 17 April, when the cyclone has weakened. The ratio between the area-averaged upward and downward cross-tropopause fluxes appears to decrease with increasing strength of the cyclone.

3.4 Discussion

In this section the parameterisation of Q -mixing in the ECMWF model and the method for calculating the flux across a Q -surface will be discussed. In section 3.4.3, the found ratios between the area-averaged upward and downward fluxes will be compared with those found in previous studies.

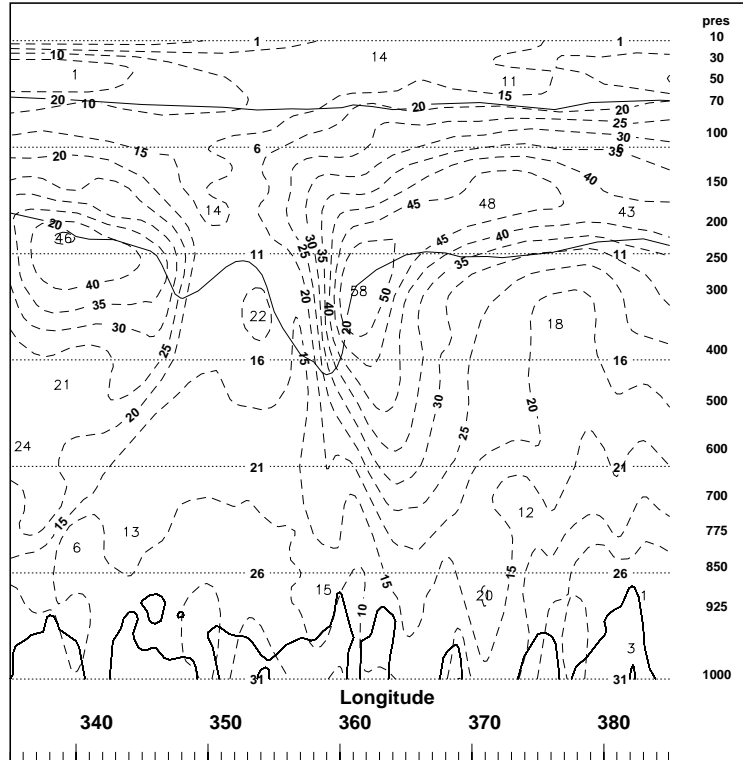


Figure 3.8: Vertical cross-section of the wind speed (dotted lines, in m s^{-1}) on 15 April 1998 12 UTC along 40°N (which is the red line in Figure 3b), with pressure as the vertical coordinate (in hPa), together with some isolines of Q (solid lines, in $\text{pvu} \times 10$).

3.4.1 Parameterisation of Q -mixing in the ECMWF model

As described in section 3.2.1, one of the sources of the gridbox-mean Q (and thus the STE as calculated in this study) is Q -mixing. In the real atmosphere, Q of a single air parcel can only be changed by diabatic heating gradients and friction. In a numerical (prognostic) model, the change of Q due to mixing is a result of the model formulation of subgrid-scale processes. A restriction of a model is that it cannot calculate the evolution of the properties of every single air parcel in the atmosphere explicitly. Instead, the quantities are calculated on a grid with a finite spatial resolution. The quantities calculated in a model are therefore gridbox-mean rather than local quantities. The same applies to Q computed along a trajectory. Therefore, in the absence of diabatic heating gradients and friction, mixing of air-masses with different Q can lead to a change in the gridbox-mean Q , although Q of

Time	F_{up}	F_{down}	F_{net}	R
98041412	1.69×10^{-3}	-2.24×10^{-3}	-5.44×10^{-4}	0.757
98041512	1.40×10^{-3}	-1.78×10^{-3}	-3.83×10^{-4}	0.785
98041612	1.52×10^{-3}	-2.39×10^{-3}	-8.77×10^{-3}	0.633
98041712	1.29×10^{-3}	-1.10×10^{-3}	1.84×10^{-4}	1.167

Table 3.1: Domain-averaged upward (F_{up}), downward (F_{down}) and net (F_{net}) fluxes (in $\text{kg m}^{-2} \text{s}^{-1}$) and the ratio of the domain-averaged upward and downward fluxes ($R = |F_{up}/F_{down}|$) across the 2 pvu surface for 14, 15, 16 and 17 April 1998, 12 UTC.

the individual air parcels is conserved.

The Q -change computed from gridbox-mean circulation data is given by (for simplicity the two-dimensional situation is considered):

$$\begin{aligned} \frac{d\overline{Q}}{dt} &= \frac{\partial \overline{Q}}{\partial t} + \overline{u} \frac{\partial \overline{Q}}{\partial x} + \overline{v} \frac{\partial \overline{Q}}{\partial y} \\ &= - \left[\frac{\partial \overline{u'Q'}}{\partial x} + \frac{\partial \overline{v'Q'}}{\partial y} \right], \end{aligned} \quad (3.5)$$

where the overbar denotes gridbox-mean values and the accent denotes deviations from those mean values.

The right-hand side of this equation, the divergence of the eddy Q -flux, is a sub-grid process, which is not computed explicitly. Instead, subgrid processes are parameterised in terms of the known gridbox-mean quantities. In the ECMWF model, the subgrid-scale fluxes of the model variables that determine Q (vorticity, divergence and temperature) are parameterised, rather than the eddy Q -flux itself. The quality of these parameterisations in the ECMWF model determines the quality of the results of this study.

A second, possibly even more important contribution to the divergence of the eddy Q flux is model numerical diffusion.

3.4.2 Method for calculating the flux across a Q -surface

Calculation of the fluxes

Because of numerical errors due to finite time and space differencing, finding an appropriate method for diagnosing the local and instantaneous flux across a Q -surface is not straightforward. *Siegmund et al.* [1996] have introduced the ‘advection method’, in which the space terms are selectively averaged over time in an Eulerian framework. In this work these time differencing problems are circumvented by working in a Lagrangian framework. The main remaining problem is that the data suffer from noise. Instant values of dQ/dt can therefore be unreliable. To cope with this problem, a

certain kind of averaging is necessary. The instant flux in a gridpoint has therefore been computed from data along 6-hour forward and backward trajectories starting at the gridpoint.

A second approximation that has been made concerns the calculation of Q along the trajectories. The gridbox-averaged Q , used in numerical atmospheric models, should be calculated according to:

$$\overline{Q} = \overline{\frac{\partial \theta}{\partial p} (\zeta + f)} = \overline{\frac{\partial \theta}{\partial p} (\zeta + f)} + \overline{\left(\frac{\partial \theta}{\partial p}\right)' (\zeta + f)'}, \quad (3.6)$$

where the overbar denotes the gridbox-mean value and the accent denotes the deviation from that value.

In the calculation of \overline{Q} we were forced to neglect the second term on the right hand side, since the ECMWF model only provides gridbox-mean quantities.

Averaging period

The averaging period for the calculation of \tilde{F} (Equation 3.3) has been varied to see how this affects the results. With decreasing period, the reduction of the noise in the results, which was made by averaging, decreases and less values of \tilde{F} are statistically significant. As a suitable time period for averaging dQ/dt and $|\partial p/\partial Q|$, 12 hours is found. Averaging over a longer period does not decrease the noise substantially, but artificially smoothes out the cross- Q fluxes.

Comparison with the Lagrangian flux calculation of *Wirth and Egger* [1999]

As described in the introduction, *Wirth and Egger* [1999] also used a Lagrangian method to diagnose the cross-tropopause air-mass flux. Although the concept of their method is similar to the method applied in this study, there are some noteworthy differences. The similarity is that in both methods a quantity is considered along a trajectory, which is Q in the present study and the pressure in their study. The pressure difference between the endpoint of a trajectory that started at the tropopause and the tropopause at that endpoint, is then taken by *Wirth and Egger* as a measure of the cross-tropopause flux.

A difference with the method of the present study is that every 3 hours a reinterpolation of their trajectories to a regular grid is performed in order to avoid a too strong accumulation or dilution of points, which introduces some smoothing. The method of the present study circumvents this problem by calculating forward and backward trajectories starting at a gridpoint and attributing the computed flux to this gridpoint.

Source	R	Averaging period	Averaging area	Method	model
<i>Spaete et al.</i> [1994]	0.4	1 day	Area around tropopause fold, travelling with system	Wei- θ across 3 pvu	Mesoscale
<i>Lamarque and Hess</i> [1994]	0.79	4 days	Area around extratropical cyclone travelling with system	Wei- Q across 2 pvu	Mesoscale
<i>Siegmund et al.</i> [1996]	0.97	Month	28°N - 90°N	Wei-p across 3.5 pvu	ECMWF, first guess data
Present study	0.63-1.17	12 hours	35°W-25°E 20°N-75°N	Trajectories, Wei- Q across 2 pvu	ECMWF, first guess data

Table 3.2: Calculations of R ($= |F_{up}/F_{down}|$) from previous studies and the present study.

A second difference is that Wirth and Egger compute the cross-tropopause flux from information at only the begin and the end of the trajectory, whereas in the present study the averaged Q -rate of change along the trajectory, estimated by a linear least square method, and the trajectory-mean value of $|\partial p/\partial Q|$ are used to calculate the flux. Our results are, therefore, expected to be less subjected to noise.

3.4.3 Comparison of F_{up}/F_{down} with previous studies

Table 3.2 shows different values of R ($= |F_{up}/F_{down}|$) found in different studies with different methods. Before comparing the values of the present study with the other values from Table 3.2, one should realise that R can be strongly case-dependent.

In the results of the present study, the largest downward fluxes have been found in tropopause folds. From Table 3.2 it appears that R decreases if less fluxes outside the tropopause fold are taken into account in the calculation of R .

In *Spaete et al.* [1994] and *Lamarque and Hess* [1994], R is calculated in a relatively small area around, respectively, a tropopause fold and an extratropical cyclone, whereas in the case of the present study, R is calculated averaged over a larger area around an extratropical cyclone. *Siegmund et al.* [1996], finally, computed R for a whole month and for a much larger area.

The domain-averaged upward (F_{up}) and downward (F_{down}) fluxes are comparable to the values found by Lamarque and Hess (1.68×10^{-3} and 2.12×10^{-3} kg m⁻² s⁻¹, respectively) and Spaete et al. (5.79×10^{-3} and 2.31×10^{-3} kg m⁻² s⁻¹, respectively).

3.5 Conclusions

In this work a Lagrangian method for diagnosing the air-mass flux across Q -surfaces, in particular across the tropopause, has been applied. Several aspects of the method are new compared to previous studies. The flux is computed from Q and $|\partial p/\partial Q|$ along 12-hour trajectories that pass the gridpoint for which the flux is estimated. The trajectories are computed from ECMWF circulation data. The error in the flux across Q -surfaces is quantified and used to determine the statistical significance of the flux.

The computed field of the air-mass flux across Q -surfaces is dominated by elongated patterns of statistically significant large downward and small upward fluxes. The downward fluxes mainly occur in regions of a tropopause fold, whereas the upward fluxes are found near tropopause ridges. The area-averaged upward (F_{up}) and downward (F_{down}) fluxes, which both lie between 1 and 2.5×10^{-3} kg m⁻² s⁻¹, are comparable to the values found in previous studies. The ratio between the area-averaged upward and downward cross-tropopause fluxes appears to decrease with increasing strength of the cyclone.

The results are thought to be reliable, at least in a qualitative sense, because the largest downward fluxes in the tropopause fold occur in regions with maximum wind shear, where Q -mixing is thought to cause STE. The geographical agreement between tropopause folds with large downward fluxes and the high total ozone values is good. Although several approximations have been made in the applied new Lagrangian method, this method appears to be an appropriate tool for diagnosing dQ/dt in general and STE in particular.

Acknowledgements We thank Rinus Scheele for his support he gave concerning the KNMI trajectory model. We also would like to thank Geert-Jan Roelofs and Anastasios Kentarchos (both from the Institute of Marine and Atmospheric Research) for their helpful suggestions. Comments of two anonymous reviewers helped improve the manuscript, and were greatly appreciated.

4

A Lagrangian computation of stratosphere-troposphere exchange in a tropopause folding event in the subtropical Southern Hemisphere

A new Lagrangian technique to calculate the air-mass flux across potential vorticity (Q) surfaces has been used to perform a case study of a tropopause folding event in the subtropical Southern Hemisphere. The flux is computed from the rate of change in Q along trajectories, which are calculated from ECMWF wind data. Because the tropopause can be defined as a Q surface, the method can be used for the calculation of stratosphere-troposphere exchange (STE). A large number of forward and backward trajectories were calculated, starting in the vicinity of the tropopause fold. This fold was observed during the TRACAS (TRANsport of Chemical species Across the Subtropical tropopause) experiment at La Reunion (21°S, 55°E) in July 1998. With the Lagrangian method the cross-tropopause air-mass flux can be calculated for the different tropopause levels, that occur in case of a tropopause folding. The computed mass exchange is about -20×10^{13} kg (i.e. downward) in 4.5 days, which is rather small compared to other (midlatitude) mass exchange studies. The ratio of the fluxes per unit of area in and outside of the fold is about 200:1. An indication of the accuracy of the calculated fluxes has been obtained with the help of the ozone soundings made during the TRACAS experiment.

4.1 Introduction

Stratosphere-troposphere exchange (STE) is one of the main processes controlling the impact of man's activities on atmospheric composition and climate forcing [Holton *et al.*, 1995]. Despite this importance, there exist no accurate estimates of STE. This is particularly true for estimates that are limited in space and time. Various versions of a general formula derived by Wei [1987] are often used to calculate mass exchange between the troposphere and the stratosphere. These calculations, however, suffer from cancellation of large terms [Wirth and Egger, 1999].

Wirth and Egger compared in their study five methods to diagnose mass exchange across the tropopause, three of which were derived from Wei's general formula, in one method the flux was evaluated directly as the difference between the motion of the air and the motion of the tropopause, and one method involved the calculation of a large number of trajectories. Their trajectory method yielded reasonable estimates for the cross-tropopause mass flux, together with Wei's general formula with potential vorticity (Q) as vertical coordinate. Disadvantage of the latter method is that the potential vorticity sources and sinks need to be estimated explicitly.

Siegmund *et al.* [1996] calculated STE with wind and temperature data at high spatial and temporal resolution. They found that the diagnosed instantaneous and local cross-tropopause fluxes do not notably depend on the horizontal and temporal resolution if these becomes higher than, respectively, $1^\circ \times 1^\circ$ latitude/longitude and 6h. A resolution decrease to $3.75^\circ \times 3.75^\circ$ and 12h, however, generally leads to quite different results for the local and instantaneous fluxes.

With previous methods the tropopause in tropopause foldings is generally truncated to a single level due to technical reasons [e.g. Wei, 1987]. The consequence of this truncation is that any stratospheric air entering the fold is assumed to be irreversibly transferred to the troposphere. The accuracy of this assumption however has never been investigated. With the Lagrangian method applied in this study all, possibly multiple, tropopause levels are taken into account.

In the present study Wei's general formula with potential vorticity as vertical coordinate is used, and the terms in this formula are determined with the help of trajectories, which are calculated at a high spatial and temporal resolution. Wirth and Egger [1999] used their trajectories to calculate the difference in tropopause pressure and trajectory pressure at the endpoint of the trajectory, and took this as a measure for the STE in the considered time interval. Sigmond *et al.* [2000] developed the Lagrangian method used in the present study for the calculation of STE. Sigmond *et al.* concentrated on the statistical significance of the method and its application to an extratropical cyclone. In the present study the method is applied to a subtropical

tropopause folding which was observed in the Southern Hemisphere during the TRACAS (TRAnsport of Chemical species Across the Subtropical tropopause) experiment. This experiment took place at the subtropical island La Reunion (21°S, 55°E). The method is evaluated with the help of TRACAS ozone soundings.

Tropopause folds in the Southern Hemisphere subtropics are believed to differ in some important aspects from the more frequently studied folds in the Northern Hemisphere midlatitudes [Ramond *et al.*, 1981]. Tropopause folds near the subtropical jet are, e.g., believed not to penetrate as deep into the troposphere in comparison with midlatitude folds, since the frontal zone is broader and the tropopause is less steeply folded [Gouget *et al.*, 1996]. Therefore, the exchange can be expected to be less in subtropical folds compared to midlatitude folds. The fold examined in this study is thought to be associated with the Hadley circulation [Baray *et al.*, 2000]. This is also an indication that care must be taken when comparing the fold of this study with Northern Hemisphere midlatitude folds.

In section 4.2 the method to calculate the cross- Q air-mass flux is explained, and a description is given of the trajectory model, its input data and the observations made during the TRACAS experiment. In section 4.3.1 the reliability of the calculated cross- Q air-mass flux F is investigated. This section is divided in two parts. In the first part a qualitative evaluation is done to analyse the geographical variability of the flux. In the second part a quantitative evaluation is done to investigate the reliability of the magnitude of the computed fluxes. Finally, in section 4.3.2, the computed area- and time-integrated flux is presented.

4.2 Method and Data

In this section first an explanation is given how the cross- Q air-mass flux (F) is derived. Next a description is given of the wind and temperature data used for the calculation of F , and the trajectory model is described. Finally a description is given of the TRACAS experiment, from which the ozone soundings are used in this study.

4.2.1 Flux calculation

For the calculation of the air-mass flux F across a potential vorticity surface the general equation derived by Wei [1987] is used. With potential vorticity (Q) as the vertical coordinate, this general formula becomes particularly simple and can be written as:

$$F = -\frac{1}{g} \frac{\partial p}{\partial Q} \frac{dQ}{dt}, \quad (4.1)$$

where g is the acceleration due to gravity, p is pressure, Q potential vorticity and t is time. The unit of F is $\text{kg m}^{-2} \text{s}^{-1}$.

The formula as given by Wei is strictly valid only for cases where $|Q|$ increases monotonously with height. It does not correctly describe the case of multiple dynamical tropopauses. If the tropopauses are numbered from the top of the atmosphere downward, a negative flux given by the Wei formula is from the stratosphere downward at odd numbers and from troposphere upward at even numbers of the tropopause. In order to take care that negative values of F are always from the stratosphere to the troposphere, F is written as:

$$F = \frac{1}{g} \left| \frac{\partial p}{\partial Q} \right| \frac{dQ}{dt}. \quad (4.2)$$

The method used in this study to compute F has been described by *Sigmond et al.* [2000], and is summarised below. At the gridpoint where F is to be determined, a 6-hour forward and a 6-hour backward trajectory is calculated. These trajectories are started on the tropopause every 12 hours, on a grid with $1^\circ \times 1^\circ$ resolution. Along these trajectories Q and $\partial p/\partial Q$ are calculated. Because the instantaneous dQ/dt is very noisy, a linear least square regression of Q along the 12-hour trajectory versus time is made, of which the slope is used as an approximation of the 12-hour mean dQ/dt . F is then approximated as

$$F \approx \frac{1}{g} \left| \overline{\frac{\partial p}{\partial Q}} \right|^{12h} \overline{\frac{dQ}{dt}}^{12h}, \quad (4.3)$$

where $\overline{|\partial p/\partial Q|}^{12h}$ is the averaged absolute $\partial p/\partial Q$ along the 12-hour trajectory.

In this study the tropopause is defined as a Q surface. Q values are generally negative in the Southern Hemisphere, so that absolute values have to be taken to make them comparable with Northern Hemisphere Q values. In the midlatitudes the tropopause is defined by a $|Q|$ value of typically 2 pvu (1 pvu= 10^{-6} K m² kg⁻¹ s⁻¹). The most suitable $|Q|$ value to define the tropopause depends on the season and the region under consideration [*Folkins and Appenzeller, 1996; Grewe and Damaris, 1995*]. A value of 1.5-2.5 pvu seems to be a reasonable range for the $|Q|$ of the subtropical tropopause. Therefore, trajectories are started at three different Q levels, i.e. -1.5 , -2 and -2.5 pvu. The derived flux is attributed to the starting point and time of these trajectories. Negative values of F correspond to fluxes towards lower values of $|Q|$, i.e. towards the troposphere. Positive values correspond to fluxes in the opposite direction, i.e. towards the stratosphere.

In this study a folding event is identified when the Q surfaces are truly folded, i.e. when the same Q value can be found three times at one gridpoint at different altitudes. For each such gridpoint, trajectories are started and F is calculated at the three different altitudes. From the uppermost level downward these fluxes are called F_1 , F_2 and F_3 (see Figure 4.5). This means that F_1 always exists, but F_2 and F_3 are

only nonzero in the case of a folding event. By adding these three separate values, the total flux, $F_{tot} \equiv F_1 + F_2 + F_3$, for that gridpoint is obtained.

The above method becomes unreliable if $\partial p/\partial Q$ becomes large. This occurs for instance when the tropopause is steep [Lamarque and Hess, 1994]. Therefore, fluxes with absolute values larger than $0.05 \text{ kg m}^{-2} \text{ s}^{-1}$ are considered to be unreliable, and are not taken into account. The threshold value of $0.05 \text{ kg m}^{-2} \text{ s}^{-1}$ was chosen on the basis of the probability density function of F given by Siegmund *et al.* [1996]. For the extratropical Northern Hemisphere, the absolute values of F hardly ever exceed $0.05 \text{ kg m}^{-2} \text{ s}^{-1}$. Although the present study concentrates on a Southern Hemisphere subtropical fold, the range of values is not expected to be larger than the range for Northern Hemisphere values [Gouget *et al.*, 1996]. If one of the separate fluxes F_1 , F_2 or F_3 is not taken into account, then also F_{tot} is not taken into account. This is the case in less than 1% of the total area.

4.2.2 ECMWF data

As input to the trajectory model ECMWF first guess wind and temperature data are used. These data are available on a $1^\circ \times 1^\circ$ grid, obtained from the T213 spectral resolution of the ECMWF model, and at 31 vertical levels. Around the tropopause the vertical resolution is about 25 hPa. The temporal resolution of the data is 6 hours.

For the comparison of the data with measurements, first guess data are used rather than analyses. This is because the latter are not physical consistent due to the addition of observations to the model data. An advantage of forecast data would have been that the data remain physical consistent during the entire trajectory computation. But the differences between a 5-day forecast and the analysis are too large to justify this approach.

4.2.3 Trajectory model

For calculating the trajectories, the KNMI trajectory model is used as described by Scheele *et al.* [1996]. This model calculates the three-dimensional displacement of air parcels for each time step using the iterative scheme after Petterssen [1940]. In the present study the trajectory time step is 10 minutes. Spatial interpolation (linear in longitude, latitude and the logarithm of pressure) and temporal interpolation (quadratic) are applied to the input data to obtain the wind at the trajectory locations. In this study three-dimensional rather than isentropic trajectories are calculated in order to include diabatic effects in the calculations of the cross- Q air-mass flux. Also, for winds from ECMWF, three-dimensional trajectories are generally more accurate at tropopause heights than isentropic trajectories, as is found, e.g., by Stohl

and Seibert [1998]. To calculate Q at location X and at time t , Q is first calculated at location X at the three 6-hourly ECMWF first guess times closest to time t , and is then quadratically interpolated to time t .

4.2.4 The TRACAS experiment

In July 1998, a measurement campaign called TRACAS (TRANsport of Chemical species Across the Subtropical tropopause) was held in the Indian Ocean region to collect ozone observations near the Southern Hemispheric subtropical jet stream. One of the objectives was to study how the dynamical processes associated with the subtropical jet control the exchange of chemical species through the tropopause. During the experiment, amongst others, ozone sondes were launched at La Reunion Island (21°S, 55°E). During the whole of July 1998 a tropopause fold persisted over a considerable longitude range from the mid-Atlantic to the mid-Pacific, i.e. from 0° to 200°E, and from 20° to 35°S. The fold is thought to be associated with the Hadley circulation [Baray *et al.*, 2000]. In this study the time interval is restricted to the part of the period when the fold was quite pronounced and over La Reunion, i.e. from 14 July 1998 00 UTC to 18 July 1998 12 UTC. Fluxes are calculated for the area between 0° to 160°E and 10° to 50°S. In the selected period four ozone sondes were launched, from which the sondes on 17 July 1998 10 UTC and 18 UTC are used for the purpose in this study, thanks to the small time interval between them.

4.3 Results

In this section the results of the exchange in the tropopause fold, calculated with the method described in section 4.2.1 is presented. In section 4.3.1, first an evaluation is done to investigate the accuracy of the calculated cross- Q air-mass flux. This section is divided in two parts, the first is the investigation of the geographical distribution, the second is a quantitative evaluation of the flux with the help of ozone soundings. In section 4.3.2 the results are given of the time and area integrated air-mass flux through the various Q levels and the various tropopause regions inside and outside the tropopause fold.

4.3.1 Evaluation of F

Geographical distribution of F

In Figure 4.1 the total flux (F_{tot}) is given for the -1.5 pvu level on 17 July 1998 12 UTC, overlaid with the $|Q|$ on the 300 hPa surface. The tropopause fold and two upper level troughs can be distinguished by the contouring of Q , which indicates

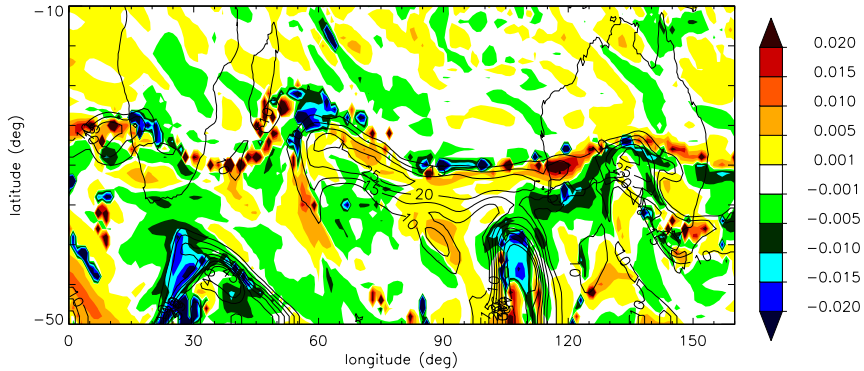


Figure 4.1: Longitude/latitude plot for the total air-mass flux (F_{tot} , in units of $\text{kg m}^{-2} \text{s}^{-1}$) across the -1.5 pvu surface (colour plot), overlaid with Q (in units of -0.1 pvu) on the 300 hPa surface (contour lines), both on 17 July 1998 12 UTC. Positive values of F correspond to fluxes towards higher, more stratospheric levels of $|Q|$, negative values correspond to fluxes in the opposite direction. The contours of Q indicate regions where the Q surfaces are located at a lower than normal position, as is the case in the upper level troughs and in tropopause foldings. These high values of Q at 300 hPa correspond to the largest fluxes.

regions where the Q surfaces are located at a lower than normal position. The fold can be found from 25° to 35°S along a large part of the longitude range, and the two upper level troughs are located from 20° to 55°E and from 100° to 120°E both below 40°S . The two upper level troughs can also be distinguished on figures of mean sea-level pressure (not shown). As can be seen in Figure 4.1 high values of the flux are found in the tropopause fold and in the upper level troughs, as would be expected [e.g. Wirth and Egger, 1999; Lamarque and Hess, 1994]. In most other regions the flux is very small. Typical values found for the calculated air-mass flux are of the order $0.02 \text{ kg m}^{-2} \text{ s}^{-1}$. This is comparable with the magnitude found by Siegmund *et al.* [1996]. However, Wirth and Egger [1999] found values of an order 5 larger in a cut-off low event at Northern Hemisphere midlatitudes. These fluxes might be larger because of the different physical mechanisms of decay in a cut-off low event and the difference in place where the event occurred, compared with the tropopause fold studied here. From this the conclusion can be drawn that the method used here to calculate the cross- Q air-mass flux is capable of detecting the areas where exchange is expected to occur and that the order of magnitude of the fluxes is in the range of what is expected.

In Figure 4.2 the fluxes through the different parts of the tropopause fold are displayed for the -1.5 pvu level on 17 July 1998 12 UTC. From these figures it can

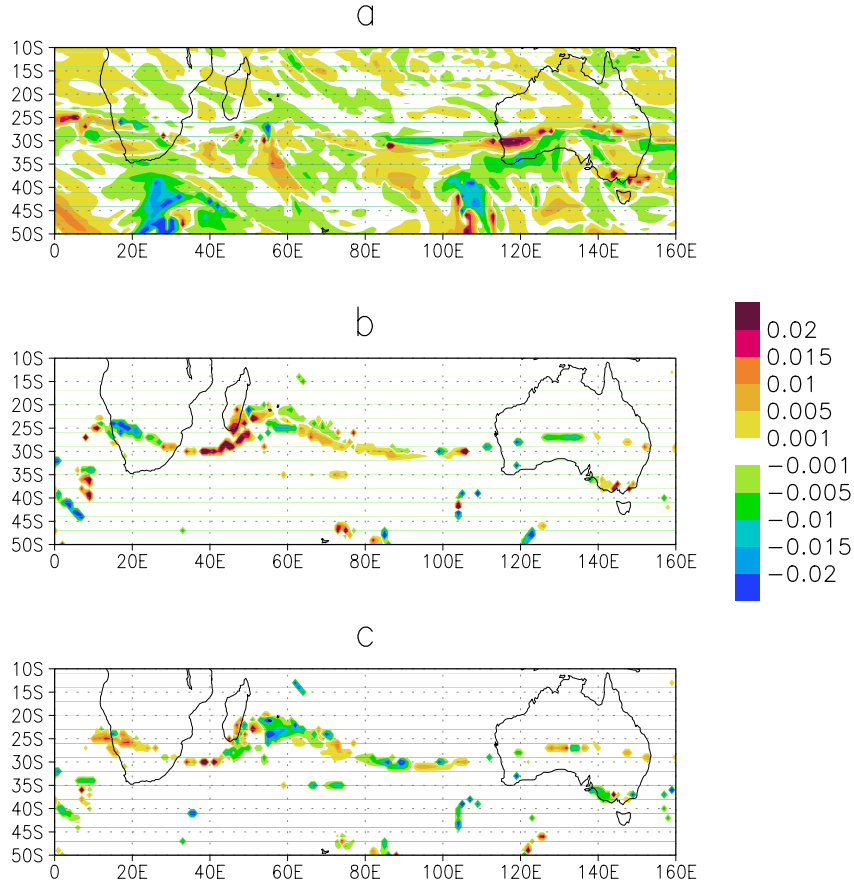


Figure 4.2: The calculated cross-Q air-mass flux (in units of $\text{kg m}^{-2} \text{s}^{-1}$) for 17 July 1998 12 UTC through the -1.5 pvu level. Panel a) represents the mass flux across the upper tropopause region (F_1 in Figure 4.5), b) through the middle tropopause region (F_2 in Figure 4.5) and c) through the lower tropopause region (F_3 in Figure 4.5). The total mass flux ($F_{tot} \equiv F_1 + F_2 + F_3$), is displayed in Figure 4.1. F_2 and F_3 are nonzero only in the case of multiple tropopauses.

be seen that the exchange in the fold takes mainly place in the middle (F_2) and lower (F_3) parts of the fold. As can be anticipated multiple tropopauses are not found for upper level troughs, and hence here large fluxes are only found for F_1 . Often regions with positive and negative fluxes are found close to each other. The reason is that small-scale mixing processes lead to bidirectional fluxes [Lamarque and Hess, 1994].

It is expected that particularly in tropopause folds the exchange is related to tur-

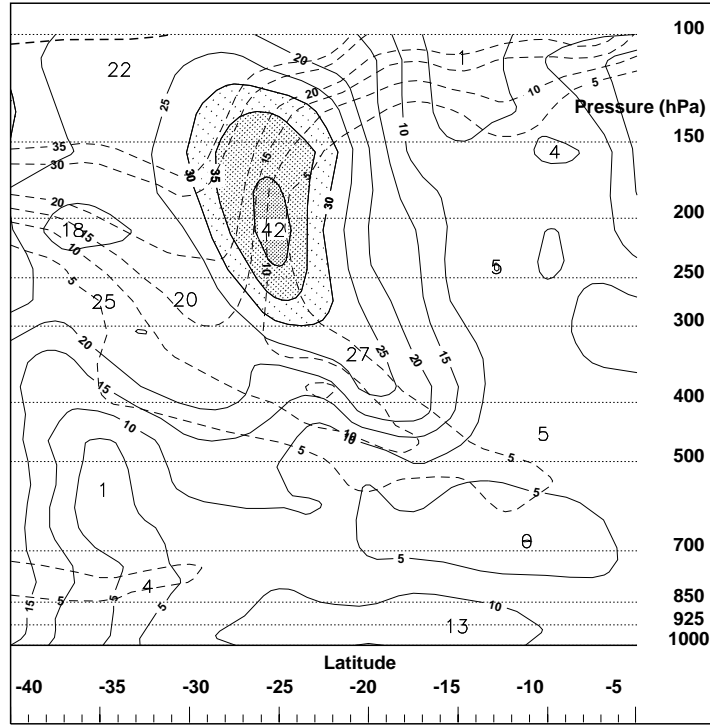


Figure 4.3: Cross section at 55°E of the wind speed (m/s) for 17 July 12 UTC 1998 (first guess model level data). Dashed lines denote values of Q (in units of -0.1 pvu), solid lines denote windspeed. As can be seen from this figure the largest windshear for the -1.5 pvu surface can be found between 20°S to 27°S , around the windspeed maximum. In the uppermost panel in Figure 4.1 (F_{tot}) can be seen that here the largest values across the -1.5 pvu surface occur.

bulent mixing of Q due to vertical windshear [Shapiro, 1980], instead of exchange by latent heating which is important in cut-off lows [Wirth and Egger, 1999]. Therefore, it is expected that in the regions with large windshear the flux will generally be large. The locations of the maximum in vertical windshear, at both sides of the maximum in windspeed, along the -1.5 pvu surface in Figure 4.3 are located between 20° and 27°S . When comparing this with the location of the maximum in the total flux in Figure 4.1 it is obvious that these areas coincide. This is another indication that the applied method is capable of detecting the areas where for physical reasons the exchange is expected to be large. The same characteristics were found for the air-mass fluxes across the -2.0 and -2.5 pvu surfaces (not shown), except for the size of the area where F_2 and F_3 are nonzero. This area decreases at higher $|Q|$ values, as can

be expected from the structure of tropopause foldings (see Figure 4.5).

In summary, the analysis of the geographical variability of the calculated flux shows that the regions where the largest fluxes occur closely correspond to locations where STE would be expected for physical reasons.

Quantitative evaluation of the magnitude of F

In the previous section it was shown that the geographical distribution of the calculated air-mass fluxes looks reasonable. Another important aspect to know is whether the magnitude of the computed fluxes corresponds to what would be expected. As follows from Equation (4.1), uncertainties in F depend on uncertainties in $\partial p/\partial Q$ and dQ/dt . We will focus the attention on the uncertainty in dQ/dt , which is expected to dominate the uncertainty in F . The dQ/dt as computed in this study from trajectories, must be interpreted as the rate of change of the mean Q of a moving air parcel with a size of about the gridbox-size of the applied circulation data. This dQ/dt strongly depends on the subgrid-scale mixing of air-masses with different Q values, which is implicitly parameterised in the ECMWF model. Although the subgrid-scale mixing is parameterised in terms of the model variables rather than Q , implicitly there is an effect on dQ/dt via the dependence of Q on the modelled temperature and horizontal velocity. In addition, numerical diffusion adds to dQ/dt . If dQ/dt would be zero, then the Q along trajectories would be constant and Q at the begin- and endpoints of the trajectories, Q_b and Q_e , would be the same. In other words, Q_e would be the result of advection of Q_b . In reality dQ/dt is generally nonzero, and Q_e is the sum of Q_b and the dQ/dt along the trajectory. The value of Q_e at some point x_0 and time t_0 , $Q(x_0, t_0)$, can be computed from ECMWF data at t_0 . The Q_b can be obtained by computing a back trajectory starting in (x_0, t_0) and ending in $(x_1, t_0 - \Delta t)$ and setting $Q_b = Q(x_1, t_0 - \Delta t)$, which can be computed from ECMWF data at $x_1, t_0 - \Delta t$ (in this study Δt has a value of 6 hours). In this section it is investigated whether Q_e is more realistic (to be defined below) than Q_b , or, in other words, whether the dQ/dt along the trajectory improves Q_e or not. This might give some qualitative information about the accuracy of the modelled dQ/dt , and hence about the accuracy of the flux F . This investigation is done by considering two ozone and Q -profiles at the same location, obtained from independent sources, at a time interval of several hours. It is assumed that during this short period the relation between ozone and Q is constant. For each point of the profiles both Q_e and Q_b are computed and it is determined whether the ozone- Q relation is more constant for Q_e or for Q_b . If it is more constant for Q_e , then it is assumed that the addition of the modelled dQ/dt along the trajectory to Q_b results in a better Q_e and, hence, that this dQ/dt is less or more realistic.

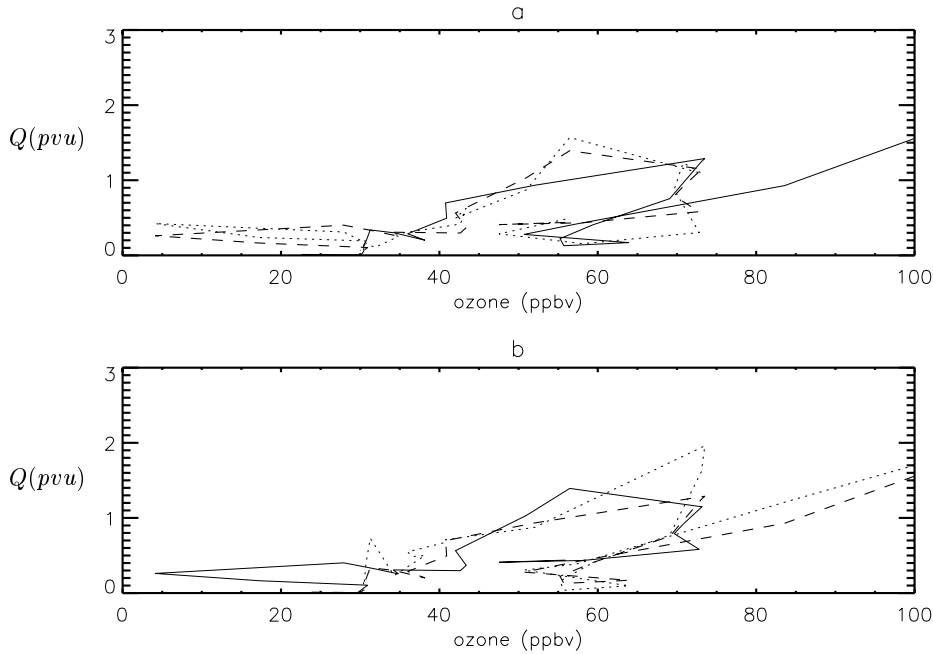


Figure 4.4: Comparison of the relation between the absolute value of Q (in units of pvu) and ozone (in units of ppbv) at times t_1 and t_2 ($t_1 = 17$ July 10 UTC 1998, $t_2 = t_1 + 8h$), where $Q(t)$ has been computed either from ECMWF data at time t (denoted by Q_e) or from 6-hour back trajectories starting at time t (denoted by Q_b). See the text for details. For a) solid line = Q_{e1} , dashed line = Q_{e2} , dotted line = Q_{b2} . For b) solid line = Q_{e2} , dashed line = Q_{e1} , dotted line = Q_{b1} .

In Figure 4.4 the solid and dashed lines show the values of ozone versus $|Q_e|$ along a vertical profile above La Reunion at times t_1 and t_2 , where $t_1 = 980717$ 10 UTC and $t_2 = t_1 + 8$ hours. These Q_e values, hereafter denoted by Q_{e1} and Q_{e2} , have been computed from ECMWF data at t_1 and t_2 for the levels at which these data are available (see section 4.2.2). The measured ozone values have been averaged over the layers to which these levels apply. Both the solid and the dashed line shows the presence of a tropopause fold: following the lines from 30 ppbv to the right in the figure, which corresponds to going up in the atmosphere, the ozone values increase to about 75 ppbv in the centre of the fold, then decrease (following the lines to the left) to about 50 ppbv in the troposphere between the fold and the stratosphere, and finally increase to more than 100 ppbv at stratospheric levels. Also the profiles of Q_{b1} and Q_{b2} have been determined, by computing 6-hour back trajectories starting at the different levels above La Reunion at, respectively, $t = t_1$ and $t = t_2$, and setting Q_b

equal to the Q at $x_1, t_0 - \Delta t$, after a linear regression of Q versus time along the 6-hour back trajectory. The values of ozone and $|Q_b|$ above La Reunion are shown by the dotted lines in Figure 4.4.

According to *Haynes and McIntyre* [1990], ‘adiabatic mixing’ does not exist. On the other hand they state that for most tropopause folds the diabatic changes in Q because of mixing will be small. *Ravetta et al.* [1999] also found that only in a small part of the fold diabatic mixing plays a role. Therefore, as a next step, it is assumed that during the period $[t_1, t_2]$ diabatic and frictional sources of Q and chemical sources of ozone can be neglected, which is a reasonable assumption for such a short time period. Under this assumption, mixing is the only ‘source’ of the gridbox-averaged ozone and Q . Also it is assumed that within an air-mass mixing does not affect the relation between ozone and Q , i.e. this relation is assumed to be linear [*Plumb and Ko*, 1992; *Danielsen*, 1990]. In Figure 4.4a two different air-masses can be identified in which at t_1 and t_2 the ozone- Q_e relation is more or less the same (i.e. where the dashed line is relatively close to the solid line): below and above the ozone maximum in the fold. This similarity might imply that the change between t_1 and t_2 is mainly due to advection. However, it is also possible that there is substantial mixing. In that case the similarity would imply that the mixing is parameterised reasonably well in the ECMWF model. Figure 4.4a shows that there is indeed substantial mixing, since there are substantial differences of about 10%, between Q_{e2} and Q_{b2} . In addition, the difference between Q_{e2} and Q_{e1} , averaged over the fold from 45 ppbv to the ozone maximum and back to 50 ppbv, is 0.2 pvu, whereas the difference between Q_{b2} and Q_{e1} is about 50% larger. Hence, the invariance of the ozone- Q relation is improved by the mixing (which determines the difference between Q_{b2} and Q_{e2}). This result improves our confidence in the accuracy of the computed dQ/dt , and of the related magnitude of F . The same conclusion applies to Figure 4.4b, in which Q_b has been determined for the Q -profile at t_1 .

4.3.2 Exchange in the fold: time and area integration

In order to evaluate the flux for various Q surfaces, outside the fold and through the different parts of the fold, and to intercompare the exchange of air inside and outside the fold, the fluxes are integrated over time and space. The result is shown in Figure 4.5. The time period over which the integration is performed is from 14 July 1998 00 UTC to 18 July 1998 12 UTC and the considered area is from 35° to 120°E and from 15° to 40°S. The flux has been integrated for the Q levels of -1.5 , -2.0 and -2.5 pvu, and for the separate fluxes, i.e. F_1 (through the upper part of the fold), F_2 (through the middle part) and F_3 (through the lower part) and F_{tot} (the total flux).

In the fold the net exchange is largest in its lower part (F_3). In the upper part

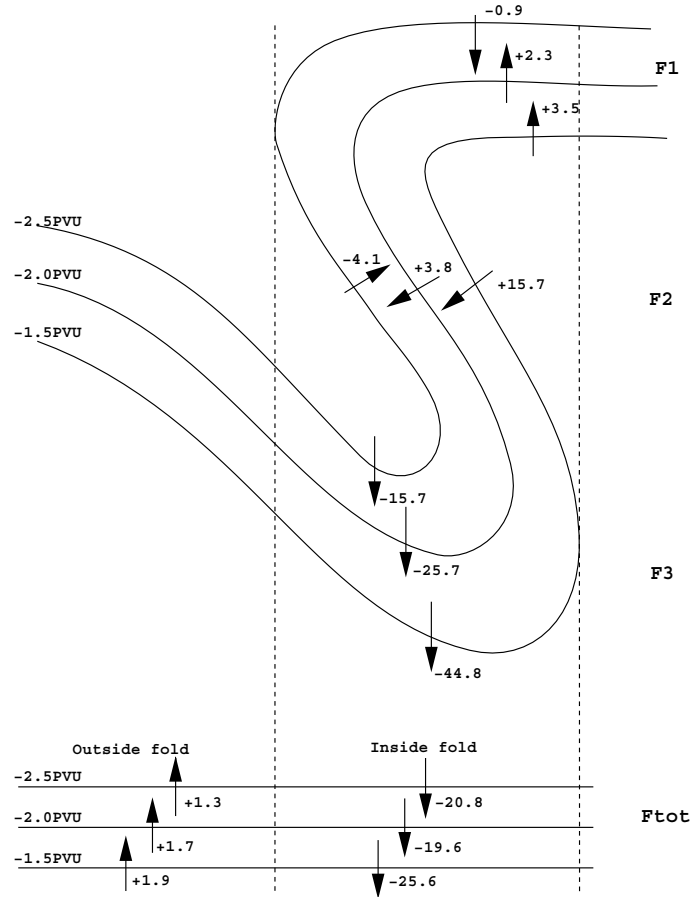


Figure 4.5: Time (14 July 1998 00 UTC-18 July 1998 12 UTC) and area (35° - 120° E/ 15° - 40° S) integrated mass flux across the -1.5 , -2 and -2.5 pvu surfaces ($\times 10^{13}$ kg). The upper part of the figure displays the integrated flux through the different tropopause regions in the fold, the lower part displays the total mass flux ($F_{tot} = F_1 + F_2 + F_3$) inside and outside the fold. On 17 July 1998 12 UTC 10% of the area was covered by the fold.

(F_1), the exchange is small, but still larger than outside the fold. The net exchange in the middle part of the fold (F_2) is about 3-5 times smaller than in the lower part. This is in agreement with Shapiro [1980], who also found the largest exchange in the lower part of the fold.

A striking feature is that for F_2 and for F_1 inside the fold opposite signs are found for the cross- Q air-mass flux through the various Q levels. This might be because the windshear maximum is found in this area, and the exchange can be expected

to be bidirectional. This is in agreement with *Ravetta et al.* [1999], who showed that the turbulent heat flux in the vicinity of large wind shear around the jet core which is situated at the middle part of the fold, is responsible for exchange towards the stratosphere. In the lowest part of the fold the exchange is directed towards the troposphere. Outside the tropopause fold the net exchange is directed towards the stratosphere.

In the fold the value for the net F_{tot} is -20×10^{13} kg, whereas in the area outside the fold the value is about 1×10^{13} kg. About 10% of the area was covered by the fold, therefore it follows from these values that the ratio of the fluxes per unit of area in and outside of the fold is about 200:1.

The net mass exchange for the total area is about -20×10^{13} kg in 4.5 days for all three Q surfaces. Not much studies of mass exchange have been performed in the subtropics yet. Compared to midlatitude studies this estimate is closest to the study of *Vaughan et al.* [1994], who estimated a mass exchange of around -20×10^{13} kg in 1.5 days. Compared to other midlatitude studies the estimate of our study is rather small. E.g., *Lamarque and Hess* [1994] found a net mass exchange of -4.9×10^{14} kg in 4 days, *Reiter and Mahlman* [1965] found -6×10^{14} kg in 2 days and *Reiter et al.* [1969] -4.8×10^{14} kg in 4 days. These larger fluxes in the midlatitudes are in agreement with *Gouget et al.* [1996], although from the lack of studies in the subtropics it cannot be said how much smaller the exchange can be expected to be in the subtropics.

It would be interesting to consider the difference in magnitude between the integrated fluxes in the lower and middle part of the fold, and to see why the integrated fluxes in the upper part of the fold and outside the fold are small. Therefore, in Figure 4.6 the probability density function is given for the local instantaneous values of F_1 for the total area where the flux was calculated for (0-160°E, 10-50°S), and for F_2 and F_3 in the tropopause fold. This figure shows that the distribution for F_1 has a smaller width and a larger symmetry than the distributions for F_2 and F_3 . As a consequence, the integrated flux for F_1 is smaller than those of F_2 and F_3 . For F_2 and F_3 the difference between the probability density functions is not as large as might be expected from the difference in magnitude in the net mass exchange of Figure 4.5, but it is clear that the distribution for F_3 is more asymmetric in such a way that a larger percentage of the values has a negative sign than for the distribution of F_2 .

The distribution in Figure 4.6a can be compared with the distribution given by *Siegmund et al.* [1996]. The mean values of the upward and downward F of the latter distribution are, respectively, 2.66×10^{-3} kg m⁻² s⁻¹ and -2.73×10^{-3} kg m⁻² s⁻¹. The values found in this study are, respectively, 2.23×10^{-3} kg m⁻² s⁻¹ and -2.54×10^{-3} kg m⁻² s⁻¹. A narrower distribution in the present results might be due

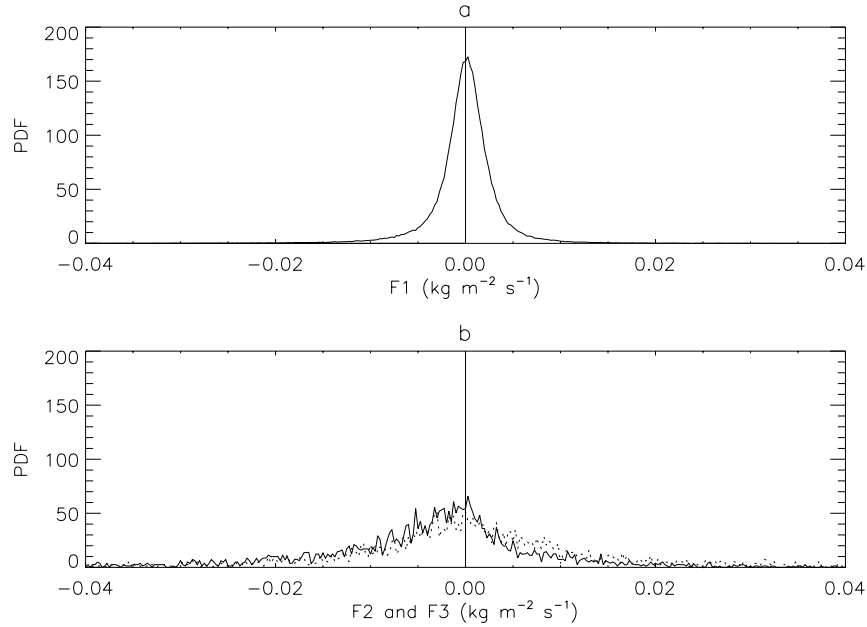


Figure 4.6: Probability density functions of the local instantaneous values of F_1 (a, for $0\text{-}160^\circ\text{E}$ to $10\text{-}50^\circ\text{S}$), and of F_2 and F_3 (b, dotted and solid line, respectively), both for the same 4.5 day period as in Figure 4.5. On the x-axis F (in $\text{kg m}^{-2} \text{s}^{-1}$) is displayed. The interval over which the F 's are summed is $0.00025 \text{ kg m}^{-2} \text{ s}^{-1}$.

to less noise, compared to the results obtained by Siegmund et al. Another reason could be that the two results are not completely comparable because the midlatitudes are also taken into account in the study of Siegmund et al., where the exchange is expected to be larger.

4.4 Discussion and conclusions

In this work a Lagrangian method to calculate the air-mass flux across Q surfaces is used for a Southern Hemisphere subtropical tropopause folding event above the Indian Ocean. A qualitative evaluation is performed to evaluate the geographical distribution of the calculated flux and a quantitative evaluation is performed to evaluate the magnitude of the flux for this tropopause folding case.

The results show that the largest fluxes are calculated in areas where the largest exchange is expected, i.e. in tropopause folds and upper level troughs, and that outside these areas the exchange is small. The largest fluxes occur in regions with strong ver-

tical windshear. In the fold the largest fluxes are found for the lowermost tropopause region. Positive and negative numbers are found close to each other, at locations where small-scale mixing is expected, leading to bidirectional exchange.

What could be the case for the method applied here is that the values found for the air-mass flux might become erroneously large near steep surfaces, where the term $\partial p/\partial Q$ becomes large. This is particularly the case for F_2 and F_3 . To investigate this, the percentage of calculated fluxes which are not taken into account, i.e. which are larger than 0.05 or smaller than $-0.05 \text{ kg m}^{-2} \text{ s}^{-1}$, are calculated. The percentage of values not taken into account is about 10% for F_2 and F_3 , and less than 1% over the total area. When taking an even higher threshold of $0.1 \text{ kg m}^{-2} \text{ s}^{-1}$, less than 1% of F_2 and F_3 is not taken into account. Hence, the problem of erroneously large values of $\partial p/\partial Q$ exists only in a small part of the total area.

Compared to other methods, it is found that the probability density function of the fluxes calculated with the new method is narrower. This is believed to be an indication that the new method is more reliable because numerical noise is expected to be partly responsible for the tails of the distributions evaluated with the other techniques. On the other hand, it could be a consequence of the fact that fluxes are expected to be smaller in the subtropics.

Because Southern Hemisphere subtropical folds have not often been investigated, and because of the special case of this fold being linked to the Hadley circulation, it is difficult to compare the results of this study with former results. As far as can be concluded now from the quantitative evaluation, the magnitude of the calculated cross- Q air-mass fluxes are within the expected range of values. When comparing the Q /ozone relation for which the Q is derived directly from the ECMWF and the relation for which the Q is derived with the help of back trajectories (Figure 4.4), it is found that the mixing included in the ECMWF model improves the invariance of the Q /ozone relation. This improves our confidence in the computed dQ/dt and the associated cross- Q air-mass flux. However, an intercomparison with other (trajectory) models or case studies would be useful.

Acknowledgements We gratefully acknowledge R. Scheele, for his help on the trajectory model and P. van Velthoven for helpful discussions. Comments of two anonymous reviewers helped improve the manuscript, and were greatly appreciated. This study has been supported by the European Union TRACAS project, EU grant ENV4-CT97-0520.

Stratosphere-troposphere exchange: model and method intercomparison

This chapter presents one of the first extensive intercomparisons of models and methods used for estimating stratosphere-troposphere exchange (STE). The study is part of the EU-project STACCATO (Influence of Stratosphere Troposphere Exchange in a Changing Climate on Atmospheric Transport and Oxidation Capacity). Nine different models and methods including three trajectory methods, one Eulerian method, two Lagrangian and one Eulerian transport model, and two general circulation models, applied a uniform initialisation. Stratospheric and tropospheric tracers have been simulated and the tracer mass fluxes have been calculated through the tropopause and the 700 hPa surface. For a 12-day case study over Europe and the north east Atlantic the simulated tracer mass fluxes have been intercompared. For this case the STE simulations show the same temporal evolution and the same geographical pattern of STE for most models and methods, but with generally different amplitudes (up to a factor four). On the other hand, for some simulations also the amplitudes are very similar. The horizontal resolution has found to be an important cause for differences between the models and methods. Also the numerical diffusion plays an important role in the simulation of the stratospheric tracer distribution in the troposphere, just as the difference between on-line and off-line models.

5.1 Introduction

Despite extensive research on stratosphere-troposphere exchange (STE) and its effect on atmospheric chemistry, there are still large uncertainties in the qualitative and quantitative characteristics of STE. For several purposes it is important to reproduce the transport processes throughout the upper troposphere and lower stratosphere correctly, e.g. for the assessment of the atmospheric impact of aircraft emissions [Rogers *et al.*, 2002], or for the estimation of the influence of stratospheric ozone on tropospheric chemistry [Roelofs and Lelieveld, 1997]. Recently, Butchart and Scaife [2001] predicted an increase of air-mass exchange from the troposphere to the stratosphere with 3% per decade due to enhanced greenhouse gas concentrations. In order to investigate the impact of enhanced greenhouse gas concentrations on STE it is important to reproduce the involved transport processes correctly. For the overall influence of STE on the dynamics and chemistry of the atmosphere not only more research on the dynamical and physical details of the exchange processes is required, but also the confidence in the used diagnostic methods needs to be increased.

For the estimation of STE a range of methods is in use. On the global-scale residual mean mass fluxes in the stratosphere have been calculated, e.g., by Holton [1990] and Rosenlof and Holton [1993] using the downward control principle. Follows [1992] estimated the global cross-tropopause mass flux from the evolution of the budget of CFCs in the troposphere and stratosphere. The net mass transport across the tropopause has been analysed by Appenzeller *et al.* [1996] by estimating the global-scale stratospheric meridional circulation and the seasonal mass variation of the stratosphere. Hoerling *et al.* [1993] made a global analysis of the monthly-mean air-mass flux across the tropopause including both the diabatic transport and the quasi-horizontal isentropic transport. The contour advection technique was used by Dethof *et al.* [2000] to quantify the global quasi-horizontal, isentropic mass transport across the dynamical tropopause due to small-scale filamentation. Other studies calculated isentropic cross-tropopause mass exchange, using a semi-Lagrangian transport model [Chen, 1995] or a two-dimensional model of isentropic turbulence [Hartjenstein, 2000].

STE has also been investigated for specific events, e.g. for stratospheric intrusions or cut-off lows. Several quantitative estimates of STE have been derived from observations of ozone and nitrogen oxides [Danielsen, 1968; Murphy *et al.*, 1993], radioactive tracers [Staley, 1960; Danielsen, 1968], or various other stratospheric constituents that are conserved on a relatively long time scale. Ancellet *et al.* [1991] combined lidar measurements with trajectories to calculate air-mass exchange for several cases. Gouget *et al.* [2000] investigated mechanisms for STE and the associated mass flux

in a cut-off low with the help of trajectories and MOZAIC (Measurement of Ozone and water vapour by Airbus In-service airCraft) data.

The exchange of air-mass between the stratosphere and the troposphere for specific events or longer time periods can also be estimated directly from the three-dimensional fields of wind and temperature, as computed by numerical weather prediction and general circulation models (GCMs). Several studies calculated instantaneous spatial distributions of air-mass exchange using the method described by *Wei* [1987], e.g. *Grewe and Dameris* [1996], *Siegmund et al.* [1996] and *Gottelman and Sobel* [2000]. A disadvantage of this method is that it is less reliable, because it suffers from an almost cancellation of large terms [*Wirth and Egger*, 1999]. In *Spaete et al.* [1994] the STE for a single event is estimated with a semi-Lagrangian transport model. Recently new methods for the calculation of STE based on trajectory calculations were developed. For instance, *Sigmond et al.* [2000] and *Meloen et al.* [2001] applied the Wei formula to trajectory model output.

Early model estimates of the vertical transport of ozone across the tropopause have been made by *Mahlman et al.* [1980] and by *Gidel and Shapiro* [1980]. They studied the effect of transport on the ozone distribution with a GCM. Recently GCMs have been interactively coupled with global chemistry, with which STE events and the associated amount of stratospheric ozone transferred into the troposphere during the event have been estimated [*Kentarchos et al.* 1999].

Quantitative comparison of the results of studies on STE with different methods is difficult, because of the use of different time periods and different events. Given the wide range of available methods it is important to perform objective intercomparisons in well-defined circumstances. Some intercomparison studies with a few different models and methods for an individual case have already been performed. *Kowol-Santen et al.* [2000], for example, implemented a trajectory based method and the method developed by *Wei* [1987] in a mesoscale model and compared the results of these two methods, which showed good agreement between the net flux values. By employing the trajectory method they also estimated STE for different meteorological situations. *Wirth and Egger* [1999] compared five methods to diagnose STE, three of which were derived from Wei's general formula, one involved the computation of a large number of trajectories, and one evaluated the flux directly as the difference between the motion of the air and the motion of the tropopause. They found that the different methods to quantify STE yield quite different results.

The present STE intercomparison study adds to the existing studies on three aspects. First, the number of applied models and methods is larger, second, also the range of the applied models and methods is larger and, finally, the model results are evaluated with measurements. Within the scope of STACCATO (Influence of

Stratosphere-Troposphere Exchange in a Changing Climate on Atmospheric Transport and Oxidation Capacity), nine different models and methods to estimate mass exchange have been applied. These models and methods range from trajectory based analyses to Lagrangian models to GCMs, with different horizontal and vertical model resolutions and different sub-grid scale parameterisations. The models and methods were applied for the calculation of idealised tracer mass exchange. This was done for a specific event, from 26 May until 7 June 1996 over central Europe. In this period a deep stratospheric intrusion took place with associated STE. The intercomparison set-up, the case study episode and the broad range of models and methods is an excellent way for an extensive intercomparison of estimated STE. The evaluation with measurements is described in the companion paper by *Cristofanelli et al.* [2002].

In section 5.2 the intercomparison set-up is described (section 5.2.1) and a summary is given of the applied models together with an outline of the quantification methods (section 5.2.2). Section 5.3 gives a short overview of the meteorological case for which the intercomparison is performed. In section 5.4 the results of the intercomparison are described, starting with the flux through the tropopause (section 5.4.1), followed by the results for the tracer fluxes across the 700 hPa surface (section 5.4.2). Finally time versus height plots are presented for the observation station Mt. Cimone (section 5.4.3). Section 5.5 provides a discussion and the main conclusions.

5.2 Intercomparison: set-up, models and methods

5.2.1 Intercomparison set-up

For the intercomparison a case has been selected that occurred from 26 May 00 UTC to 7 June 00 UTC 1996. All models and methods have generated output for the region of interest that extends from 20°N to 70°N and from 20°W to 40°E. Models which require a spin up time (FLEXPART, ECHAM4, MA-ECHAM4 and TM3), are started on 1 May 1996.

All models are initialised as similarly as possible. The tropopause is defined at a potential vorticity (Q) value of 2 pvu ($1 \text{ pvu} = 10^{-6} \text{ K m}^2 \text{ kg}^{-1} \text{ s}^{-1}$). Ideal stratospheric and tropospheric tracers with a mixing ratio of 1 kg/kg are then inserted in the stratosphere and troposphere, respectively. Stratospheric tracers are only inserted above the 700 hPa surface, to exclude tropospheric air with high Q values due to friction or diabatic heating in the boundary layer. If a stratospheric (tropospheric) air parcel crosses the tropopause and enters the troposphere (stratosphere), the tracer mass decays exponentially with a time constant of 2 days. The stratospheric (tropospheric) tracer mixing ratios are kept at a constant value of 1 kg/kg in the stratosphere (troposphere).

A tracer decay has been used, because this gives the atmosphere the possibility to establish an equilibrium between supply and decay of the tracers. Without this decay the troposphere (stratosphere) would slowly fill up with stratospheric (tropospheric) tracer. A decay time of 2 days has been chosen in order to limit the trajectory calculations to 10 days, a period beyond which the accuracy of the trajectories gets low.

If the tracer crosses the tropopause several times, different approaches are applied by the different methods. For the trajectory methods (LAGRANTO, FLEXTRA and TRAJKS) the decay only starts after the last crossing, i.e. every time the tracer returns to its original reservoir, the tracer mixing ratio is reset to 1 kg/kg, and no exchange takes place before the last crossing. The other approaches (FLEXPART, Wei method, STOCHEM, TM3, ECHAM4 and MA-ECHAM4) are not able to use such a method, because they cannot follow air parcels. Therefore, with these other approaches mixing takes place every time a certain amount of air passes the tropopause.

Because the 700 hPa surface is situated entirely in the troposphere for the considered case study, the stratospheric tracer flux at this pressure surface can be used as a measure of deep STE (see section 5.4.2). Therefore, every 3 hours upward and downward fluxes of the inserted stratospheric and tropospheric tracers are calculated at this pressure surface. In addition, the vertical velocity and the tracer concentrations are considered. As a direct measure of STE air-mass fluxes through the tropopause have been calculated by some of the models and methods. To highlight the meteorological events, 24-hour running means have been calculated for all model output.

For ten measurement sites, the models computed vertical profiles of the stratospheric tracer concentration, that also will be intercompared. The complementary study by *Cristofanelli et al.* [2002], compares the model results from this study with vertical profile measurements or surface measurements of water vapour, ozone and radio nuclides at some of these measurement sites.

5.2.2 Models and methods

The nine models which are used to simulate STE are briefly described in Table 5.1. In Table 5.2 the methods applied for calculating STE are summarised. For the three methods that are based on trajectories, three trajectory models, LAGRANTO, FLEXTRA and TRAJKS, have been used. These models (but not the methods) have been intercompared by *Stohl et al.* [2001]. The methods of the flux calculation through the 700 hPa surface applied by LAGRANTO and FLEXTRA are similar. They used the formula $F = cw$, where c denotes the tracer concentration (kg m^{-3}), and w denotes the vertical velocity (m s^{-1}). The concentration is determined by means of 10-day backward trajectory calculations, starting on the pressure surface every 3 hours on

Table 5.1 Overview of models and methods used in the intercomparison.

Model	LAGRANTO	FLEXTRA	TRAJKS	FLEXPART	Wei method	STOCHEM	TM3	ECHAM4	MA-ECHAM4
Institute	ETHZ	TUM	KNMI	TUM	KNMI	MetO	KNMI	IMAU	MPI
Type of model	Trajectory	Trajectory	Trajectory	Lagrangian	Direct use of ECMWF data	Lagrangian transport	Eulerian transport	mudged GCM	mudged GCM
Reference	<i>Wernli and Davies</i> [1997]	<i>Stohl et al.</i> [1995]	<i>Scheele et al.</i> [1996]	<i>Stohl et al.</i> [1998]		<i>Collins et al.</i> [1997]	<i>Meyer et al.</i> [2000]	<i>Roegner et al.</i> [1996]	<i>Mansini and McFarlane</i> [1998]
	<i>Stohl et al.</i> [2001] for trajectory intercomparison		Trajectory model	<i>Stohl and Thomson</i> [1999]		<i>Collins et al.</i> [2002]		Nudging: <i>Jeuken et al.</i> [1996]	
Updates since reference							Fluxes computed from spectral fields directly		Advection scheme SPITFIRE (<i>Rasch and Lawrence</i> , 1998) applied
Input data									
Horizontal resolution	$1^\circ \times 1^\circ$	$1^\circ \times 1^\circ$	$1^\circ \times 1^\circ$	$1^\circ \times 1^\circ$	$0.5^\circ \times 0.5^\circ$	$3.75^\circ \times 2.5^\circ$	$2.5^\circ \times 2.5^\circ$	$1.85^\circ \times 1.85^\circ$	$3.75^\circ \times 3.75^\circ$
Vertical resolution	31	31	31	31	31	38	31	19	39 (top 0.01 hPa)
Temporal resolution input data	6 hours	3 hours	6 hours	3 hours	3 hours	6 hours	6 hours	6 hours	6 hours
Convection scheme	No	No	No	Yes	No	Yes	Yes	Yes	Yes
Planetary Boundary layer scheme	No	No	No	Yes	No	Yes	Yes	Yes	Yes

a $1^\circ \times 1^\circ$ grid. Along the trajectory Q is computed, thereby allowing to determine tropopause crossings. To calculate the concentration of the stratospheric and tropospheric tracers on the pressure surfaces, it is only necessary to know the time of the last crossing through the tropopause.

With LAGRANTO also the flux through the tropopause is calculated. The approach to obtain fluxes across the 2 pvu surface is identical to the method described by *Wernli and Bourqui* [2002]. Trajectories are started in the entire Northern Hemisphere every 24 hours on a regular grid with a horizontal (vertical) spacing of 80 km (30 hPa) between 80 and 600 hPa. The air parcels represented by these trajectories are only considered as exchange events if they cross the tropopause within 24 hours and if they reside for at least 1 day in the stratosphere before crossing the 2 pvu surface and at least 1 day in the troposphere after the crossing or vice versa for troposphere to stratosphere exchange. With this second criterion, parcels that move transiently across the tropopause on short time scales are eliminated. By keeping up a budget of when and where the trajectories pass the tropopause, the flux in the domain specified for this case study can be calculated.

With the TRAJKS trajectory model only fluxes through the tropopause are calculated, with a different method compared to LAGRANTO [*Meloen et al.*, 2001]. For the TRAJKS method the equation derived by *Wei* [1987] is used, with Q as the vertical coordinate. Every 3 hours a 48-hour forward and 48-hour backward trajectory is calculated at the tropopause from a regular grid with $1^\circ \times 1^\circ$ resolution. In the present study the method used in *Meloen et al.* [2001] is extended with a residence time criterion [*Wernli and Bourqui*, 2002]. This means that the flux is calculated only for those air parcels which reside 48 hour in the stratosphere and troposphere before and after the exchange. This is done to eliminate air parcels that move rapidly to and fore across the tropopause. Of those air parcels that satisfy the residence time criterion, only the first 12 hours are used as input for the *Wei* equation, from which the flux is derived.

Apart from the trajectory methods, two Lagrangian transport models, FLEXPART and STOCHEM, are used in this intercomparison. In these models, 8 million and 100.000 particles are initialised, respectively. Unlike the trajectory models, these models contain parameterisations of sub-grid scale convection and turbulence. Tracer concentrations are determined by the tracer masses of the particles located within a grid cell. Upward and downward tracer fluxes are determined by keeping a budget of the particle tracer masses crossing the surfaces within 3-hour periods.

With the Eulerian *Wei* method the mass flux across the tropopause has been calculated by applying *Wei*'s equation in isobaric coordinates [*Siegmund et al.*, 1996]. The cross-tropopause flux for the time interval $[t_0, t_0+3h]$ is computed from data at

Table 5.2 Overview of the applied methods.

Model	LAGRANTO	FLEXTRA	TRAJKS	FLEXPART	STOCHEM	Wei method	TM3	MA-ECHAM4	ECHAM4
Flux calculated for	700 hPa +	700 hPa	2 pvu	700 hPa +	700 hPa	2 pvu	700 hPa	700 hPa	700 hPa
Method for calculating flux through 700 hPa surface	2 pvu $F = [\text{tracer}] \times w$ Tracer concentration: determined with backtrajectories, starting at 700 hPa	2 pvu	2 pvu	Lagrangian advection of 8 million particles.	100.000	–	Direct calculation of flux from vertical transport of tracers.	–	$F = \frac{1}{g} \times \omega \times \text{mixing ratio}$
Method for calculating flux through 2 pvu surface	Budget study of when and where trajectories pass the tropopause. Trajectories are started in the troposphere and stratosphere in the entire Northern Hemisphere.	–	Trajectory model output used as input for Wei's [1987] equation. Trajectories are started on the tropopause.	Budget study of particles that crossed the 2 pvu surface.	–	ECMWF model output directly used as input for Wei's [1987] equation.	–	–	–

t_0 and t_0+3h . To ensure physical consistency, they are taken from the same ECMWF forecast. For example, the flux for the 9-12 UTC time interval is computed from the 3-hour and 6-hour forecasts based on the analysis at 6 UTC. Fluxes with an amplitude smaller than $0.005 \text{ kg m}^{-2} \text{ s}^{-1}$ are considered as noise and are not taken into account.

Besides FLEXPART and STOCHEM, three other global models, TM3, ECHAM4 and MA-ECHAM4, are used to calculate the stratospheric tracer flux through and the concentration on the 700 hPa surface. Like FLEXPART and STOCHEM, TM3 is driven by ECMWF wind fields. ECHAM4 and MA-ECHAM4 are atmospheric general circulation models. TM3 and MA-ECHAM4 calculate the stratospheric tracer fluxes directly from the vertical transport of the tracers. ECHAM4 calculated the stratospheric tracer fluxes through the 700 hPa surface as $(1/g) \times \omega \times \text{mixing ratio}$ of the tracer on the pressure surface, where g is the acceleration due to gravity and ω the vertical velocity in pressure coordinates. With STOCHEM, TM3, ECHAM4 and MA-ECHAM4 the fluxes through the tropopause have not been calculated, because the tropopause is not a predefined model level and rapidly moves up- and downward. As a consequence, interpolation to it would lead to large errors in the computed fluxes.

5.3 Meteorological situation

The period for which the model simulations have been performed, is from 26 May 00 UTC until 7 June 00 UTC 1996. This period has been considered previously in studies by e.g. *Bonasoni et al.* [2000], *Stohl et al.* [2000] and *Eisele et al.* [1999]. Extensive observations made in this period indicate a deep stratospheric intrusion with associated STE. Therefore, this period is an attractive case for this model intercomparison. During this period several weather systems developed and decayed within the region of study, as described by *Stohl et al.* [2000]. An example is shown in Figure 5.1. Q on the 320 K isentropic surface on 28 May 1996 12 UTC shows a southward extrusion of stratospheric air over central Europe (Figure 5.1a). A vertical cross-section through this stratospheric filament (Figure 5.2), reveals the considerable depth of the extrusion into the troposphere. During the next day, the extrusion transformed into a cut-off low (Figure 5.1b), which decayed rapidly over the eastern Mediterranean (Figure 5.1c).

5.4 The model and method intercomparison

In this section the results of the intercomparison are described. In section 5.4.1 the computed cross-tropopause mass fluxes are presented. In section 5.4.2 emphasis is laid on the results for the 700 hPa surface, by discussing the time series of the

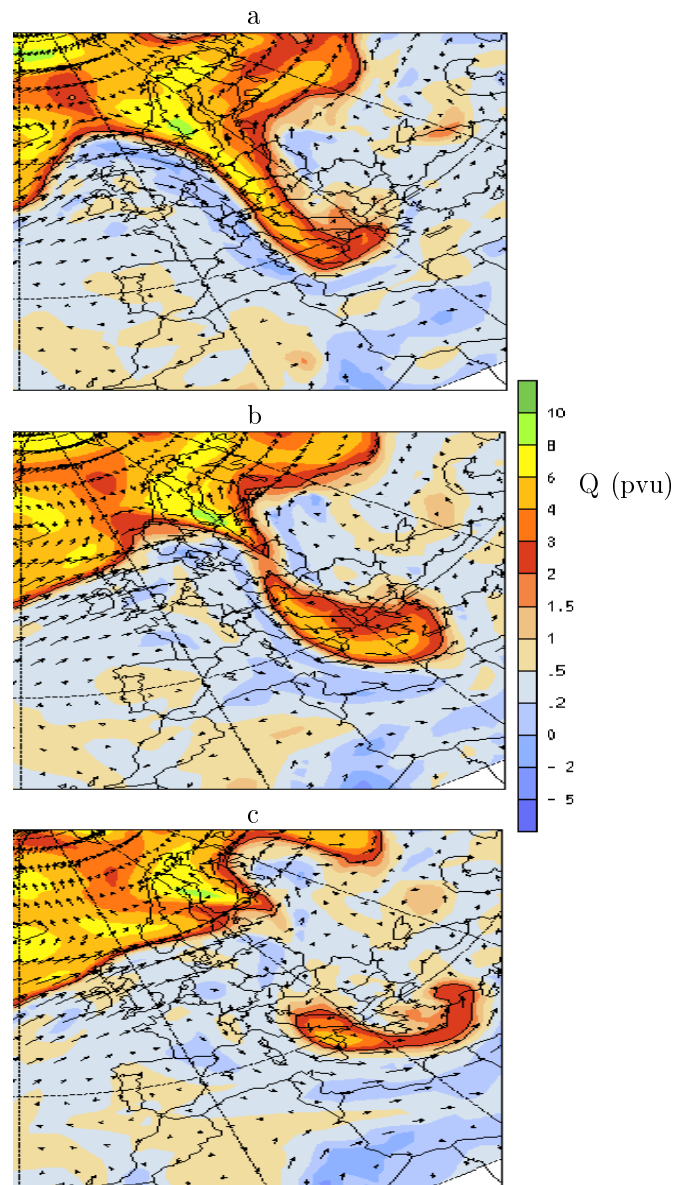


Figure 5.1: Potential vorticity on the 320 K isentropic surface for 28 May 12 UTC (a), 29 May 00 UTC (b) and 29 May 12 UTC 1996 (c), computed from ECMWF analyses.

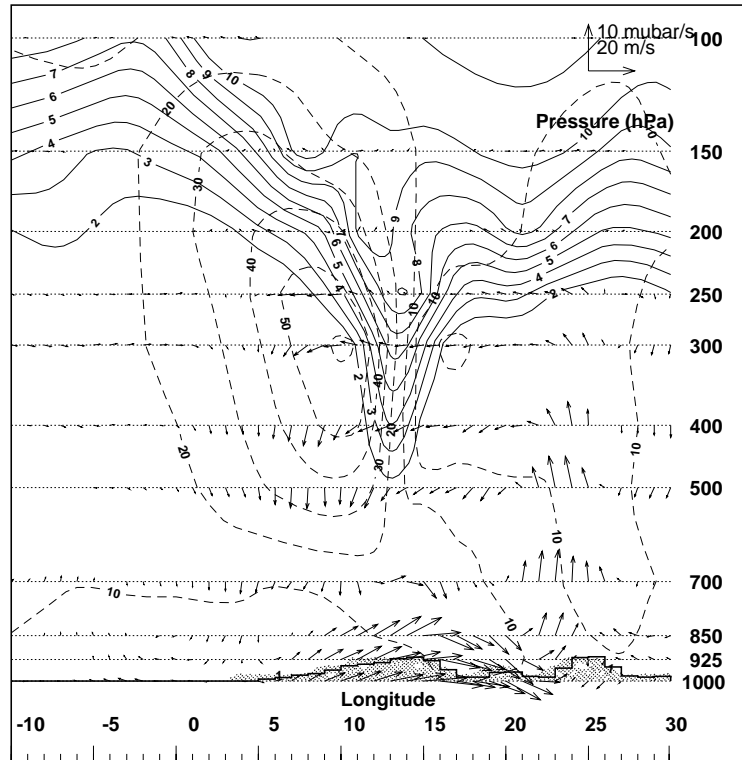


Figure 5.2: Vertical cross-section of the potential vorticity (in pvu, solid lines), the wind field (in m/s, dashed lines) and ageostrophic wind vectors on 28 May 1996 12 UTC, computed from ECMWF analysis. The vertical cross-section is made at 48°N.

domain-integrated stratospheric tracer concentration (5.4.2), the tropospheric tracer flux (5.4.2), the stratospheric tracer flux (5.4.2) and the latitude/longitude fields of the stratospheric tracer flux (5.4.2). Finally, in section 5.4.3 time versus height plots are shown for the station Mt. Cimone (44°N, 10.5°E, 2165 m asl).

5.4.1 Cross-tropopause mass fluxes

A direct measure of STE is the air-mass flux through the tropopause, which was defined in this study as the 2 pvu surface. Unfortunately only four of the nine models are able to calculate the air-mass flux through the 2 pvu surface. From Figure 5.3 which displays the net and the individual up- and downward fluxes, it can be seen that TRAJKS and LAGRANTO give very similar results. Although both methods use ECMWF data and trajectories, this similarity is quite surprising since the applied

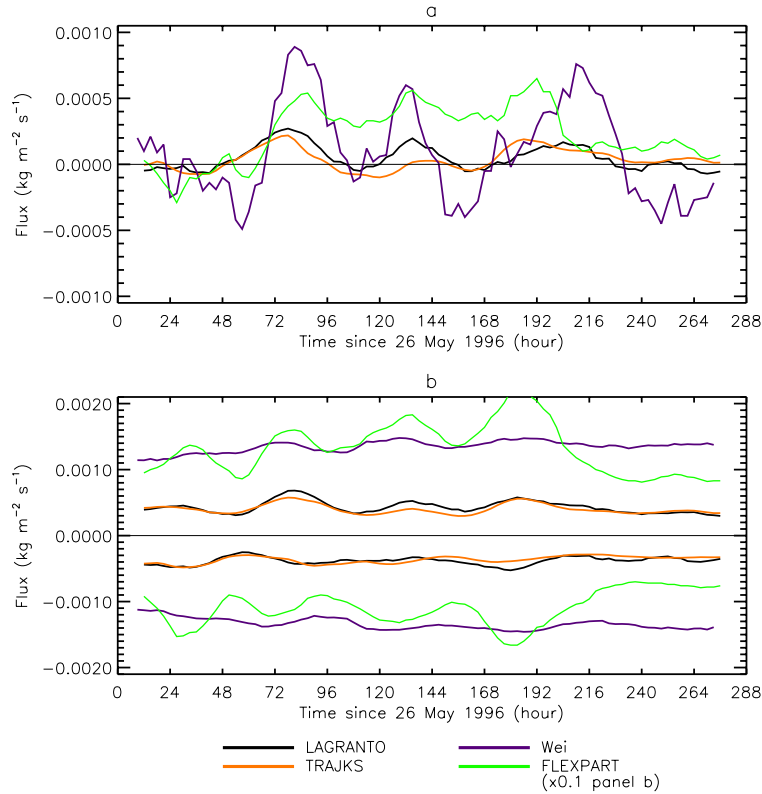


Figure 5.3: Time series of the net air-mass flux (a) and the up- and downward air-mass fluxes (b) through the tropopause. The legend is valid for both panels. In panel (b) the results of the FLEXPART model have been multiplied by 0.1. Positive values correspond to downward fluxes, negative values to upward fluxes.

methods are very different. The LAGRANTO method starts trajectories through almost the entire troposphere and stratosphere and keeps a budget of trajectories passing the tropopause, whereas the TRAJKS method only starts trajectories on the tropopause and uses the potential vorticity along the trajectories to solve the Wei formula which gives the air-mass exchange through the tropopause.

The Eulerian Wei method and the FLEXPART model show the same events as LAGRANTO and TRAJKS, but with a larger amplitude. This is most clearly illustrated by the up- and downward tracer fluxes through the tropopause in Figure 5.3b. Especially FLEXPART, whose results have been multiplied by 0.1 in Figure 5.3b, yields about ten times larger up- and downward mass fluxes than the three

other methods. The difference with the LAGRANTO and TRAJKS method is, that there is no residence time criterion applied in FLEXPART. In *James et al.* [2002] it is found that most of the air parcels that cross the tropopause, return to their original reservoir within 24 hours. Thus, if these fluxes would have been excluded, results would have likely been more similar to the LAGRANTO and TRAJKS results. Furthermore, turbulent and convective fluxes are included in the FLEXPART model, possibly explaining the larger FLEXPART net fluxes.

5.4.2 Stratospheric tracer concentration and flux at the 700 hPa surface

The pressure surface of 700 hPa has been chosen for the intercomparison of the models and methods because it is entirely located in the troposphere for this case study (cf. Figure 5.2). The 700 hPa stratospheric tracer concentration and flux are therefore indirect measures of deep STE. Pressure surfaces above 500 hPa are in this case situated partly in the stratosphere and partly in the troposphere. On these levels differences in the fluxes between the models can therefore not only be attributed to differences in STE, but also partly to slight differences in tropopause height in the models. When comparing the 700 hPa stratospheric tracer results with results for pressure surfaces at higher altitudes, it is found that the different model results are more similar for the higher altitude pressure surfaces. This is as expected, because these surfaces are closer to the stratospheric tracer's source region, and because they are situated partly in the stratosphere. For the 700 hPa surface, the obtained stratospheric tracer concentrations and fluxes are entirely due to STE and the subsequent transport of the stratospheric tracer down into the lower troposphere.

Time series of the stratospheric tracer concentration

The time series of the domain-averaged stratospheric tracer concentration at 700 hPa is shown for several models in Figure 5.4. It can be seen that MA-ECHAM4 and ECHAM4 (which results have been multiplied by 0.5 in Figure 5.4) give much larger stratospheric tracer concentrations than the other models. This is partly due to numerical diffusion. Especially in the presence of large gradients, as is the case for the stratospheric tracer at the tropopause level, these models tend to decrease this gradient by numerical diffusion, bringing stratospheric tracer into the troposphere. It is then rapidly transported throughout the troposphere by vertical mixing, convection and turbulence. The tracer advection scheme as used in ECHAM4 is more diffusive than the scheme used by MA-ECHAM4, which explains why the stratospheric tracer concentrations are much larger for ECHAM4 than for MA-ECHAM4. An increased vertical resolution around the tropopause, as MA-ECHAM4 has, also reduces the

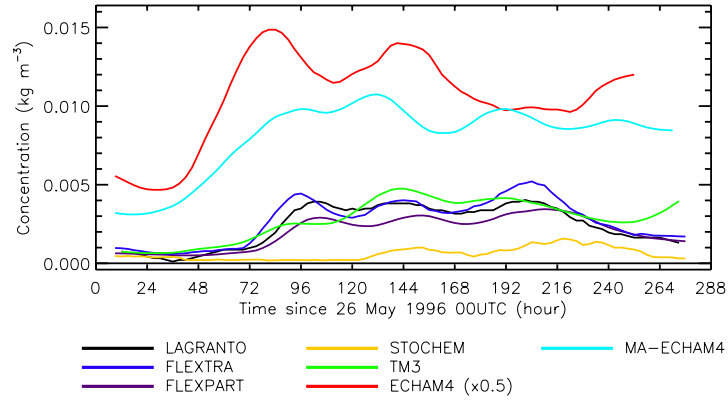


Figure 5.4: Time series of the 24-hour running mean stratospheric tracer concentration at the 700 hPa surface. The data of the ECHAM4 model have been multiplied by 0.5.

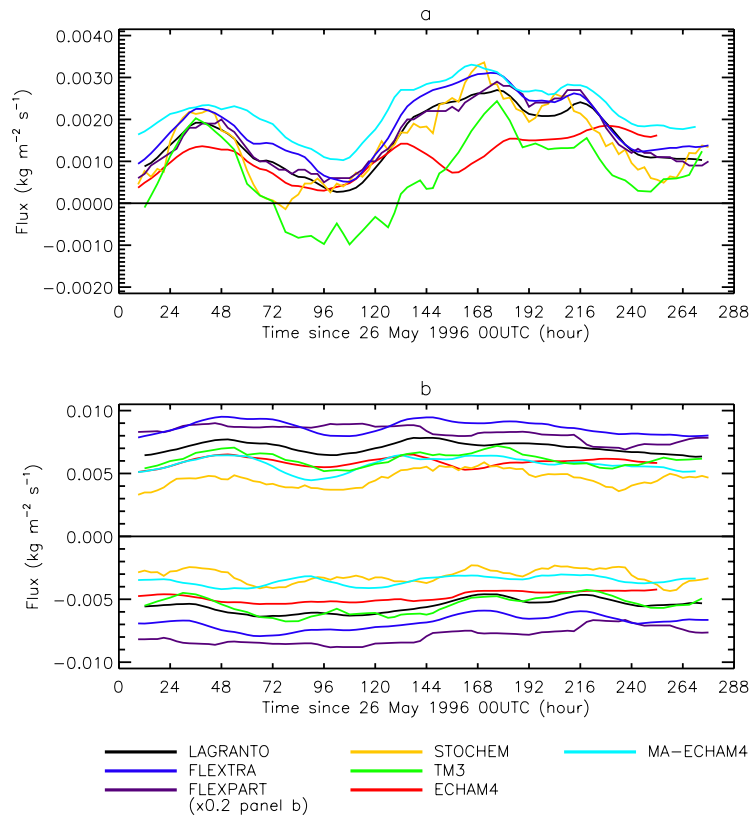


Figure 5.5: Time series of the 24-hour running means of net tropospheric tracer flux (a), and the up- and downward tropospheric tracer fluxes (b) through the 700 hPa surface. The legend is valid for both panels. In panel (b) the results of the FLEXPART model have been multiplied by 0.2. Positive values correspond to downward fluxes, negative values to upward fluxes.

numerical diffusion. The tracer advection scheme as used by TM3 is less diffusive than the scheme used by MA-ECHAM4. The other models and methods only suffer from weak numerical diffusion.

What adds up to this diffusion effect is that the ECHAM4 and MA-ECHAM4 models are on-line, whereas the other models are off-line. The off-line models use the ECMWF wind fields every 6 or 3 hours, and interpolate between these two values to obtain the wind field in between. ECHAM4 and MA-ECHAM4 on the other hand are nudged by the 6-hourly ECMWF meteorology but produce wind fields every time step. This means that for the on-line models the vertical winds can display a larger variability compared to the interpolated, hence smoother, vertical wind fields in off-line models. As a result of these more fluctuating winds the mixing around the tropopause is larger in the GCMs, and the stratospheric tracer is transported faster throughout the troposphere. Consequently, the stratospheric tracer concentration at 700 hPa will be larger.

The nudging is not supposed to bias the stratospheric tracer concentration on the 700 hPa surface. The nudging is applied each time step. But even though this additional tendency is not physical, the perturbation of the balance of the model's physics has found to be much smaller than the physical tendencies. Therefore, it is assumed that the nudging reproduces the observed meteorology without introducing noise [*Jeuken et al., 1996*].

The difference between the results of ECHAM4 and MA-ECHAM4 are due to the different horizontal resolutions, the different advection schemes and the different treatment of subgrid-scale processes.

Time series of the tropospheric tracer flux

The tropospheric tracer flux gives an indication of the vertical velocity in the models. An accurate vertical velocity is necessary for a correct representation of STE in general, and for a correct representation of the stratospheric tracer fluxes. In Figure 5.5 the time series of the domain-averaged net (a) and the up- and downward tropospheric tracer fluxes (b) at 700 hPa are shown. Because the 700 hPa surface lies entirely in the troposphere, where the tropospheric tracer concentration is 1 kg/kg, the tropospheric tracer flux is in principle equal to ω/g . There might be deviations due to different interpolation techniques and due to parameterisations in some of the models (e.g. convective parameterisations in FLEXPART). As can be seen in Figure 5.5a, the net tropospheric tracer fluxes computed by the different models are qualitatively similar, but the absolute values differ about a factor of two. The net tropospheric tracer flux for TM3 has relatively low, and even negative values.

These differences are mainly due to differences in the vertical velocity ω , which

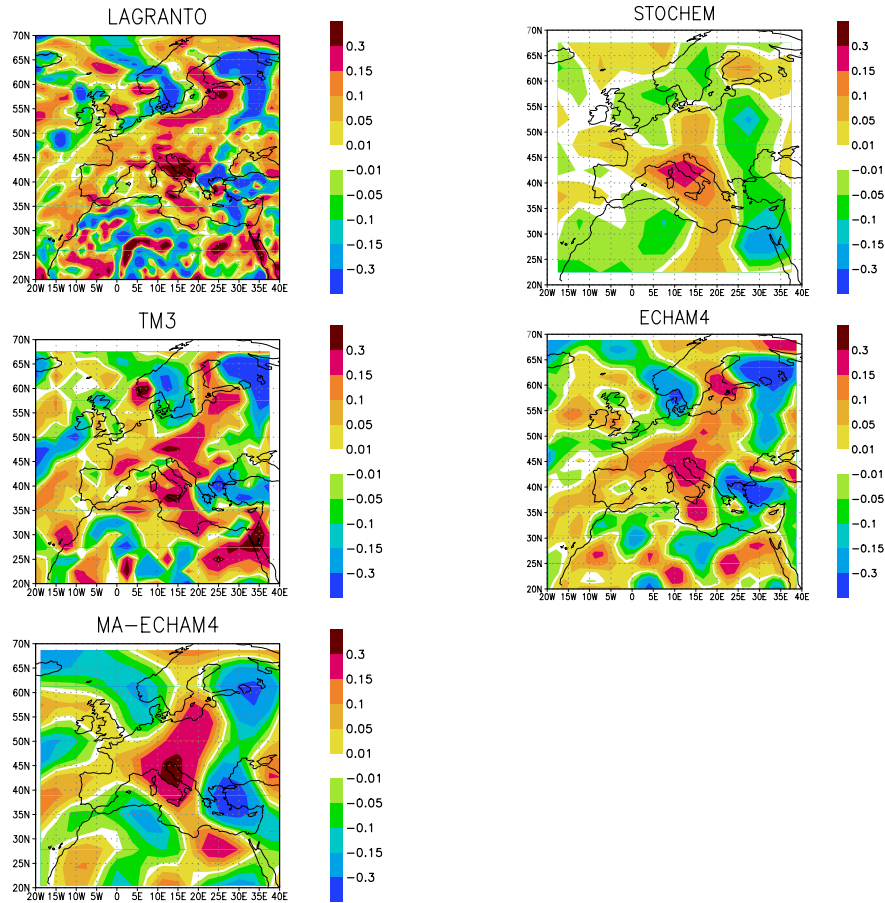


Figure 5.6: Latitude/longitude fields for the 3-hour mean omega (Pa/s) at the 700 hPa surface for 29 May 1996 9-12 UTC. Positive values correspond to downward vertical velocity, negative values to upward vertical velocity.

depends e.g. upon the model resolution. Figure 5.6 shows the latitude/longitude fields of ω at a particular time. These results indicate that differences are partly due to resolution differences between the models, i.e. finer resolution of ECHAM4, TM3 and LAGRANTO versus coarser resolution of MA-ECHAM4 and STOCHEM. Such differences in ω imply differences in the calculated stratospheric and tropospheric tracer fluxes.

The net tropospheric tracer flux (Figure 5.5a) is a residual from relatively large

up- and downward fluxes (Figure 5.5b). Especially FLEXPART displays very large up- and downward fluxes compared to the net flux and also compared to the up- and downward fluxes of other models. These large FLEXPART fluxes arise because in some parts of the domain the 700 hPa surface lies within the boundary layer. In the boundary layer the particles are rapidly transported up- and downward by the parameterised turbulent eddies, causing larger fluxes than when the effects of boundary layer turbulence are neglected or treated in a mean sense. The absolute differences between the other models are about a factor of three, with LAGRANTO, FLEXTRA and FLEXPART giving relatively large net tropospheric tracer fluxes, and the others relatively small fluxes, likely because of their coarser resolution.

Time series of the stratospheric tracer flux

In Figure 5.7 the time series of the domain-averaged net (panel a) and up- and downward (panel b) stratospheric tracer fluxes at 700 hPa are shown. The events in the stratospheric tracer fluxes are more comparable to the stratospheric tracer concentration (Figure 5.4) than to the tropospheric tracer fluxes (Figure 5.5). The differences between the fluxes and the concentration of the stratospheric tracer are entirely due to differences in the vertical velocity including parameterised turbulence and convection, which are, as already explained, mainly due to resolution differences.

Unlike the results of FLEXPART for the cross-tropopause flux in Figure 5.3 and the tropospheric tracer flux in Figure 5.5, the up- and downward stratospheric tracer fluxes of FLEXPART are comparable to those of the other models. Comparing FLEXTRA and FLEXPART, the latter being an expansion of the first, it can be seen that FLEXPART gives in general larger fluxes than FLEXTRA. This is as expected, because in FLEXPART more physical processes are included, such as boundary layer turbulence, which enhance the stratospheric and tropospheric tracer fluxes. STOCHEM produces relatively small stratospheric tracer fluxes, probably because this model has less vertical transport and less mixing.

Comparing the time series of the stratospheric and tropospheric tracer fluxes it can be seen that they show signatures of various events, as expected. The tropospheric tracer flux (Figure 5.5a) has a maximum around 36 hours and a minimum around 96 hours, which is reverse in most of the modelled stratospheric tracer fluxes (Figure 5.7a). At the time of the intrusion of stratospheric air into the troposphere (Figure 5.1a, $t = 60$ hours), the net tropospheric tracer fluxes at 700 hPa are enhanced (Figure 5.5a). The net stratospheric tracer flux at 700 hPa (Figure 5.7a), becomes large only when the low has been cut off and is decaying (Figure 5.1c, $t = 84$ hours). In the latter situation the tropospheric tracer flux is reduced. TRAJKS, which was used to calculate the flux through the tropopause displays the same features, i.e. less

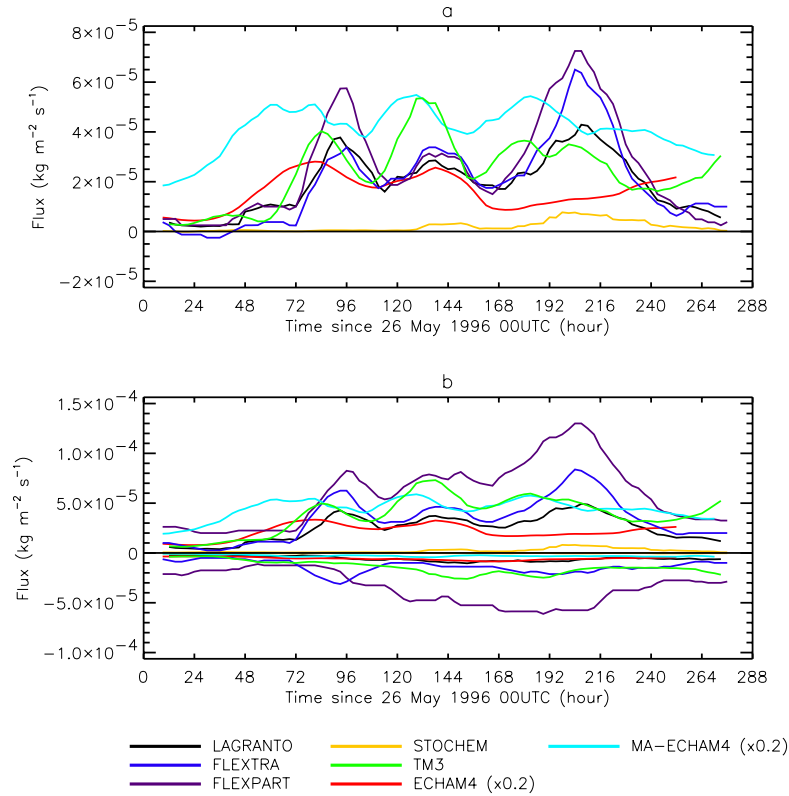


Figure 5.7: Time series of the 24-hour running means of net stratospheric tracer flux (a), and the up- and downward stratospheric tracer fluxes (b) through the 700 hPa surface. The legend is valid for both panels. The results of the ECHAM4 and MA-ECHAM4 model have been multiplied by 0.2 in both panels. Positive values correspond to downward fluxes, negative values to upward fluxes.

exchange at the time of the intrusion of stratospheric air into the troposphere and more exchange from the stratosphere to the troposphere at the time and place of the decaying cut-off low (not shown).

Latitude/longitude fields of the stratospheric tracer flux

Figure 5.8 shows the latitude/longitude fields of the stratospheric tracer flux through the 700 hPa surface on 29 May 1996 9-12 UTC. Here the differences between the GCMs and the other models and methods can be clearly seen. The fluxes of the stratospheric tracer in ECHAM4 and MA-ECHAM4 are larger than those in the other models and

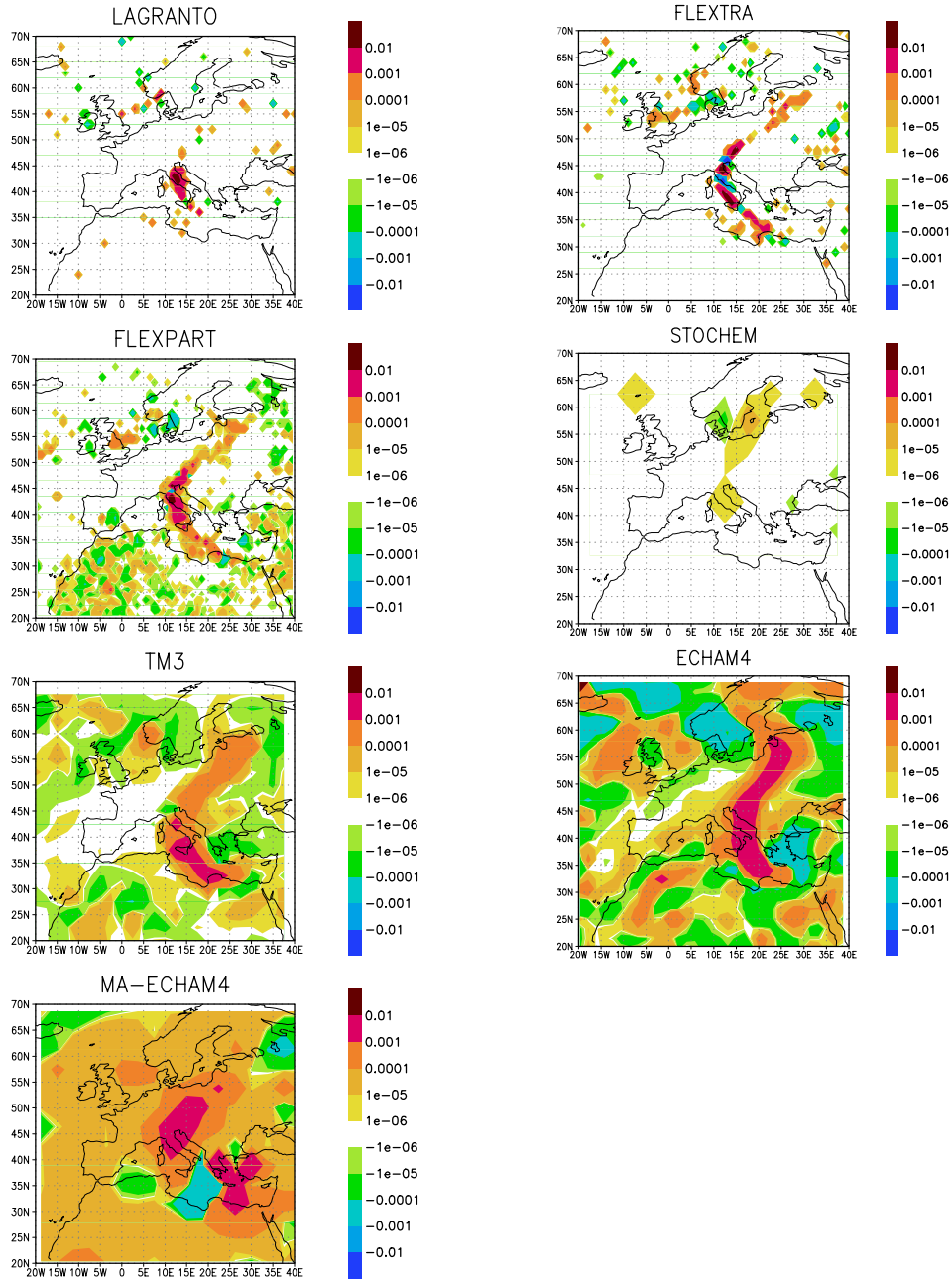


Figure 5.8: Latitude/longitude fields of the 3-hour mean net stratospheric tracer flux ($\text{kg m}^{-2} \text{s}^{-1}$) through the 700 hPa surface on 29 May 1996 9-12 UTC. Positive values correspond to downward fluxes, negative values to upward fluxes.

methods, as explained in section 5.4.2. The patterns are similar for all models and methods except for STOCHEM where the flux equals zero in most regions. This is because in STOCHEM the number of air parcels is relatively small, leading to only a small chance of a parcel crossing the 700 hPa surface in a $5^\circ \times 5^\circ$ grid cell in a 3-hour time period.

5.4.3 Time versus height plots of the stratospheric tracer concentration

In Figure 5.9 the time versus height plots of the stratospheric tracer concentration above the station Mt. Cimone are shown for the different models and methods. In this figure the tropopause heights, which correspond to where the gradient of stratospheric tracer concentration is largest, are at about the same altitudes in all models. They display some similar features, i.e. enhanced stratospheric tracer concentrations in the first 24 hours of the period and an intrusion of stratospheric air into the troposphere around 48 hours. However, the penetration depth into the troposphere differs in the models. All models and methods except STOCHEM show a pattern of high stratospheric tracer concentration around 96 hours at an altitude of about 600 hPa. At the end of the period all models and methods again show a slightly increased stratospheric tracer concentration whose duration and penetration depth into the troposphere differs again for the several models and methods.

In Figure 5.9 it can be seen that the ability of capturing the intrusion depends very much on the model resolution. STOCHEM that has the coarsest resolution hardly shows the intrusion, and MA-ECHAM4 shows a broader intrusion than ECHAM4. A coarser model resolution also implies a decreased spatial variability (not shown). TM3 shows, in spite of the relatively large resolution, a relatively small maximum of stratospheric tracer around 96 hours and 600 hPa.

The similarity between LAGRANTO and FLEXTRA is not surprising, since the applied methods are similar. These are the only two methods in Figure 5.9 that do not allow mixing in air parcels that cross the tropopause several times. This could be the reason for the smaller amount of stratospheric tracer in the troposphere for LAGRANTO and FLEXTRA, and for the very localised patches of the stratospheric tracer in the troposphere.

ECHAM4 and MA-ECHAM4 show a larger stratospheric tracer concentration in the troposphere compared to the other models and methods. This is due to numerical diffusion and more varying vertical winds, as explained in section 5.4.2, resulting in a continuous stratospheric signal at the mountain top.

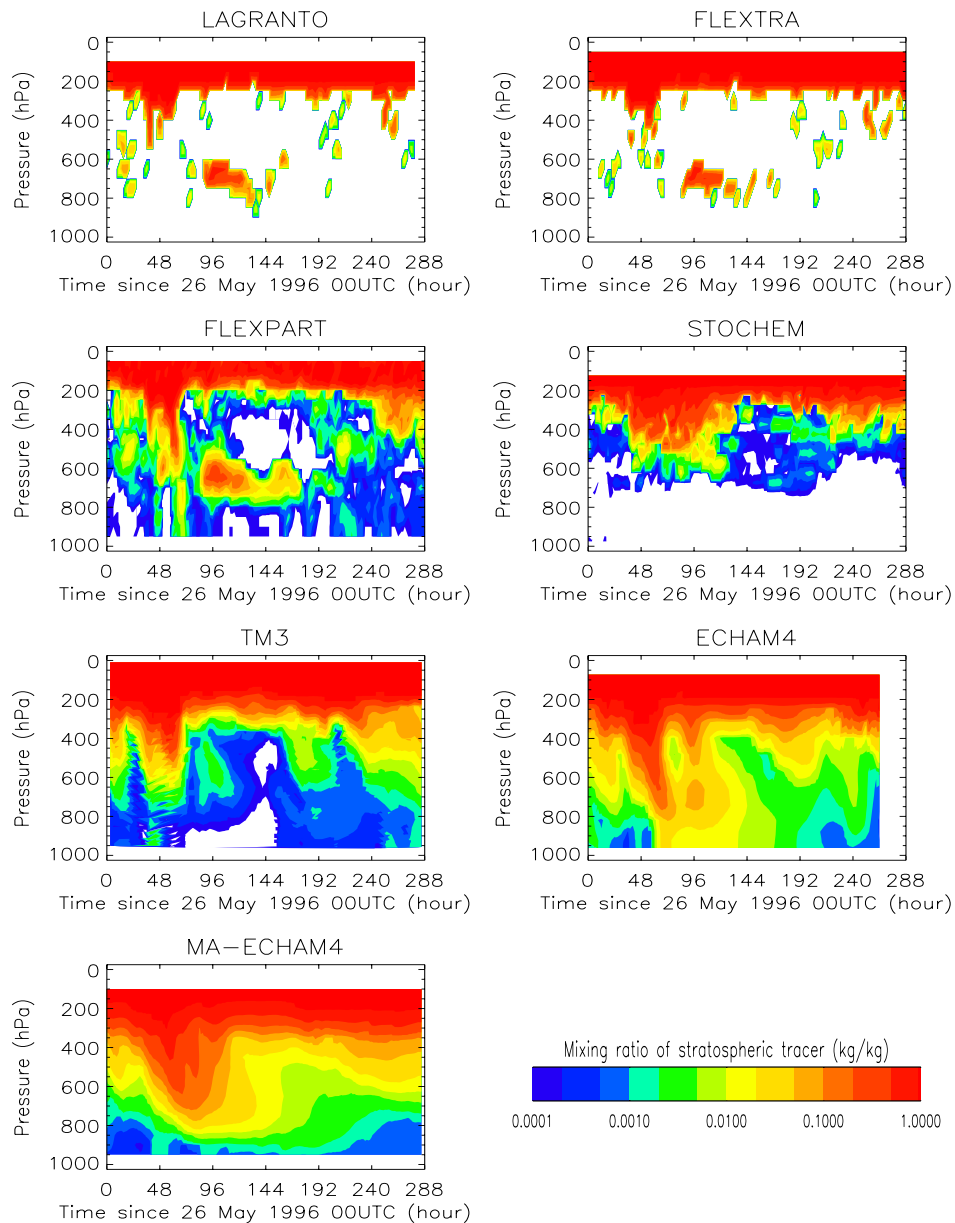


Figure 5.9: Time-height plots for the instantaneous stratospheric tracer concentration (kg/kg) at the Mt. Cimone station (44°N, 10.5°E, 2165 m asl)

5.5 Discussion and conclusions

This chapter presents one of the first extensive case study intercomparisons of models and methods used for estimating stratosphere-troposphere exchange (STE). In the present study the number and range of applied models and methods is larger than in other similar studies. Also, the model and method results are evaluated with measurements in a companion paper by *Cristofanelli et al.* [2002]. The intercomparison has been performed in the framework of the EU-project STACCATO. Hereto, nine different models and methods inserted an idealised stratospheric tracer in the stratosphere and an idealised tropospheric tracer in the troposphere. When this tracer leaves the stratosphere or troposphere, it decays exponentially with a time constant of 2 days. Three trajectory methods (LAGRANTO, FLEXTRA and TRAJKS), one Eulerian method (the Wei method), two Lagrangian transport models (FLEXPART and STOCHEM), one Eulerian transport model (TM3) and two nudged GCMs (ECHAM4 and MA-ECHAM4) participated in this intercomparison.

For a correct representation of STE several processes need to be captured by the models. For a correct representation of the spatial and temporal distribution of STE, synoptic-scale weather systems, like tropopause foldings and cut-off lows, need to be correctly represented. Another important quantity affecting STE is the vertical velocity, that is related to diabatic processes, especially the release of latent heat, and by turbulent mixing in the tropopause region. For the models and methods in which the dynamics entirely depend on ECMWF data (i.e. all models and methods except the two GCMs), these processes are captured by the ECMWF analyses. The ECMWF analyses have a high horizontal ($0.5^\circ \times 0.5^\circ$) and vertical (31 levels) resolution, which make them an excellent source of input data for the models and methods used to calculate STE. For the GCMs the representation of the spatial and temporal distribution of STE depends on the chosen horizontal and vertical resolution, as is obvious from some of the differences between the ECHAM4 and MA-ECHAM4 results.

Except for physical processes that lead to STE, there are also several artificial sources for STE. In the ECMWF model the addition of measurements disturbs the dynamical balance in the model every analysis time step. In the GCMs there is strong numerical diffusion restricting the reliability of the results.

The results of this study indicate that ECHAM4 and MA-ECHAM4 are influenced by numerical diffusion, especially in the vicinity of large tracer gradients, and by a larger variability of the vertical winds because of the GCMs being on-line, such that the tracer mass exchange in these models is much larger than in the other models and methods. This is partly inherent to the applied intercomparison set-up. The stratospheric tracer mixing ratio is 0 kg/kg in the troposphere and 1 kg/kg in the

stratosphere. Therefore, the stratospheric tracer gradient near the tropopause is very large, and, consequently, also the numerical diffusion near the tropopause is very large, as well as the exchange due to more varying vertical winds. In reality, tracers do not have such a sharp gradient. Ozone, for example, is initialised a few model levels above the tropopause, with concentration increasing upward in the stratosphere. Therefore, the numerical diffusion and more varying vertical winds will not have such a large impact on the ozone transport into the troposphere. Simulations with GCMs of the exchange of ozone are therefore expected to be more realistic than the simulation of the exchange of the stratospheric tracer in this study, which was also found by *Cristofanelli et al.* [2002].

From the results of the present study it is not possible to conclude which of the applied models or methods simulated the most realistic STE. Therefore, in the complementary study by *Cristofanelli et al.* [2002] the simulations are compared with measurements. Nevertheless, the results from the present study give insight in the dependence of the simulated STE on several aspects of the models and methods, such as the spatial resolution or the strength of the numerical diffusion. What is important for a correct spatial and temporal distribution of STE is a high horizontal and vertical resolution, as has already been shown by *Velthoven and Kelder* [1996]. This can be seen comparing ECHAM4 and MA-ECHAM4, the latter having a coarser horizontal resolution (but a slightly higher vertical resolution in the vicinity of the tropopause), and by comparing STOCHEM with the other models, STOCHEM having a relatively coarse resolution.

LAGRANTO, FLEXTRA, TRAJKS and FLEXPART all show the same events, with only slightly differing amplitudes. The results for the flux through the tropopause for TRAJKS and LAGRANTO are even almost identical. That these models show similar results is perhaps not surprising, because they are all based on trajectories, and LAGRANTO and FLEXTRA are even identical apart from the applied trajectory models and the temporal resolution of the input data. LAGRANTO, FLEXTRA, TRAJKS and FLEXPART also have the same resolution, which favours similar results. TM3 shows a similar amplitude as these models, but has a slightly different pattern in the events. STOCHEM shows the same events but has an amplitude that is two to three times smaller than that shown by the majority of the other models and methods. This is due to the relatively coarse resolution of the model which leads to smaller vertical transport and mixing. The crude meteorological assimilation scheme used in this model may also be responsible for this underestimation, because an improved assimilation scheme lead to results (not shown) that were more in line with the other models.

In conclusion, for the period and region considered in the present study the STE

simulations with nine different models and methods show the same temporal evolution and the same geographical pattern of STE, but with generally different amplitudes. On the other hand, for some simulations also the amplitudes are very similar. However, any model estimate of STE should be confronted with observations. Because of the use of a hypothetical stepwise tracer distribution a comparison with measurements is not straightforward. It requires a further analysis of the results discussed in this study, which is presented in the companion paper by *Cristofanelli et al.* [2002].

6

Summary and outlook

6.1 Summary

In this chapter a summary of this thesis is given and the main conclusions are presented. This thesis has been focussed on four subjects:

1. The differences between the moist potential vorticity and the commonly used potential vorticity.
2. A new Lagrangian method to diagnose stratosphere-troposphere exchange.
3. Application of this method to a subtropical Southern Hemisphere tropopause fold.
4. Intercomparison of nine different models and methods that are used for the simulation and diagnosis of stratosphere-troposphere exchange.

The first subject is described in Chapter 2, the second in Chapter 3, the third in Chapter 4, and the fourth subject in Chapter 5.

1. The fact that the atmosphere is not perfectly adiabatic and dry, while this is assumed in the use of potential vorticity, motivated the work of the second chapter. An important source of potential vorticity (Q_d) is related to the release of latent heat. A moist potential vorticity (Q_m) can be defined in which this source is absent. However, a new source arises that is related to baroclinicity. In Chapter 2 the differences and similarities between Q_d and Q_m are investigated.

It is found that the differences between Q_m and Q_d are mainly determined by the vertical gradient of the specific humidity. In the higher atmosphere, Q_m differs little from Q_d because here the humidity and its vertical gradient are very small. At lower levels, below about 6 km, the differences are larger. Differences in material conservation between Q_d and Q_m have been investigated by considering Q_d and Q_m along trajectories. It was found that for altitudes above 600 hPa, Q_m is indeed better

conserved than Q_d . For altitudes below 600 hPa Q_m is less well conserved than Q_d , for which several reasons are discussed in Chapter 2.

2. Lagrangian methods have only recently been applied to estimate cross-tropopause fluxes. Traditionally cross-tropopause fluxes were computed using the Eulerian diagnostic developed by Wei [1987]. However, numerical problems with the cancellation of large terms make this method inaccurate. In Chapter 3 a new Lagrangian technique is developed, and the results of this technique are evaluated. With this Lagrangian method spatial and temporal distributions of the air-mass flux across potential vorticity surfaces can be calculated. Because the tropopause can be approximated by a potential vorticity surface, this Lagrangian method can be applied for the calculation of cross-tropopause air-mass fluxes. The results are thought to be reliable, at least in a qualitative sense, because the largest downward fluxes in the tropopause fold occur in regions with maximum wind shear, where mixing is thought to cause stratosphere-troposphere exchange (STE). Although several approximations have been made in the applied Lagrangian method, this method appears to be an appropriate tool for diagnosing STE.

3. The Lagrangian method developed in Chapter 3 has been used in Chapter 4 to perform a case study of a tropopause folding event in the subtropical Southern Hemisphere. Both for the Southern Hemisphere and for the subtropics in general, little is known about STE. For this study a large number of forward and backward trajectories was calculated, starting in the vicinity of the tropopause fold. This particular fold was observed during the EU-project TRACAS (TRANsport of Chemical species Across the Subtropical tropopause) at La Reunion (21°S, 55°E) in July 1998. With the Lagrangian method the cross-tropopause air-mass flux has been calculated for the different tropopause levels which occur in case of a tropopause fold.

The results show that the largest fluxes occur in tropopause folds and upper level troughs, and that outside these areas the exchange is small. The largest fluxes occur in regions with strong vertical windshear. In the fold the largest fluxes are found for the lowermost tropopause region. Up- and downward fluxes are found close to each other, in regions of strong vertical wind shear, leading to bi-directional exchange. The computed net mass exchange in the considered region is about -20×10^{13} kg (i.e. downward) in 4.5 days. Because Southern Hemisphere subtropical folds not often have been investigated, it is difficult to compare the results of this study with former results. As far as can be presently concluded, the magnitudes of the calculated cross potential vorticity surface air-mass fluxes are rather small. The ratio of the fluxes per unit of area in- and outside the fold is about 200:1.

4. Chapter 5 presents one of the first extensive intercomparisons of models and methods used for estimating STE. In this study the number and range of applied

models and methods is much larger than in earlier studies. The intercomparison has been performed in the framework of the EU-project STACCATO (Influence of Stratosphere Troposphere Exchange in a Changing Climate on Atmospheric Transport and Oxidation Capacity). Nine different models and methods, including three trajectory methods, one Eulerian method, two Lagrangian and one Eulerian transport model and two general circulation models, applied a uniform initialisation. Stratospheric and tropospheric tracers were simulated and the tracer mass fluxes were calculated through the tropopause and the 700 hPa surface, the latter being an indirect measure of STE because this surface lies entirely in the troposphere. For a 12-day case study over Europe the simulated tracer mass fluxes were intercompared.

For this case the STE simulations show the same temporal evolution and the same geographical pattern of STE for most models and methods, but with rather varying amplitudes (up to a factor four). However, for some simulations also the amplitudes are very similar. The horizontal resolution is found to be an important cause for differences between the models and methods. Also the numerical diffusion in the general circulation models appears to play an important role in the simulation of the stratospheric tracer distribution in the troposphere, especially in the vicinity of large tracer gradients. Finally the difference between on-line and off-line models has proven to be important, because of the larger variability of the vertical winds in the on-line models.

6.2 Outlook

Scientific research often leaves you with more questions than you began with. This is also true for the research done in this thesis. Below several interesting questions are summarised which should be addressed in the future.

In Chapter 2, an unsolved question is why the moist potential vorticity is worse conserved in the lower troposphere than the potential vorticity. To resolve this question all source terms should be analysed carefully for the (moist) potential vorticity, including a decomposition of the diabatic heating into its parts, i.e. latent heating, radiative heating and sensible heating. Also the contribution of mixing, friction and baroclinicity to the change of the (moist) potential vorticity should be quantified.

Concerning Chapter 3, any method used to calculate STE has its advantages and disadvantages. There is no method with which all questions concerning STE can be answered. Therefore, combination of different models or methods can be expected to give new and useful results. For example, combination of Lagrangian methods, for the flux calculation, and general circulation models coupled to chemistry models, to simulate the accompanying chemistry, is expected to give better estimates of cross-

tropopause fluxes of various trace gasses.

Another question concerns mixing of potential vorticity along trajectories. Here rise two difficulties. First, in a region of mixing a trajectory loses its identity, i.e., it does not have a specific position any more. However, in these regions of mixing STE occurs. A second difficulty concerns the mixing of potential vorticity. This mixing is a subgrid-scale process which is not explicitly parameterised in the ECMWF model. Instead, the subgrid-scale fluctuations of the model variables are parameterised. It is unclear what the effect is of the parameterised mixing on quantities that are computed from the model variables, such as potential vorticity.

In Chapter 4 it is attempted to validate the used trajectory method with measurements. However, for a thorough validation, high time and spatial resolution measurements are necessary. Potentially useful data for this purpose are e.g. ozone data from satellites. Presently these data still have a very low horizontal and vertical resolution in the troposphere. The problem with validating the method with ozone soundings is the rather coarse time resolution with which these soundings are made, and the inability to follow the atmospheric event with consecutive soundings.

In Chapter 3 and 4 emphasis is put on the mixing as a cause for changing potential vorticity along the trajectories. Of course there are also other mechanisms which can change potential vorticity, as described in Chapter 2. Most of these mechanisms are implicitly taken into account when calculating trajectories, but more research could be done on the importance of the different physical mechanisms which can change the potential vorticity.

With the trajectory method of Chapter 3 and 4 more research can be done on the different aspects of STE. Those trajectories which display STE can, e.g., be prolonged which gives information about the origin and fate of the exchanged air. Another possibility is to calculate ozone fluxes with this trajectory method, if the fluxes are combined with a simultaneous ozone distribution as will become available from ECMWF. Also an estimation can be made of the reversibility of the exchange.

An open question concerning Chapter 4 is the lack of knowledge of STE in the Southern Hemisphere and in the subtropics. It would be interesting to know whether the differences between the folding event in the subtropics studied in Chapter 4 and folding events in midlatitudes are systematic.

Concerning the model intercomparison performed in Chapter 5, some issues would have improved the intercomparison. One of them is the different resolutions of the models. The models were applied using their 'standard resolution', in order to enable an intercomparison between old and new simulations with the separate models. Another improvement would have been to use a more realistic tracer distribution. With such a distribution the general circulation models would have suffered less from

numerical diffusion and their results would be likely to be more comparable with the other models and methods. There are also other differences in set-up which make the model results less easy to compare, e.g. the different treatment of multiple tropopause crossings. A general remark is that for an intercomparison the set-up should be as similar as possible for all models and methods, so that differences in model results can be attributed to inevitable model differences.

During the STACCATO project, our knowledge of STE has substantially increased. The confidence in the methods has increased, and multi-year, high resolution global distributions of STE have been obtained. Also future changes in STE because of a changing climate have been investigated. However, despite the amount of research done on STE in the last decades, there are still uncertainties on several aspects of STE and its effects on the composition and chemistry of stratosphere and troposphere, and continuing research will be necessary.

References

- Ambaum, M. H. P., Large-scale dynamics of the tropopause, Ph.D. thesis, Technical University Eindhoven, ISBN 90-386-0249-9, Eindhoven, 1997.
- Ancellet, G., J. Pelon, M. Beekmann, A. Papayannis, and G. Megie, Ground-based lidar studies of ozone exchanges between the stratosphere and the troposphere, *J. Geophys. Res.*, **96**, 22401-22421, 1991.
- Appenzeller, C., H. C. Davies, and W. A. Norton, Fragmentation of stratospheric intrusions, *J. Geophys. Res.*, **101**, 1435-1456, 1996.
- Appenzeller, C., J. R. Holton, and K. H. Rosenlof, Seasonal variation of mass transport across the tropopause, *J. Geophys. Res.*, **101**, 15071-15078, 1996.
- Baray, J.-L., G. Ancellet, F. G. Taupin, M. Bessafi, S. Baldy, and P. Keckhut, Subtropical tropopause break as a possible stratospheric source of ozone in the tropical troposphere, *J. of Atmos. and Solar-Terrestrial Phys.*, **60**, 27-36, 1998.
- Baray, J.-L., V. Daniel, G. Ancellet, and B. Legras, Planetary-scale tropopause folds in the Southern subtropics, *Geophys. Res. Lett.*, **27**, 353-356, 2000.
- Bénard, P., J.-P. Lafore and J.-L. Redelsperger, Nonhydrostatic simulation of frontogenesis in a moist atmosphere. Part 2: Moist potential vorticity budget and wide rainbands, *J. Atmos. Sci.*, **49**, 2218-2235, 1992.
- Bolton, D., The computation of equivalent potential temperature, *Mon. Wea. Rev.*, **108**, 1046-1053, 1980.
- Bonasoni, P., F. Evangelisti, U. Bonafè, F. Ravegnani, F. Calzolari, A. Stohl, L. Tositti, O. Tubertini, and T. Colombo, Stratospheric ozone intrusion episodes recorded at Mt. Cimone during the VOTALP project: case studies, *Atmospheric Environment*, **34**, 1355-1365, 2000.
- Brewer, A. M., Evidence for a world circulation provided by the measurements of helium and water vapour distribution in the stratosphere, *Quart. J. Roy. Meteor. Soc.*, **75**, 351-363, 1949.
- Butchart, N., and A. A. Scaife, Removal of chlorofluorocarbons by increased mass exchange between the stratosphere and troposphere in a changing climate, *Nature*, **410**, 799-802, 2001.
- Cao, Z. and H.-R. Cho, Generation of moist potential vorticity in extratropical cyclones, *J. Atmos. Sci.*, **52**, 3263-3281, 1995.
- Chen, P., Isentropic cross-tropopause mass exchange in the extratropics, *J. Geophys. Res.*, **100**, 16661-16673, 1995.

- Collins, W. J., D. S. Stevenson, C. E. Johnson, and R. G. Derwent, Tropospheric ozone in a global-scale three-dimensional Lagrangian model and its response to NO_x emission controls, *J. Atmos. Chem.*, **26**, 223-274, 1997.
- Collins, W. J., R. G. Derwent, C. E. Johnson, and D. S. Stevenson, A comparison of two schemes for the convective transport of chemical species in a Lagrangian global chemistry model, *Quart. J. Roy. Meteor. Soc.*, **128**, 991-1009, 2002.
- Cristofanelli, P., W. Collins, C. Land, J. Meloen, G. J. Roelofs, A. Stohl, T. Trickl, P. Zanis, H. Wernli, and P. Bonasoni, Stratosphere-troposphere exchange: model and method evaluation of model results with measurement data during the STACCATO project, submitted, *J. Geophys. Res.*, 2002.
- Danielsen, E. F., Stratospheric-tropospheric exchange based on radioactivity, ozone and potential vorticity, *J. Atmos. Science*, **25**, 502-518, 1968.
- Danielsen, E. F., In defense of Ertel's potential vorticity and its general applicability as a meteorological tracer, *J. Atmos. Sci.*, **47**, 2013-2020, 1990.
- Dethof, A., A. O'Neill, and J. Slingo, Quantification of the isentropic mass transport across the dynamical tropopause, *J. Geophys. Res.*, **105**, 12279-12293, 2000.
- Dobson, G. M. B., Origin and distribution of polyatomic molecules in the atmosphere, *Proc. Roy. Meteor. Soc.*, **A236**, 187-193, 1956.
- Eisele, H., H. E. Scheel, R. Sladkovic, and T. Trickl, High-resolution lidar measurements of stratosphere-troposphere exchange, *J. Atmos. Science*, **56**, 319-330, 1999.
- Folkens, I. and C. Appenzeller, Ozone and potential vorticity at the subtropical tropopause break, *J. Geophys. Res.*, **101**, 18787-18792, 1996.
- Folkens, I., M. Loewenstein, J. Podolske, S. J. Oltmans, M. Proffitt, *J. Geophys. Res.*, **104**, 22095-22102, 1999.
- Follows, M. J., On the cross-tropopause exchange of air, *J. Atmos. Science*, **49**, 879-882, 1992.
- Gettelman, A., and A. H. Sobel, Direct diagnosis of stratosphere-troposphere exchange, *J. Atmos. Science*, **57**, 3-16, 2000.
- Gidel, L. T., and M. A. Shapiro, General circulation model estimates of the net vertical flux of ozone in the lower stratosphere and the implications for the tropospheric ozone budget, *J. Geophys. Res.*, **85**, 4049-4058, 1980.
- Gouget, H., J.-P. Cammas, A. Marenco, R. Rosst, and I. Jonquierès, Ozone peaks associated with a subtropical tropopause fold and with the trade wind inversion: a case study from the airborne campaign TROPOZ II over the Caribbean in winter, *J. Geophys. Res.*, **101**, 25979-25993, 1996.
- Gouget, H., G. Vaughan, A. Marenco, and H. G. J. Smit, Decay of a cut-off low and contribution to stratosphere-troposphere exchange, *Quart. J. Roy. Meteor. Soc.*, **126**, 1117-1141, 2000.
- Grewe, V., and M. Damaris, Calculating the global mass exchange between stratosphere and troposphere, *Ann. Geophys.*, **14**, 431-442, 1996.

- Hartjenstein, G., Diffusive decay of tropopause folds and the related cross-tropopause mass flux, *Mon. Wea. Rev.*, **128**, 2958-2966, 2000.
- Haynes, P. H. and M. E. McIntyre, On the conservation and impermeability theorems for potential vorticity, *J. Atmos. Sci.*, **47**, 2021-2031, 1990.
- Hoerling, M. P., T. K. Schaack, and A. J. Lenzen, A global analysis of stratospheric-tropospheric exchange during northern winter, *Mon. Wea. Rev.*, **121**, 162-172, 1993.
- Holton, J. R., On the global exchange of mass between the stratosphere and troposphere, *J. Atmos. Science*, **47**, 392-395, 1990.
- Holton, J.R., Introduction to Dynamic Meteorology. Academic Press, 507 pp., 1992.
- Holton, J. R., P. H. Haynes, M. E. McIntyre, A. R. Douglass, R. B. Rood, and L. Pfister, Stratosphere-troposphere exchange, *Rev. Geophys.*, **33**, 403-439, 1995.
- Hoskins, B. J., Towards a PV- θ view of the general circulation, *Tellus*, **43**, 27-35, 1991.
- Hoskins, B. J., M. E. McIntyre and A. W. Robertson, On the use and significance of isentropic potential vorticity maps, *Quart. J. Roy. Meteor. Soc.*, **111**, 877-946, 1985.
- IPCC (Intergovernmental Panel on Climate Change), special report on 'Aviation and the global atmosphere', Cambridge University Press, 1999.
- James, P., A. Stohl, C. Forster, S. Eckhardt, P. Seibert, and A. Frank, A 15-year climatology of stratosphere-troposphere exchange with a Lagrangian particle dispersion model, Part B: Seasonal and interannual variations, submitted, *J. Geophys. Res.*, 2002b.
- Jeuken, A., P. Siegmund, L. Heijboer, J. Feichter, and L. Bengtsson, On the potential of assimilating meteorological analyses in a global climate model for the purpose of model validation, *J. Geophys. Res.*, **101**, 16939-16950, 1996.
- Kentarchos, A. S., G.-J. Roelofs, and J. Lelieveld, Model study of a stratospheric intrusion event at lower midlatitudes associated with the development of a cut-off low, *J. Geophys. Res.*, **104** 1717-1727, 1999.
- Kowol-Santen, J., H. Elbern, and A. Ebel, Estimation of cross-tropopause air mass fluxes at midlatitudes: comparison of different numerical methods and meteorological situations, *Mon. Wea. Rev.*, **128**, 4045-4057, 2000.
- Lamarque, J. and P. G. Hess, Cross-Tropopause Mass Exchange and Potential Vorticity Budget in a Simulated Tropopause Folding, *J. Atmos. Sci.*, **51**, 2246-2269, 1994.
- Lyttekens, E., Standard Errors of Regression Coefficients in the Case of Autocorrelated Residuals, from: 'Time Series Analysis', edited by M. Rosenblatt, John Wiley and Sons, Inc., p. 38-60, 1963.
- Mahlman, J. D., H. Levy II, and W. J. Moxim, Three-dimensional tracer structure and behavior as simulated in two ozone precursor experiments, *J. Atmos. Science*, **37**, 655-684, 1980.
- Meijer, E. W., P. F. J. van Velthoven, A. M. Thompson, L. Pfister, H. Schlager, P. Schulte, and H. Kelder, Model calculations of the impact of NO_x from air traffic, lightning, and surface emissions, compared with measurements, *J. Geophys. Res.*, **105**, 3833-3850, 2000.

- Manzini, E., and N. A. McFarlane, The effect of varying the source spectrum of a gravity wave parameterization in a middle atmosphere general circulation model, *J. Geophys. Res.*, **103**, 31523-31539, 1998.
- Meloan, J., P.C. Siegmund, and M. Sigmond, A Lagrangian computation of stratosphere-troposphere exchange in a tropopause folding event in the subtropical Southern Hemisphere, *Tellus*, **53**, 367-378, 2001.
- Meloan, J., P. Siegmund, P. van Velthoven, H. Kelder, M. Sprenger, H. Wernli, A. Kentarchos, G. Roelofs, J. Feichter, C. Land, C. Forster, P. James, A. Stohl, W. Collins, and P. Cristofanelli, Stratosphere-troposphere exchange: a model and method intercomparison, submitted, *J. Geophys. Res.*, 2002.
- Meloan, J., W. Verkley, P. Siegmund, P. van Velthoven, and M. Scheele, On the conservation of moist potential vorticity versus potential vorticity, submitted, *J. Atmos. Sci.*, 2002.
- Moustaoui, M., H. Teitelbaum, P. F. J. van Velthoven and H. Kelder, Analysis of gravity waves during the POLINAT experiment and some consequences for stratosphere-troposphere exchange, *J. Atmos. Science*, **56**, 1019-1030, 1999.
- Murphy, D. M., W. H. Fahey, M. H. Proffitt, S. C. Liu, K. R. Chan, S. C. Eubank, S. R. Kawa, and K. K. Kelly, Reactive nitrogen and its correlation with ozone in the lower stratosphere and upper troposphere, *J. Geophys. Res.*, **98**, 8751-8773, 1993.
- Pedlosky, J., *Geophysical Fluid Dynamics*, Springer, 710 pp., 1987.
- Peixoto, J. P. and A. H. Oort, *Physics of climate*, American Institute of Physics, 520 pp., 1992.
- Petterssen, S., *Weather Analysis and Forecasting*. McGraw-Hill, p. 221-223, 1940.
- Plumb, A., 'Tropical pipe' model of stratospheric transport, *J. Geophys. Res.*, **101**, 3957-3972, 1996.
- Plumb, R. A. and M. K. W. Ko, Interrelationships between mixing ratios of long-lived stratospheric constituents, *J. Geophys. Res.*, **97**, 10145-10156, 1992.
- Ramond, D., H. Corbin, M. Desbois, G. Szejwach, and P. Waldteufel, The dynamics of polar jet stream as depicted by the Meteosat WV Channel radiance Fields, *Mon. Wea. Rev.*, **109**, 2164-2176, 1981.
- Rasch, P. J. and M. Lawrence, Recent development in transport methods at NCAR, in: MPI Workshop on conservative transport schemes, Report No. 265, edited by B. Machenhauer, Max-Planck-Institute for Meteorology, ISSN 0937-1060, Hamburg, 65-75, 1998.
- Ravetta, F., G. Ancellet, J. Kowol-Santen, R. Wilson, and D. Nedeljkovic, Ozone, temperature, and wind field measurements in a tropopause fold: comparison with a mesoscale model simulation, *Mon. Wea. Rev.*, **127**, 2641-2653, 1999.
- Reiter, E. R. and J. D. Mahlman, Heavy radioactive fallout over the southern United States, November 1962, *J. Geophys. Res.*, **70**, 4501-4520, 1965.
- Reiter, E. R., M. E. Glasser, and J. D. Mahlman, The role of the tropopause in stratospheric-tropospheric exchange process, *Pure Appl. Geophys.*, **75**, 185-218, 1969.

- Roeckner, E., K. Arpe, L. Bengtsson, M. Christoph, M. Claussen, L. Dmenil, M. Esch, M. Giorgetta, U. Schlese, and U. Schulzweida, The atmospheric general circulation model ECHAM-4: Model description and simulation of present-day climate, Rep. 218, Max-Planck-Institute for Meteorology, Hamburg, Germany, 1996.
- Roelofs, G.-J., and J. Lelieveld, Model study of the influence of cross-tropopause O₃ transports on tropospheric O₃ levels, *Tellus*, **49**, 38-55, 1997.
- Rogers, H. L., H. Teyssedre, G. Pitari, V. Grewe, P. van Velthoven, and J. Sundet, Model intercomparison of the transport of aircraft-like emissions from sub- and supersonic aircraft, in press, 2002.
- Rosenlof, K. H., and J. R. Holton, Estimates of stratospheric residual circulation using the downward control principle, *J. Geophys. Res.*, **98**, 10465-10479, 1993.
- Saraber, M. J. M. and L. C. Heijboer, A modern teaching tool for cyclone development and structure, *Meteorol. Appl.*, **1**, 135-139, 1994.
- Scheele, M. P., P. C. Siegmund, P. F. J. and van Velthoven, Sensitivity of trajectories to data resolution and its dependence on the starting point: in or outside a tropopause fold, *Meteorol. Appl.*, **3**, 267-273, 1996.
- Schubert, W. H., S. A. Hausman, M. Garcia, K. V. Ooyama, and H.-C. Kuo, Potential vorticity in a moist atmosphere, *J. Atmos. Sci.*, **58**, 3148-3157, 2001.
- Shapiro, M. A., Turbulent Mixing within Tropopause Folds as a Mechanism for the Exchange of Chemical Constituents between the Stratosphere and Troposphere, *J. Atmos. Sci.*, **37**, 994-1004, 1980.
- Siegmund, P. C., P. F. J. van Velthoven, and H. Kelder, Cross-tropopause transport in the extratropical northern winter hemisphere, diagnosed from high resolution ECMWF data, *Quart. J. Roy. Meteor. Soc.*, **122**, 1921-1941, 1996.
- Sigmond, M., J. Meloen, and P. C. Siegmund, Stratosphere-troposphere exchange in an extratropical cyclone, calculated with a Lagrangian method, *Ann. Geophys.*, **18**, 573-582, 2000.
- Spaete, P., D. R. Johnson, and T. K. Schaack, Stratospheric-tropospheric mass exchange during the presidents' day storm, *Mon. Wea. Rev.*, **122**, 424-439, 1994.
- Staley, D. O., Evaluation of potential-vorticity changes near the tropopause and the related vertical motions, vertical advection of vorticity, and transfer of radioactive debris from stratosphere to troposphere, *J. Meteorol.*, **17**, 591-620, 1960.
- Starr, V. P., and M. Neiburger, Potential vorticity as a conservative property, *J. Marine Res.*, **3**, 202-210, 1940.
- Stohl, A., G. Wotawa, P. Seibert, and H. Kromp-Kolb, Interpolation errors in wind fields as a function of spatial and temporal resolution and their impact on different types of kinematic trajectories, *J. Appl. Meteor.*, **34**, 2149-2165, 1995.
- Stohl, A., M. Hittenberger, and G. Wotawa, Validation of the Lagrangian particle dispersion model FLEXPART against large scale tracer experiments. *Atmos. Environ.*, **32**, 4245-4264, 1998.

- Stohl A. and P. Seibert, Accuracy of trajectories as determined from the conservation of meteorological tracers, *Quart. J. Roy. Meteor. Soc.*, **124**, 1465-1484, 1998.
- Stohl, A., and D. J. Thomson, A density correction for Lagrangian particle dispersion models, *Boundary-Layer Meteorology*, **90**, 155-167, 1999.
- Stohl, A., N. Spichtinger-Rakowsky, P. Bonasoni, H. Feldmann, M. Memmesheimer, H. E. Scheel, T. Trickl, S. Hübener, W. Ringer, and M. Mandl, The influence of stratospheric intrusions on alpine ozone concentrations, *Atm. Environment*, **34**, 1323-1354, 2000.
- Stohl, A., L. Haimberger, M. P. Scheele, and H. Wernli, An intercomparison of results from three trajectory models, *Meteorol. Appl.*, **8**, 127-135, 2001.
- Vaughan, G., Stratosphere-troposphere exchange of ozone, in: Tropospheric ozone, D. Reidel Publishing Company, 125-135, 1988.
- Vaughan, G., J. D. Price, and A. Howells, Transport into the troposphere in a tropopause fold, *Quart. J. Roy. Meteor. Soc.*, **120**, 1085-1103, 1994.
- Velthoven van, P. F. J., and H. Kelder, Estimates of stratosphere-troposphere exchange: sensitivity to model formulation and horizontal resolution, *J. Geophys. Res.*, **101**, 1429-1434, 1996.
- Wei, M.-Y., A new formulation of the exchange of mass and trace constituents between the stratosphere and the troposphere, *J. Atmos. Science*, **44**, 3079-3086, 1987.
- Wernli, H. and H. C. Davies, A Lagrangian-based analysis of extratropical cyclones. I: The method and some applications. *Quart. J. Roy. Meteor. Soc.*, **123**, 467-489, 1997.
- Wernli, H., and M. Bourqui, A Lagrangian "one-year climatology" of (deep) stratosphere-troposphere exchange in the extratropical northern hemisphere, *J. Geophys. Res.*, **107**, 2002.
- Wirth, V., Diabatic heating in an axisymmetric cut-off cyclone and related stratosphere-troposphere exchange, *Quart. J. Roy. Meteor. Soc.*, **121**, 127-147, 1995.
- Wirth, V., and J. Egger, Diagnosing extratropical synoptic-scale stratosphere-troposphere exchange: a case study, *Quart. J. Roy. Meteor. Soc.*, **125**, 635-655, 1999.
- WMO, 'Scientific assessment of ozone depletion: 1994'. Global ozone research and monitoring project, Report No. 37 World Meteorological Organization, Geneva, Switzerland, 1995.
- Zhang, D.-L. and H.-R. Cho, The development of negative moist potential vorticity in the stratiform region of a simulated squall line, *Mon. Wea. Rev.*, **120**, 1322-1341, 1992.
- Zierl, B., and V. Wirth, The influence of radiation on tropopause behavior and stratosphere-troposphere exchange in an upper tropospheric anticyclone, *J. Geophys. Res.*, **102**, 23883-23894, 1997.

Curriculum vitae

Op 8 juli 1972 ben ik in Nieuwkoop geboren. Na twee verhuizingen kwam ik op mijn zesde in Aarlanderveen terecht, waar ik naar hartelust tussen de schapen, koeien, pony's, konijnen, kippen en de grassprietjes kon hobbelen. Op mijn twaalfde ben ik begonnen aan de tweejarige brugklas van het Albanianea in Alphen aan den Rijn. Na het eerste jaar was ik nog intelligent genoeg voor de 'latijnklas' (gymnasium), maar vanwege weerzin voor talen (toen al) wilde ik daar niet toe. In de tweede klas trokken de schapen, koeien enzovoort zo hard, dat mijn intelligentie daalde naar het HAVO-niveau. Dat werd het dus. Gelukkig verhuisden mijn ouders, zus en ik meteen naar Berg aan de Maas (Zuid-Limburg), zodat ik niet continu geconfronteerd zou worden met dit 'gezichtsverlies'. Daar ben ik verder gegaan met mijn schoolcarrière op het College Sittard in Sittard. De overgang van het tamelijk losbollige Albanianea (huiswerk? nee hoor, het is veel te mooi weer om jullie huiswerk te geven vandaag) naar het strenge Colleej verliep in het begin tamelijk moeizaam. Na een half jaar was ik zodanig geconditioneerd dat ik als vanzelf begreep dat alleen de omslachtigste manier moeilijk genoeg was. Op mijn zestiende heb ik de schaap-, koe- enzovoortloze jaren vervangen door elke zaterdag in Dierenpark Born te gaan werken op de kinderboerderij. Na verloop van tijd mocht ik ook af en toe tussen de roofvogels en kleine roofdieren vertoeven (voor zover je een Europese lynx nog klein kan noemen). In 1989 heb ik mijn HAVO-diploma gehaald en daarna ben ik eindelijk in mijn element geraakt op het Atheneum. Daar waren zowaar mensen die op mij leken en zich wat meer bezig hielden met de vraag wat ze zouden gaan studeren en wat minder met waar ze in het weekend uit zouden gaan. Hier heb ik in 1991 Cum Laude mijn Atheneum diploma gehaald. Ondanks mijn lage lotingsnummer (in mijn lotingsgroep had ik nummer negen van in totaal dertien) werd ik twee weken na aanvang van het collegejaar nog nageplaatst bij de studie Diergeneeskunde in Utrecht. Zat ik toch weer tussen de schapen, koeien enzovoort, alleen waren de meeste dood. In 1992 haalde ik mijn propedeuse (Met Genoegen) en ben ik doorgedaan in het tweede jaar. Aan het eind van dit tweede jaar, in 1993, met nog vier jaar pilletjes en poedertjes, schimmels en bacteriële infecties, koliek en keizersneden maakte ik toch maar een ommezwaai

naar de studie Natuurkunde (ook in Utrecht). Hier heb ik het eerste jaar erg veel moeite gehad om het spannend leren weer onder de knie te krijgen. In 1995 had ik dan ook pas mijn propedeuse Natuurkunde binnen, maar toen ik weer door had hoe het moest ging het tweede jaar Natuurkunde vrij soepel. Ik ging verder met de (toen nog) bovenbouwstudie Meteorologie en Fysische Oceanografie. In 1998 ben ik hier, na in totaal 4.5 jaar, Met Genoegen afgestudeerd. Ik kon meteen verder gaan als onderzoeksmedewerker op het KNMI, waar ik ook mijn afstudeeronderzoek had gedaan. Bij de sectie Atmosferische Samenstelling ben ik in totaal vier jaar en vier maanden bezig geweest om dit proefschrift te voltooien. In totaal heb ik op twee verschillende projecten gewerkt en heb ik onderweg zes contractsverlengingen gehad. Ik ben elf keer op dienstreis geweest, waarvan één zomerschool, vier conferenties en zes project meetings. In totaal ben ik zes keer met het vliegtuig gegaan, de andere keren met de trein. Tijdens deze dienstreizen heb ik één praatje op een conferentie en één colloquium gegeven, twee posters gepresenteerd en vier praatjes op project meetings gegeven. St. Jean-de-Luz was het interessantst, Nice het gezelligst, Tenerife het verst qua afstand en St. Jean-de-Luz het verst qua reistijd. Ik heb een beetje het idee dat 20 juni 2002 de dag is waar ik mijn hele leven naartoe gewerkt heb. Maar misschien is elke dag wel de dag waar je je hele leven naartoe werkt. Het was in ieder geval zeker de moeite waard!



Stellingen

behorende bij het proefschrift

Simulation and diagnosis of stratosphere-troposphere exchange

1.

Minder oorzaken van verandering, betekent niet altijd minder verandering.

Hoofdstuk 2.

2.

De nauwkeurigheid van een model kan vaak beter worden bepaald door te vergelijken met andere modellen dan door de fouten van het model te schatten.

Hoofdstuk 5.

3.

Vanwege tuning van de meeste modellen is de kans dat een model beter gaat presteren bij het vinden en verbeteren van een fout klein.

4.

Het nut van klimaatonderzoek zou groter zijn als de bereidheid van de mens om het milieu te ontzien groter was.

5.

Elke berg wordt een dal door het perspectief erover te veranderen.

6.

De meest eigenwijze mensen zijn vaak die mensen die van zichzelf vinden dat ze helemaal niet eigenwijs zijn.

7.

Er is een grote verscheidenheid in soort, type en kleur van auto's. Dit is terug te voeren op de verschillen in soort, type en kleur van de eigenaren. De verscheidenheid in auto's is volkomen geaccepteerd, de verscheidenheid in eigenaren daarentegen nog niet.

8.

Per jaar sterven ruim 20 miljoen mensen, waarvan 12 miljoen kinderen, onnodig. (Dit zijn per dag 13.600 mensen door gebrek aan schoon water en basishygiëne, 5.500 kinderen door gebrek aan vaccinaties, 24.000 mensen door ondervoeding, 2.750 mensen door malaria, 8.200 mensen door tuberculose en 1.370 vrouwen bij de bevalling.)

9.

Luister eens naar je lichaam, je lichaam luistert tenslotte ook naar jou.

10.

Eerlijkheid loont vaak niet in deze wereld.
Het is hooguit beter voor je eigen gemoedsrust.

Jojanneke Meloen

14 mei 2002